DISTRIBUTION SYSTEM SERVICE RESTORATION BY DYNAMIC PROGRAMMING CONSIDERING SWITCH CHARACTERISTICS

A Dissertation
Presented to
The Academic Faculty

by

Bai Cui

In Partial Fulfillment
of the Requirements for the Degree
Doctor of Philosophy in the
School of Electrical and Computer Engineering

Georgia Institute of Technology
August 2018

DISTRIBUTION SYSTEM SERVICE RESTORATION BY DYNAMIC PROGRAMMING CONSIDERING SWITCH CHARACTERISTICS

Approved by:

Dr. A. P. Meliopoulos, Advisor
School of Electrical and Computer Engineering
Georgia Institute of Technology

Dr. Ying Zhang
School of Electrical and Computer Engineering
Georgia Institute of Technology

Dr. Andy Sun, Co-advisor
H. Milton Stewart School of Industrial and Systems Engineering
Georgia Institute of Technology

Dr. Lukas Graber
School of Electrical and Computer Engineering
Georgia Institute of Technology

Dr. Maryam Saeedifard
School of Electrical and Computer Engineering
Georgia Institute of Technology

Dr. Shijie Deng
H. Milton Stewart School of Industrial and Systems Engineering
Georgia Institute of Technology

Date Approved: July 20, 2018

ACKNOWLEDGEMENTS

I have been very fortunate to have two mentors guide and support me during my time at Georgia Tech. Firstly, I would like to express my deepest gratitude to my advisor, Professor A. P. Sakis Meliopoulos, for his motivation, encouragement, and guidance throughout the years. He exemplifies that a good engineer needs to have a solid background in both natural sciences and practical skills. His perspective on research and engineering will have a long-lasting influence on me.

I'm also extremely grateful to my co-advisor, Professor Andy Sun, who introduced me to the field of operations research and showed me the beauty of mathematics. The countless hours he spent introducing and discussing fascinating power system and optimization problems have been a great pleasure. His dedication to research was, and continues to be, a source of inspiration for me.

I would also like to express my gratitude to the committee members in ECE and ISyE: Professor Maryam Saeedifard, Professor Ying Zhang, Professor Lukas Graber, and Professor Shijie Deng, for providing me with valuable and constructive suggestions on my work, and for kindly agreeing to serve on my Ph.D. defense committee.

My thanks go to all colleagues in the current and former labs. I would like to thank Dr. Zhaoyu Wang, Dr. Namhun Cho, Dr. Rajatha Bhat, Dr. Dongbo Zhao, Dr. Renke Huang, Dr. Rui Fan, Dr. Zhenyu Tan, Dr. Liangyi Sun, Dr. Yu Liu, Dr. Aniemi Umana, Yi Du, Orestis Vasios, Hussain F Albinali, Boqi Xie, Chiyang Zhong, Yuan Kong, Kai Tian, Jiahao Xie, Kaiyu Liu, Kaizhao Sun, Shixuan Zhang, and Amin

Gholami, for their friendship and support. Thank you for making my Ph.D. journey such a unique and enjoyable one.

Above all, no words can express my gratitude to my parents Jichun Cui and Li Bai, for their unconditional love, support, and faith in me. They have always stood by my side and allowed me to pursue my path freely. To them this thesis is dedicated.

A special thanks to my lovely wife Weiting for the many late night drives from and to the airport, for all the beautiful memories we shared, and for always being there and cheering me up during difficult times. It is a blessing to have her around during my doctoral years.

TABLE OF CONTENTS

LIST OF TABLES

LIST OF FIGURES

SUMMARY

The objective of the proposed research is to develop a systematic approach of finding the optimal switching sequence leading to optimal post-fault topology in distribution system restoration (DSR) problem. The purpose of DSR is to reconfigure the topology of distribution system through switching actions to restore power to customers subject to system faults. Many existing methods formulate DSR problems as single-step optimization problem where the only control devices are remotely controllable sectionalizers. The problem with this approach is that when various kinds of switches are present in the distribution system, certain sequence of switching actions need to be followed based on the different characteristics of the switches, which is not considered by the single-step optimization formulations. To the best of our knowledge, there hasn't been research reported in the literature that considers the characteristics of switches and couples the constraints in the optimization problem to derive feasible switching sequences in a systematic and mathematically rigorous way. By formulating the DSR problem as a dynamic programming (DP) problem, the solution can be found in a systematic way with guaranteed optimality. Switch current limits as well as system operational constraints are considered in the formulation. Scalability to larger systems and related computational issues are discussed.

CHAPTER 1. INTRODUCTION

1.1 Problem Statement

Distribution systems are undergoing unprecedented changes with new utility and customer owned resources that promise the ability of a more controllable and resilient system with fast recovery capability from system anomalies. The advancement in metering and communication technologies facilitates the coordination of geographically dispersed control devices in modern distribution systems. For example, automatic switches, capacitors and reclosers are being integrated in the distribution automation system with many pilot programs such as the Pacific Northwest smart grid demonstration project [1]. The integration of these devices as well as the communications among them enables a centralized coordination scheme for better system restoration that takes full advantage of the hardware and communication infrastructure.

When a fault occurs in a distribution system, protective devices such as reclosers and circuit breakers will act to isolate the fault. Some customers will inevitably lose power in the process, which is referred to as service interruption. The purpose of distribution service restoration (DSR) is to reconfigure the distribution system topology through switching actions to restore power to as many customers as possible while isolating system faults. Subsequently the faulty parts can be repaired. Many existing methods formulate the DSR problem as a single-step optimization problem where the only control devices are sectionalizers. The problem with this approach is that when various kinds of switches are present in the distribution system, certain sequence of switching actions need to be followed based on the characteristics of the different

switches. These caharacteristics are not considered in many single-step optimization approaches appearing in the literature.

The switches in distribution systems can be categorized into reclosers, circuit breakers, load break switches, and sectionalizers. During DSR, the switching sequence of open/close the switches should be considered based on their specific characteristics: reclosers and circuit breakers can be opened and closed under load, and they can break a fault current. In addition, circuit breakers and reclosers can operate automatically when a fault is detected. Load break switches can be opened and closed under load, but they cannot break fault current. Sectionalizers can only be opened and closed at no-load. The appropriate sequencing of switching actions is demonstrated in the following example:

Consider the two-feeder distribution system shown in Figure 1 with 9 buses and 9 switches

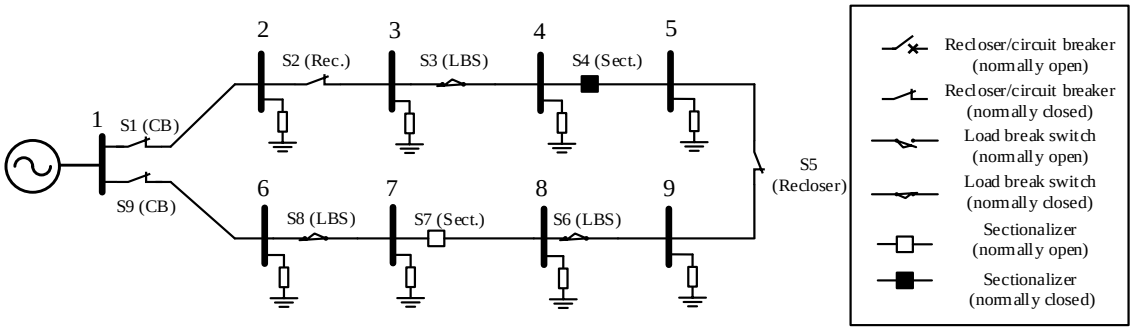

Figure 1 Two-feeder distribution system.

Assume there is a short-circuit between S4 (sectionalizer) and S5 (recloser). In response to the fault, S2 (recloser) opens automatically to isolate the fault, which isolates loads between S2 and S7. In the optimal post-fault topology, S4 and S5 should be opened to isolate the fault instead of S2 and S7, so that buses 1 – 4 form one new feeder and buses

1, 6, 7, 8, 9 forms the other. Considering the characteristics of the switches, the appropriate switching sequencing is: open S2 (automatically); open S4; close S2; open S5; open S8; close S7; close S8. The final topology is shown in Figure 2.

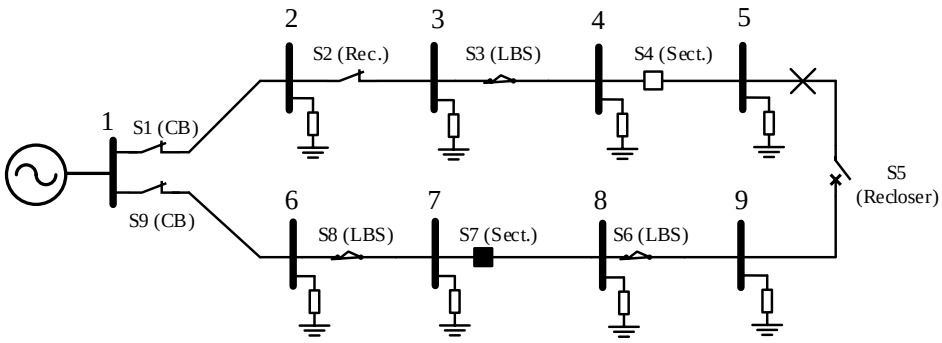

Figure 2 Optimal post-fault topology for the example system.

The above procedures can be generalized as follows: when a fault occurs, the upstream recloser or circuit breaker is opened (open recloser 2). If there are extra switches between the open recloser/circuit breaker and the fault location, then to minimize the isolated area, the switch between the fault location and the open recloser/circuit breaker that is closest to the fault location is opened (open sectionalizer 4), which is followed by closing the upstream recloser/circuit breaker (close recloser 2). This sequence of switching actions restores the upstream section of the feeder. To restore the downstream section, the affected loads need to be picked up by another feeder. First, open the downstream switch closest to the fault location (open recloser 5). Then close the normally open tie switch (close sectionalizer 7) so that the loads can be picked up by another feeder. If the tie switch is a sectionalizer, the closing of the sectionalizer needs to be preceded by opening the upstream recloser/circuit breaker/load break switch (open circuit breaker 8) to de-energize the circuit.

For small distribution networks, simple logic as described above employed by distribution management systems suffices to find optimal or near optimal switching sequences that lead to post-fault topologies. However, as the systems are being operated ever closer to their operational boundaries while their topologies get more complicated at the same time, it becomes increasingly difficult to find the optimal solution, or even a feasible solution, by this simple approach. As mentioned earlier, many algorithms in the literature formulate the DSR problem as a single-stage optimization problem that only provides the final configuration. However, to the best of our knowledge, there hasn't been research reported in the literature that considers the characteristics of switches and couples this type of constraints in the optimization problem to derive feasible switching sequences in a systematic and mathematically rigorous way. The dissertation therefore proposes a systematic way to find the optimal switching sequence in DSR problems considering switch characteristics. By formulating the DSR problem as a dynamic programming (DP) problem, the solution can be found in a mathematically rigorous way with guaranteed optimality. In addition, different operational constraints can be considered in the DP framework such as nodal voltage bounds and line flow limits, so that the impact of operational constraint violation in the switching process can be controlled.

1.2 Thesis Outline

The rest of the dissertation is outlined as follows:

In Chapter 2, literature survey on distribution system reconfiguration and service restoration problems is presented. Both single-stage optimization which optimizes the

final system topology and sequential optimization which optimizes the switching operations leading to the final system topology are reviewed. Five classes of single stage optimization approaches are discussed, namely expert systems, local search, meta-heuristic, exhaustive search, and mixed-integer programming-based approaches. Sequential optimization based on mixed-integer programming is also discussed. The limitations of existing methods are discussed.

Chapter 3 presents the proposed DP-based sequential service restoration scheme considering switch characteristics. Specifically, transition cost, cost of operation, as well as the optimal total cost are introduced to model system states associated with topologies during the service restoration process. Stopping criterion of the algorithm is defined and the overall algorithmic description of the proposed approach is summarized.

Chapter 4 presents two numerical test cases to evaluate the performance of the proposed service restoration algorithm. The capability to reliably derive the optimal switching sequence considering switch current upper bounds is demonstrated and verified.

Chapter 5 presents the extension of the proposed services restoration algorithm incorporating system operational constraints. To be specific, nodal voltage, line current, and radiality constraint violations are penalized in the cost of operation of system states. Simulation results with and without consideration of the operational constraints show the effectiveness of the proposed extension.

Chapter 6 presents distribution system state estimation using switch measurements. It is shown that the entire system states can be successfully recovered

given enough measurements on switch voltages and currents. This algorithm can be used to obtain system loading conditions which is an essential piece of information for service restoration algorithms.

Chapter 7 presents an exhaustive search method for service restoration. The method uses a two-level search scheme to limit the number of candidate radial topologies. This algorithm can be used as a tool to find the appropriate subsystem to apply the proposed DP-based service restoration when the number of switches is too large. The proposed DP-based approach is then tested on a reduced distribution system with a large number of switches (20) to examine its scalability.

Finally, chapter 8 summarized the research work and contributions of the work and outlines some directions of future work.

CHAPTER 2. LITERATURE SURVEY

2.1 Overview

The classical distribution service restoration problem, when viewed as a reconfiguration problem, seeks the optimal radial topology by opening and closing different combinations of protective and sectionalizing switches. The problem was first formulated and solved in the 1970's [2] and has gain considerable attention ever since.

In addition to simply finding the optimal topology in a single-stage optimization, a more important and relevant objective is to find the sequence of switching operations that leads to the optimal topology such that operational constraints are not violated and intermediate operating costs are taken into consideration. The latter problem can be viewed as a sequential optimization problem. Compared to its single-stage counterpart, the sequential one has drawn little attention.

Solutions to distribution service restoration as a single-stage reconfiguration problem has been derived using a wide variety of ways ranging from expert systems and fuzzy logic, local search, meta-heuristics, special exhaustive search to mixed-integer programming approaches. In Section 2.2, existing researches on single-stage DSR problem are reviewed and the limitations for each class of methods are identified. DSR considering switching sequences will be reviewed in Section 2.3. It is noted that this problem has been predominantly solved for using mixed integer programming (MIP) approaches. The drawbacks of this approach will also be discussed in Section 2.3. The chapter concludes with a summary.

2.2 Survey of Service Restoration and Reconfiguration Techniques

2.2.1 Expert System

Expert system has been one of the first systematic methods applied for DSR in the 1980s [3]. An expert system is a computer system that emulates the decision-making ability of a human expert. The system has a knowledge base, which contains rules for decision-making under various scenarios. The work in [3] divides solution of DSR problem into five segments as 1) group restoration, 2) zone restoration, 3) load transfer, 4) switching action determination, and 5) inference control. If-then-type of rules are designed for each segment. The rules in each segment are then applied sequentially given specific system scenarios to formulate the optimal restoration plan. Subsequent researches have applied G-Nets or Petri Net as inference mechanisms for the expert system based on pre-defined heuristic rules [4–5]. The effectiveness of an expert system depends largely on pre-defined rules. For complicated problems, it is generally difficult to design a list of rules that can encompass all possible scenarios and yield ideal results under drastically different scenarios. This is especially the case when considering complicating factors arising in modern distribution systems such as DG output uncertainties and bi-directional power flow.

2.2.2 Local Search Methods

When viewed as a specific kind of reconfiguration problem where the objective function is load re-energization, DSR is essentially a mixed-integer programming (MIP) problem. Because of its relatively large size and the combinatorial nature, the problem has long been solved for by local search methods and its variants as well as other

heuristic methods, before the proliferation of commercial mixed-integer programming software in the last decade or so. These simple and robust methods served as the foundation of some production grade computer programs and have subsequently influenced the development of various techniques [12].

A local search algorithm called “successive branch exchange” is proposed for distribution reconfiguration problem in [6], where the idea of “branch exchange” is first proposed in [7]. The algorithm starts with a feasible system topology. At each iteration, a pair of switches is chosen, and the on/off status of the switches are swapped to achieve maximum cost function reduction while the radial structure is maintained. The algorithm terminates at a local optimal solution when no switch pair that improves the cost function can be found. Some developments and extensions on this approach can be found in [8–12]. The work in [13] applies similar idea but partitions the system topology into groups and perform reconfiguration within each group for scalability purposes. An advantage of the method lies in the fact that every intermediate step is an improved solution to the reconfiguration problem, so the algorithm can be terminated early. However, it may suffer from slow convergence and the results are sensitive to initial condition. A related approach proposed in [14] assumes all switches are initially closed. They are then opened successively based on maximum cost function reduction until the system topology is radial. For this algorithm, the number of iterations is bounded by the number of redundant switches. However, when applied in real-time, the resulting topology may be quite different from the current operating one, and the large number of switching actions may be unfavorable from system operation perspective. The two approaches can also be combined to form two-stage algorithms where successive switch opening is followed by

branch exchange [15]. Other variants of the two-stage algorithm include [16–17]. It is interesting to note that empirical results have suggested the superiority of the two-stage methods over individual ones.

2.2.3 Metaheuristic Approaches

Many metaheuristic and artificial intelligence-based methods has been proposed for distribution system reconfiguration since 1990s. These algorithms, typically inspired by metaphors from physics or biology, can be considered as variants of local search. They can be roughly divided into three categories: local search metaheuristics, constructive metaheuristics, and population-based metaheuristics.

Local search algorithms update the solution based on maximum cost improvement among the neighbors. The main problem is that the converged solution may only be a local optimum. Simulated annealing improves the original local search algorithm by accepting moves to a worse solution with certain probability, thus granting the possibility to escape from a local optimum. This solution algorithm is adopted in [18-19] for distribution system reconfiguration where the problem is formulated as a multi-objective mixed-integer constraint optimization problem. Tabu search is another local search heuristic in which the recently-visited solutions are temporarily forbidden. See [20] for application to distribution reconfiguration by Tabu search. Constructive metaheuristics construct solutions from their constituting elements rather than improving complete solutions. A notable example is ant colony optimization, which builds solutions by mimicking the foraging behavior of ants. The application of this method and its variants in reconfiguration problem has resulted in many publications, for example, [21-22].

Population-based metaheuristics find good solutions by iteratively selecting and then combining existing solutions. The most important methods of this class are evolutionary algorithms (EA), which is an umbrella name that compasses the wide range of methods based on evolution. This include genetic algorithms [23–26], differential evolutionary [27–28], and many others [29]. Comparative studies and evaluation of various metaheuristic algorithms for DSR can be found in [30]. Metaheuristic algorithms are robust enough to achieve a relatively good performance on a wide spectrum of problem types, however, for specific problems like DSR or distribution reconfiguration problem in general, their performance may not be as good as mixed-integer programming solvers in terms of solution quality and computation time, as the latter approach exploits specific problem structures in solving them. Another problem with metaheuristic algorithms is that the performance of these algorithms depends critically on the setting of the parameters, which requires a very good understanding of both the problem at hand and the inner working of the algorithm.

2.2.4 Exhaustive Search Methods

Exhaustive search methods have also been considered for reconfiguration problem. In [31], an efficient exhaustive spanning tree search algorithm has been proposed for reconfiguration problem which exploits system sparsity patterns by using semi-sparse transformations of current sensitivity matrix. A recent work [1] also relies on the exhaustive algorithm for finding all spanning trees [32] as well as graph reduction techniques to find optimal post-fault system topology in the presence of distributed generators (DGs). The main problem of the approach is its scalability to larger systems.

When the optimal state is easy to characterize, e.g., when the optimal state corresponds to a topology with no unserved loads in DSR problem, instead of performing exhaustive search and then looking for the switching sequence to the optimal final topology, a simpler approach is to directly find a shortest path that leads to the optimal state without listing all potential solutions. This is computationally friendlier than exhaustive search, and it provides a switching sequence from the initial topology to the final one. This approach is adopted in [33] where A^* algorithm, a variant of general shortest path algorithm, is applied.

2.2.5 Mixed Integer Programming Approaches

In the last decade or so, MIP techniques have been widely used in distribution reconfiguration problems including loss minimization, service restoration, and DG integration due to the proliferation of mature academic and commercial MIP solvers.

A mixed-integer linear programming (MILP) formulation based on polyhedral approximations has been proposed in [34] for system reconfiguration. Mixed-integer quadratic, quadratically constrained, and second-order conic programming (MISOCP) models are derived for reconfiguration problems in [35]. MISOCP model as well as its polyhedral approximation is adopted in [36]. To deal with uncertainties in DG output and load demands, information gap decision theory is proposed in [37]; a robust MILP model for DSR problem is proposed in [38], in which column-and-constraint generations are applied to improve computation time. To reduce computation time, more efficient formulation utilizing linear current flow models has been proposed for MILP model in [42]. The reconfiguration problem can also be coupled with OPF problem to form a two-

stage problem where the reconfiguration problem is solved in the first stage and OPF is performed in the second stage with known system topology. This two-stage structure naturally lends itself to a Bender's decomposition-based solution technique [43]. There have been some growing interests in applying the developed linear and conic models for DG integration and real time operation. For example, a recent work in [44] has considered time-varying loads and DG output in the reconfiguration problem. Other works include [37–45]. MIP is generally more efficient and effective for reconfiguration problems including DSR compared with metaheuristic algorithms. However, most of the above works focus on optimizing only the final topology, while optimizing switching sequences is still a challenge both in terms of problem formulation and computation time especially when the number of switching actions is unknown in advance.

In addition to minimization of unserved loads, many alternative objectives are sought after for DSR problems, in which some specialized approaches are used: the work in [46] proposes a strategy for restoring critical load based on shortest path search which takes system dynamic stability into consideration by coupling optimization with dynamic simulation. The work in [47] models manual and automatic switches with different costs and proposes a minimum spanning tree-based reconfiguration strategy that minimizes the total switching cost. Instead of focusing on system reconfiguration, [48] considers the problem of avoiding frequency disturbance brought about by generation/load unbalance in the process of service restoration. The sequence of load integration over a time horizon is determined using dynamic programming with state reduction technique.

Transmission switching problem [49–53] is a closely related problem to DSR. It can also be viewed as a reconfiguration problem and solved using similar MIP

formulations. A major difference from a formulation perspective is that the radiality constraint, normally strictly enforced in DSR [54–55], can be dropped. Thanks to recent advancement in conic programming relaxation techniques in power system optimizations [56–59], more elaborated models can be used [60], which relies on tight conic relaxation and strong valid inequalities through problem structure exploitation.

2.3 Survey of Sequential Service Restoration

Sequential service restoration takes the entire service restoration process into consideration which not only finds the final optimal system topology but also the sequence of switching operations that lead to the final topology. This viewpoint of the service restoration problem has been largely overlooked in the past. In this section, we review the limited literature on this topic that emerged in the last year or two.

The research in [61] proposed a MINLP model for the service restoration problem minimizing the overall cost of load de-energization and switching operation over the entire switching horizon while the operational constraints are enforced throughout the switching process. The model is then linearized using disjunctive constraints, Taylor expansion, and approximations including piecewise linear functions, to obtain a MILP model. DGs are also considered in the formulation to provide additional support to the de-energized zones. A similar approach is taken in the series of papers in [39–41]. In contrast to [61] where the main motivation is to avoid operational constraints violation during switching process, the papers in [39–41] focus on ensuring normal operation of system components that have inter-temporal characteristics, such as DGs with ramp constraints, load demand under cold load pickup, state-of-charge of energy storage

systems, generators with frequency response, and so on. In these papers, MILP models are used where the linearized power flow equations based on the celebrated distflow model [6] are used. However, none of the above formulations considers the switch current upper bound when the switch is being operated.

The sequential service restoration problems introduced above are all formulated and solved using MIP. MIP has received considerable attention lately as a proven powerhouse for many power system optimization problems with combinatorial nature. However, it should be pointed out that the approach suffers from several drawbacks for this specific multi-stage problem: First of all, the maximum number of switching actions needs to be known in advance, which may not be practical even when the system topology and number of switches are known a priori. For example, a switch may be opened or closed multiple times during the restoration process in certain scenario, such as when a section needs to be temporarily de-energized to allow the sectionalizers to be operated but will then be re-energized. Second, the optimization formulation requires a fixed number of variables for each stage of the restoration process, which means the size of the formulation goes up quickly when the maximum number of stages is increased. This in turn discourages the generous estimation of the maximum number of stages as this will increase the problem size and consequently affect the computation time. Third, it is hard to tell from the optimal solution whether the preset maximum number of stages is sufficient, or the algorithm will converge to a better solution if more stages are given.

2.4 Summary

Literature survey on distribution system reconfiguration and service restoration problems is conducted in this chapter. In particular, Section 2.2 gives a comprehensive review of the primary classes of algorithms proposed for single-stage distribution reconfiguration problem in rough chronological order. These methods are: 1) expert systems; 2) local search; 3) meta-heuristic; 4) exhaustive search; and 5) mixed-integer programming-based approaches. The advantages and limitations of each class of methods are briefly discussed at the end of the respective sections. Section 2.3 reviews the literatures on MIP-based sequential service restoration which consider intermediate switching operations. The drawbacks of the approach are identified.

CHAPTER 3. DISTRIBUTION SERVICE RESTORATION VIA DYNAMIC PROGRAMMING

As introduced in preceding chapters, the DSR problem can be solved effectively by dynamic programming (DP). In this chapter, the solution of the DSR problem via DP is introduced. By controlling the on/off status of switches, the distribution system can transition from one topology (state) to another. DP provides a systematic way to find the optimal sequence of switching actions that leads to the post-fault optimal system topology. The DSR problem can be divided into two steps: 1) fault locating and 2) service restoration. After introducing the distribution system modeling in Section 3.1, fault locating and service restoration via DP will be discussed in Section 3.2 and 3.3, respectively.

3.1 Distribution System Modeling

We model a primary distribution system as consisting of buses, distribution lines (branches), switches, and constant power loads. Each branch of the distribution system is modeled as a single-phase π-equivalent circuit. As introduced previously, there are three types of switches in the system, namely reclosers/circuit breakers, load break switches, and sectionalizers. They have different current upper bounds when being opened/closed. The system topology can be modeled as an undirected graph $G = (N, E)$ where N is the set of buses and E is a set of two-element subsets of V corresponding to distribution lines. The buses in the system are modeled as slack, PV, and PQ buses. The slack bus represents a substation connected to a transmission system receiving bulk power. The

voltage magnitudes and phase angles of slack buses are regulated. Load buses are modeled as PQ buses, whose power consumptions are regulated (distributed generators can be modeled as loads with negative real power consumptions). We also model generator buses as PV buses, whose real power injections and voltage magnitudes are regulated.

A binary variable ξ_{ik} is related to each distribution line (*i*, *k*) with a switch in the subset $E^s \subseteq E$, which indicates the on/off status of a switch. We let $\xi_{ik} = 1$ if the switch on the branch (*i*, *k*) is closed, and $\xi_{ik} = 0$ if the switch on the branch (*i*, *k*) is open. For a system with *n* switches, switch statuses are represented by an *n*-dimensional binary vector *u*. Each switch has associated current upper bound when breaking/making current:

$$I_{ij} \le \bar{I}_{ij}, \quad \forall (i, j) \in E^s \tag{1}$$

The bus-oriented model described above can be extended to a more versatile breaker-oriented model, which allows more accurate representation of switch topologies. However, we introduce the DP formulation with bus-oriented model due to its simplicity.

3.2 Fault Locating

A prerequisite for designing effective restoration strategies is to determine the fault location after a fault occurs in the distribution system. To obtain the fault location, we assume each switch can 1) measure current magnitude flowing through the switch, and 2) detect current direction. Based on the two sets of information collected from protective relays, the fault location can be pinpointed as follows.

3.2.1 Determining Fault Current Threshold

The switches detect fault current when the measured current magnitudes are abnormally high. To determine the threshold for fault current, consider a distribution feeder where the rated voltage and rated power are V_r and S_r, then the rated current is calculated as $I_r = S / (\sqrt{3} V_r)$. A reasonable setting for fault current threshold would be twice of the rated current. That is, a fault is declared when current through the switch exceeds $2I_r$.

When a fault results in higher fault current than fault current threshold set by protective relays, the fault current can be detected and the fault location can be pinpointed. On the other hand, switches may have different fault current thresholds and some may detect current while others may not. In this case the fault cannot be detected exactly. Another possibility is that fault currents are small so that all switches don't detect it.

3.2.2 Fault Current-Based Fault Locating

In the remainder of the proposal we assume fault currents can be detected accurately. We consider a radial distribution network where currents flow unidirectionally from the source (possibly a substation) downstream. In this case, the switches that detect fault currents form a path starting from a source. Tracing the path from the source downstream, the fault can be located within the last switch in the path and its downstream neighboring switches. For example, consider the system in Figure 3:

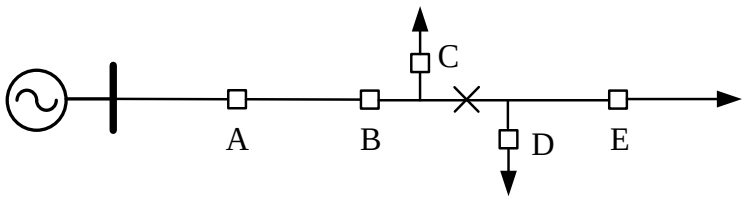

Figure 3 Sample system with five switches

When a fault occurs among switches B, C, D and E, the fault current flows through switches A and B. Since B is the last switch that detects fault current along the path from the source, the fault can be located between B and its neighboring switches downstream, which are C and D.

3.3 Application of Dynamic Programming to Distribution Service Restoration

In service restoration problem, system topology and operating conditions of a given distribution system is uniquely determined by switch status vector *u*. The objective of service restoration is to find the optimal switching sequence that leads to the optimal system topology which minimizes total real power of disconnected loads while accounting for switching constraints (1). The optimal switching sequence is defined in the sense that it results in minimum cumulative transition cost from the initial post-fault topology to the optimal topology.

In the DP formulation, the system topology transitions are broken down into stages k = 1, 2, …, K. Stage k corresponds to the set of topologies resulted from k switching actions from the initial post-fault topology. The loading levels are considered constant throughout the stages. Every switch has a certain on/off status in stage k. For the j-th switch, let $u_j(k)$ be the switch status at stage k. Then $u_j(k)=1$ when the switch is

closed and $u_j(k) = 0$ when the switch is open. At each stage, the state of the system is defined as the set of switch status for all switches:

$$x[k][i] = \left\{ u_j(k),\ j = 1, 2, \ldots n \right\} \tag{2}$$

The initial state of the system is set to be the initial post-fault switch statuses. We define this state $x[0][1]$ as the only state at stage 0. A state $x[k][i]$ represents that the system topology is at state i at stage k.

3.3.1 Transition Cost

At stage k, the system can assume N possible states ($x[k][i]$, $i = 1, 2, \ldots N$) corresponding to all possible system topologies. A state transition from $x[k][m]$ at stage k state $x[k+1][i]$ at stage $k+1$ is feasible when the switch statuses differ by at most one and the switching operation is feasible, i.e. it does not violate switch operating constraints. Note, the state transition is feasible when a state transitions to itself. We may consider the case when $m \neq i$ and let the switch index of the switch whose status changes be j. Then we have $\left| u_j(k) - u_j(k+1) \right| = 1$. Under this condition, the state transition is feasible if and only if the current flowing through switch j does not exceed its upper limit when switch j is closed either in state $x[k][m]$ or $x[k+1][i]$.

When the transition is feasible, the transition cost TransitionCost($x[k][m]$, $x[k+1][i]$) is 0; when the transition is infeasible, it is set to ∞:

$$\text{TransitionCost}(x[k][m], x[k+1][i]) = \begin{cases} 0, & \text{the transition from } m \text{ to } i \text{ is feasible} \\ \infty, & \text{the transition from } m \text{ to } i \text{ is infeasible} \end{cases} \tag{3}$$

3.3.2 Cost of Operation

The cost of operation of an infeasible topology is infinite. On the other hand, for a feasible topology, the cost of operation is defined as the total real power of disconnected loads. The cost of operation Cost[k+1][i] is defined as

$$\text{Cost}[k+1][i] = \begin{cases} U(x[k+1][i]), & \text{State } i \text{ is feasible} \\ \infty, & \text{Otherwise} \end{cases} \quad (4)$$

where $U(x[k+1][i])$ is the total real power of disconnected loads (in MW) at stage k+1, state i. Note that the cost of operation only depends on system topology and it is independent of stage number, without loss of generality we can write Cost[k][i] = Cost[i].

The cost of operation can be extended to incorporate more comprehensive indices in addition to total disconnected loads. For example, cost of system real power loss and harmonics can be included. Note that these additional costs are not integrated in the current algorithm, but the algorithm is flexible for incorporating these additional costs as well as others. The following paragraphs briefly introduce these additional costs and their inclusion in the cost of operation.

First, the system real power loss can be calculated as the sum of real power loss $I_i^2 R_i$ of all circuits i (distribution lines, transformers, etc.), where I_i and R_i are the current through circuit i and total resistance of circuit i, respectively.

The harmonic bus voltage and current through circuits at various frequencies can be calculated based on harmonic power flow algorithm. Let $V_{i,k} = |V_{i,k}| e^{j\theta_{i,k}}$ be the k^{th} harmonic voltage at bus i and $I_{i,k} = |I_{i,k}| e^{j\varphi_{i,k}}$ be the k^{th} harmonic current at circuit i, where k ranges from 1 to 13. The harmonic distortion of a bus or circuit can be measured

based on Total Harmonic Distortion (THD), which is defined as the ratio of the RMS amplitude of higher harmonics to the amplitude of the fundamental frequency:

$$THD_i = \frac{\sqrt{\sum_{k=2}^{13} |V_{i,k}|^2}}{|V_{i,1}|} \tag{5}$$

Then the cost of operation Cost[k+1][i] considering loss and harmonic minimization is defined as

$$\text{Cost}[k+1][i] = w_1 \frac{U(x[k+1][i])}{\text{baseMVA}} + w_2 \frac{\sum_{i \in E} I_i^2 R_i}{\text{baseMVA}} + w_3 \sum_{i \in N} THD_i + w_4 \sum_{i \in E} THD_i \tag{6}$$

where the second term is the total real power loss in per unit, the third and fourth terms are the sum of total harmonic distortions at all buses and all circuits, respectively, and w_i, i = 1,2,3,4 are weighting factors controlling the relative importance of different costs.

Another possible extension is to consider DGs in the system with variable output so that the cost of operation can be minimized over possible DG output through an optimal power flow (OPF) algorithm instead of power flow / harmonic power flow calculation where system operational and stability constraints can be enforced.

3.3.3 Computation of Optimal Cost

When the states at each stage are defined, the optimal transition from a state at stage k to a state at stage k+1 depends only on the parameters at stages k and k+1. Consider $x[k][i]$ at stage k, state i. Let OptimalTotalCost($x[k][i]$) be the optimal total cost of the transition of the system from the state at the initial stage to the present stage k, state

i. Assume the optimal total cost has been computed for all states at stage *k*, then the algorithm to compute the optimal total cost for stage *k*+1, state *i* is given by the following recursive formula:

$$\text{OptimalTotalCost}(x[k+1][i]) = \text{OptimalTotalCost}(x[k][m]) + \text{TransitionCost}(x[k][m], x[k+1][i]) + \text{OperatingCost}(x[k+1][i]) \quad (7)$$

where OptimalTotalCost($x[k+1][i]$) is the optimal total cost at stage k+1, state i. The state with minimum optimal total cost at a stage is called the optimal state. The computation of optimal total cost of $x[k+1][1]$ by DP is shown in Figure 4.

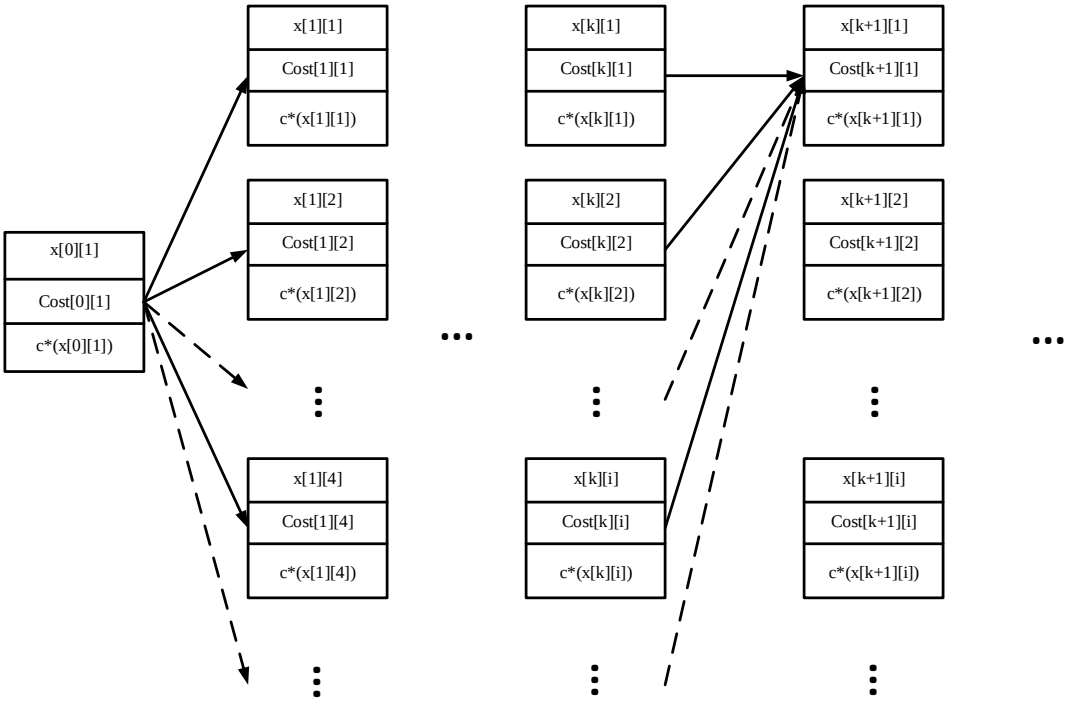

Figure 4 Computation of optimal total cost $c^*(x[k+1][1])$.

Every state i at stage k also has a variable $D[k][i]$, which stores the state number of the previous stage that is in the optimal path from initial state at stage 0 to the current state, this state is called the parent state of the current one. The parent states are not

necessary for computation of the optimal cost, but are needed for backtracking the optimal path (control sequence) from the final to the initial state.

3.3.4 Stopping Criterion

The objective of the algorithm is to find an optimal trajectory from an initial topology to the post-fault topology. When the algorithm reaches a state with sufficiently low operating cost, it tends to stay at the same state afterwards since transitioning to other states incurs a higher cost. The algorithm terminates when the optimal state does not change for a certain number of stages s, or we say the algorithm converges to the state. This corresponds to a local optimal solution since no trajectories with sufficiently short length other than staying at the same state leads to lower optimal total cost. For example, by setting $s = 3$ we assume DP converges to the optimal solution whenever it doesn't change for the last 3 stages.

Before DP algorithm starts, the costs of operation of all states are calculated. An n-switch system will have 2^n possible topologies. However, some topologies may be inadmissible when the fault is not isolated or the power flow does not converge, the cost of operations of which are infinite. The flowchart of the initialization is shown in Figure 5. The flowchart of implementation of DP algorithm is shown in Figure 6.

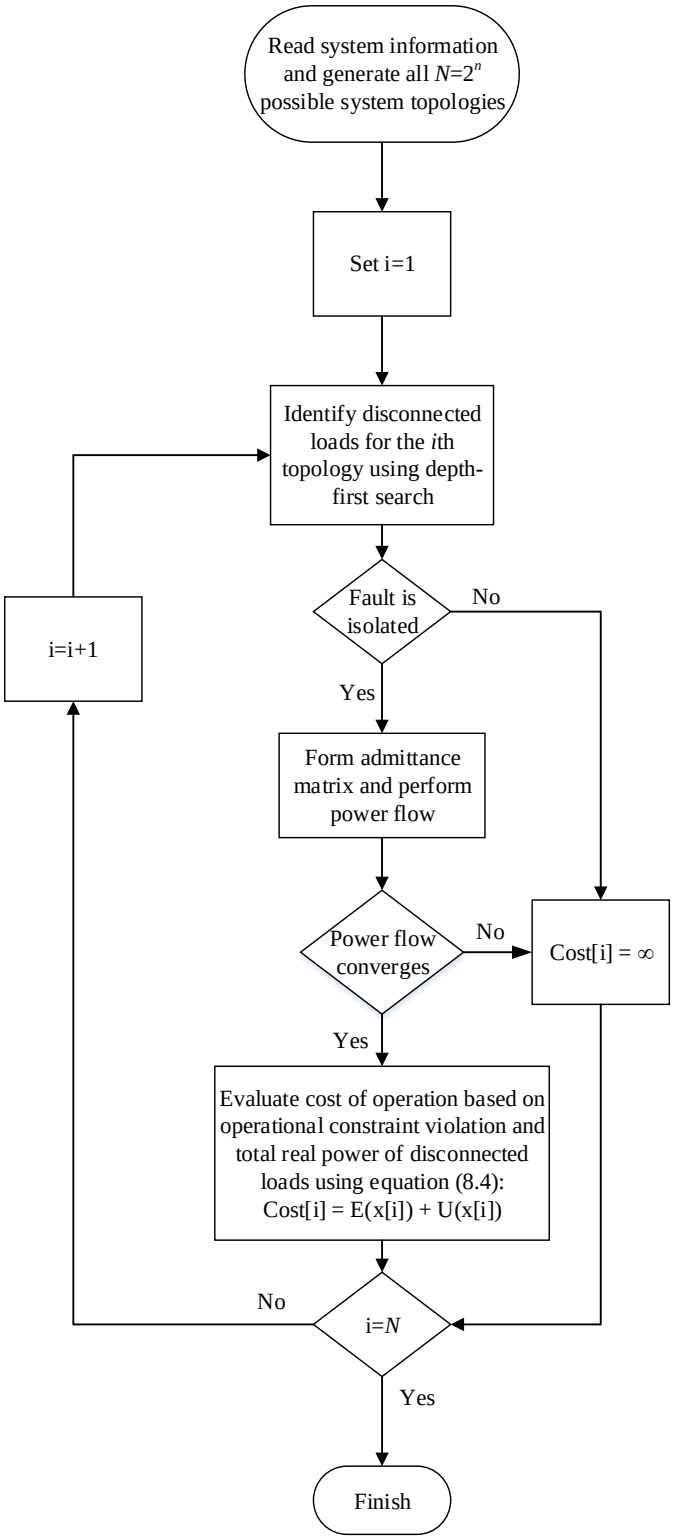

Figure 5 Flowchart of initialization of system states and associated costs of operation (stage number is omitted in Cost[i] and x[i] as the values of the variables are independent of stages).

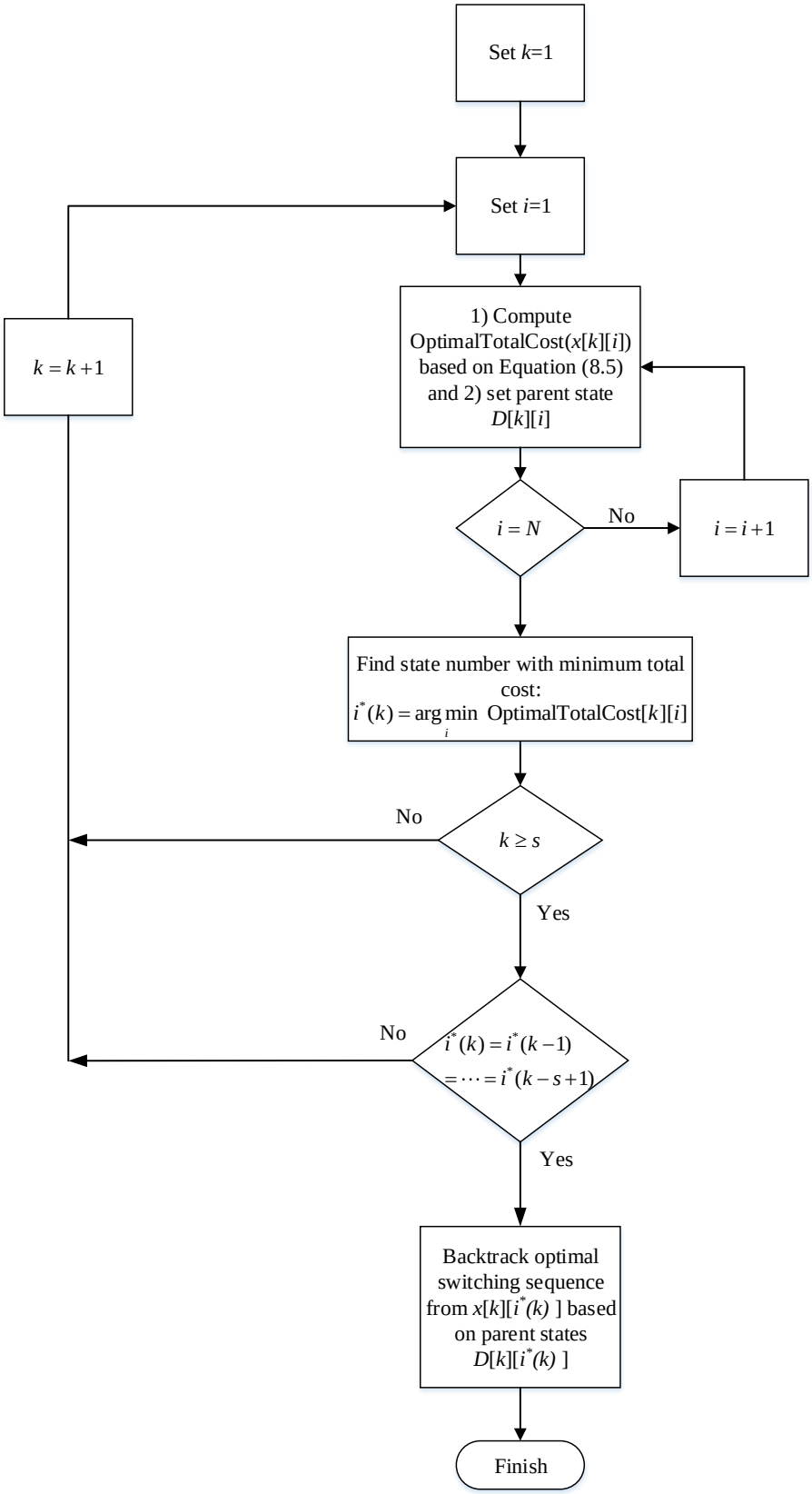

Figure 6 Flowchart of implementation of DP for service restoration problem.

CHAPTER 4. SIMULATION RESULTS ON PROPOSED SERVICE RESTORATION SCHEME

This section presents simulation results of the proposed DP-based service restoration scheme. Two examples with four and nine switches are used to demonstrate the effectiveness of the method.

4.1 Test System 1

A distribution system with four buses and four switches is shown in Figure 7. The goal is to determine the optimal switching sequence to reach post-fault optimal system topology subject to load interruptions following a fault.

4.1.1 System Modeling

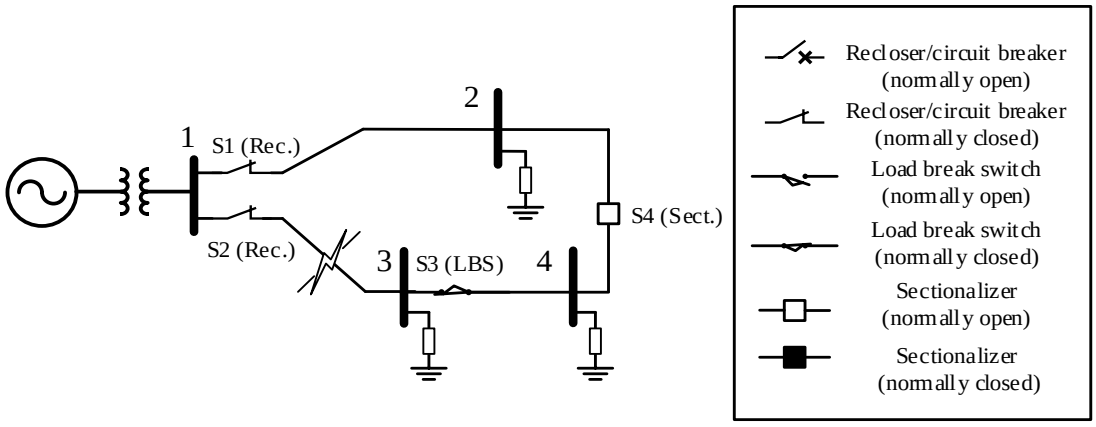

Figure 7 One-line diagram of the test distribution system.

The one-line diagram of the test distribution system is shown in Figure 7. For the system, we assume the feeder head is rated 110 kV, buses 2-4 have voltage ratings of 13.8 kV and the loadings are 5 MW+j2 MVAr. The system base MVA is 100 MVA. The

distribution lines have impedance 0.1524 + j0.2095 Ω between adjacent buses. Switches S1 and S2 are reclosers with current upper limit of 20 kA, S3 is a load break switch and its current upper limit is 600 A. S4 is a sectionalizer, which can only break at no-load, so its current upper limit is 0 A.

Suppose a fault occurs between S2 and S3. In response to the fault, recloser S2 opens automatically, thus isolating buses 3 and 4.

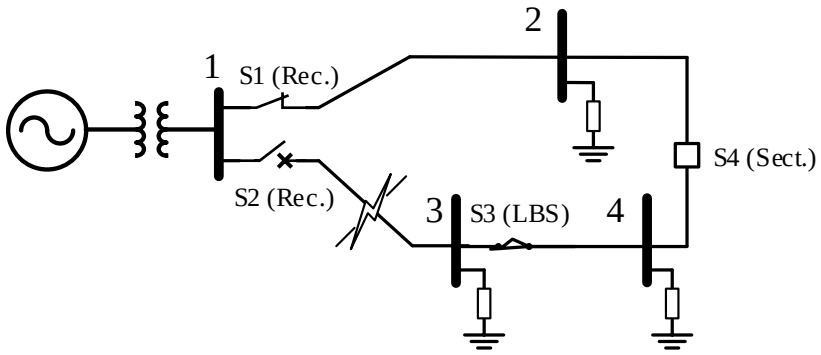

Figure 8 One-line diagram of the test distribution system when a fault occurs between S2 and S3. Recloser opens automatically.

The DP-based service restoration algorithm will be initiated at this moment to restore the interrupted loads. Therefore, the control variable $u(0)$ at stage 0 is

$$u(0) = [1, 0, 1, 0] \tag{8}$$

By definition, the cost of operation and total cost in this state are both 0.

4.1.2 Initialization

In DP formulation for service restoration, the states are initialized at the beginning of the algorithm. That is, for stage i, we need to specify the control variable $u(i)$ and cost

of operation Cost[i][j] for all states j. Since there are 4 switches, the total number of states at one stage is $2^4 = 16$.

To compute the cost of operation of all states, we compute the total real power of disconnected loads, which can be obtained by adding the real power of the loads that are not connected to any source based on the connectivity information. As introduced previously, the state is feasible if and only if the fault is isolated. The cost of operation of an infeasible state is ∞ based on Equation (3). Table 1 below shows the switch statuses, feasibility, and cost of operation of all states.

Table 1 Switch statuses, feasibility, and cost of operation of all states for the test system.

State	Switch status (0/1)				Feasibility	Cost of Operation (MW)
	1	2	3	4		
1	1	0	1	0	Yes	10
2	0	0	0	1	Yes	15
3	0	0	1	0	Yes	15
4	0	0	1	1	Yes	15
5	1	0	0	0	Yes	10
6	1	0	0	1	Yes	5
7	0	0	0	0	Yes	15
8	0	1	0	0	No	∞
9	0	1	0	1	No	∞
10	0	1	1	0	No	∞
11	0	1	1	1	No	∞
12	1	0	1	1	No	∞
13	1	1	0	0	No	∞
14	1	1	0	1	No	∞
15	1	1	1	0	No	∞
16	1	1	1	1	No	∞

Since states 8–16 are infeasible, they are not part of any feasible switching sequences and can be removed from the subsequent DP computation. Table 2 shows the

transition costs between the seven feasible states. Note that the transition cost is 0 when the transition is feasible and it is ∞ otherwise.

Table 2 Transition costs between feasible states.

State	1	2	3	4	5	6	7
1	0	∞	0	∞	0	∞	∞
2	∞	0	∞	0	∞	0	0
3	0	∞	0	0	∞	∞	0
4	∞	0	0	0	∞	∞	∞
5	0	∞	∞	∞	0	∞	0
6	∞	0	∞	∞	∞	0	∞
7	∞	0	0	∞	0	∞	0

4.1.3 Forward Computation

Equation (7) is used to compute the optimal total cost of all stage/state pairs. For stage 1, since there is only one state at stage 0, the computation of optimal total cost for each state *i* is

$$\begin{aligned}\text{OptimalTotalCost}\,(x[1][i]) = \text{OptimalTotalCost}\,(x[0][1]) + \\ \text{TransitionCost}(x[0][1], x[1][i]) + \text{Cost}(x[1][i])\end{aligned} \tag{9}$$

The computation continues for subsequent stages based on Equation (7) until the stopping criterion is met.

4.1.4 Stopping Criterion

The DP algorithm stops when the optimal solution doesn't change for the last 10 stages. That is, the algorithm stops at stage $K \geq 10$ if and only if

$$i^*(K) = i^*(K\text{-}1) = \ldots = i^*(K\text{-}9) \tag{10}$$

where $i^*(k)$ is defined as

$$i^*(k) = \arg\min_i \ \text{OptimalTotalCost}[k][i]. \tag{11}$$

Based on the stopping criterion, the algorithm stops at stage 15, and the optimal state is 10. Figure 9 to Figure 12 show the DP computation for states from stage 0 to 15. Table 3 below shows the optimal state at each stage and the associated optimal total cost:

Table 3 State number with minimum OptimalTotalCost and associated OptimalTotalCost for stages 1 to 15.

Stage number	State number with minimum OptimalTotalCost	Minimum OptimalTotalCost (MW)
1	1, 5	10
2	1, 5	20
3	1, 5	30
4	1, 5	40
5	1, 5, 6	50
6	6	55
7	6	60
8	6	65
9	6	70
10	6	75
11	6	80
12	6	85
13	6	90
14	6	95
15	6	100

The optimal trajectory is shown in red in Figure 9 to Figure 12. The optimal trajectory is 1 – 5 – 7 – 2 – 6 – 6 – 6 – 6 – 6 – 6 – 6 – 6 – 6 – 6 – 6 – 6. After eliminating transitions from a state to itself, the optimal switching sequence is 1 – 5 – 7 – 2 – 6. The switching sequence corresponds to the following switching actions: open S3, open S1, close S4, close S1.

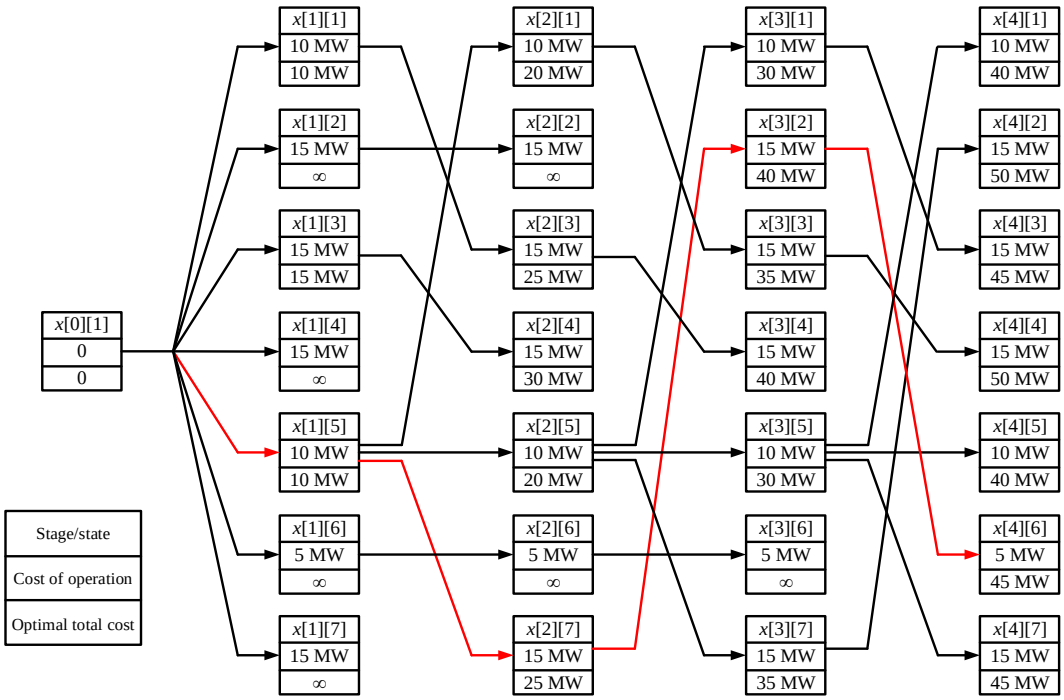

Figure 9 DP computations for the example system from stage 0 to 4 (optimal trajectory marked by red).

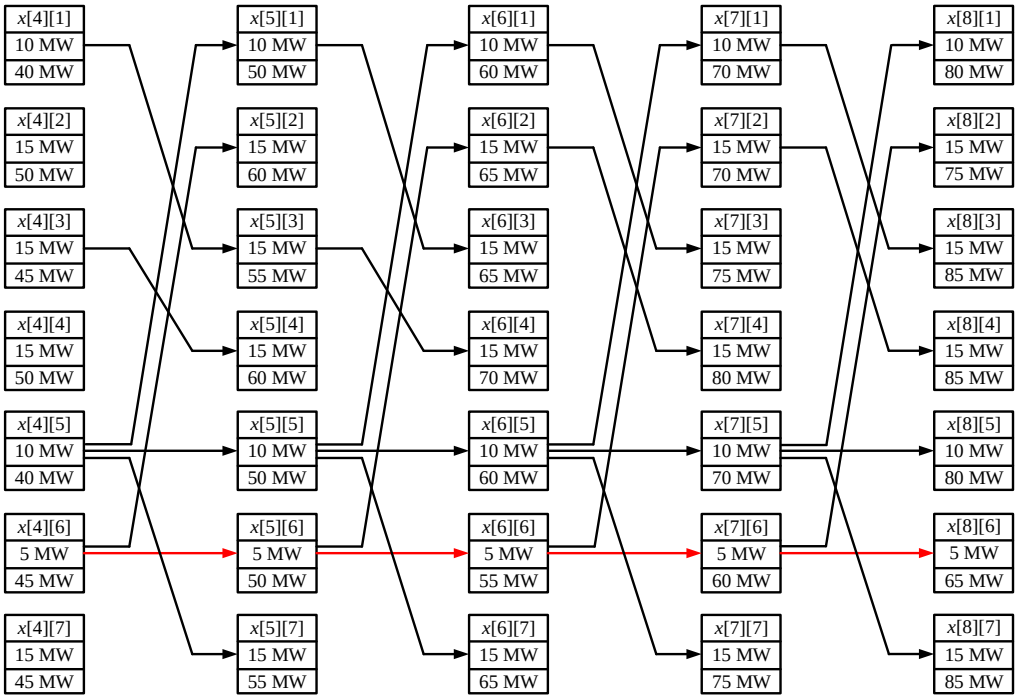

Figure 10 DP computations for the example system from stage 4 to 8 (optimal trajectory marked by red).

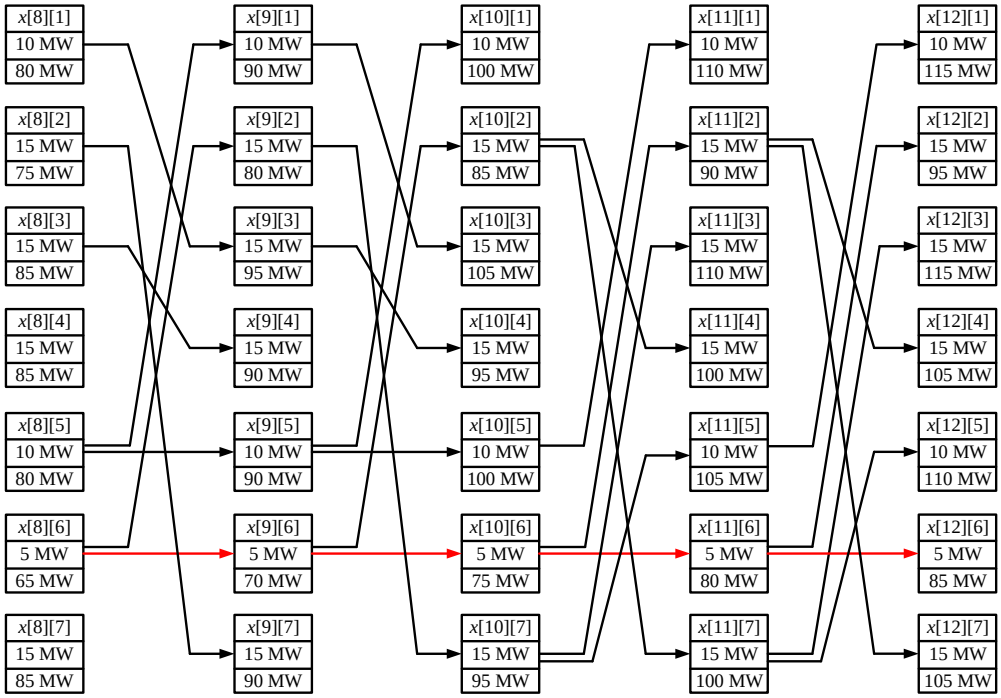

Figure 11 DP computations for the example system from stage 8 to 12 (optimal trajectory marked by red).

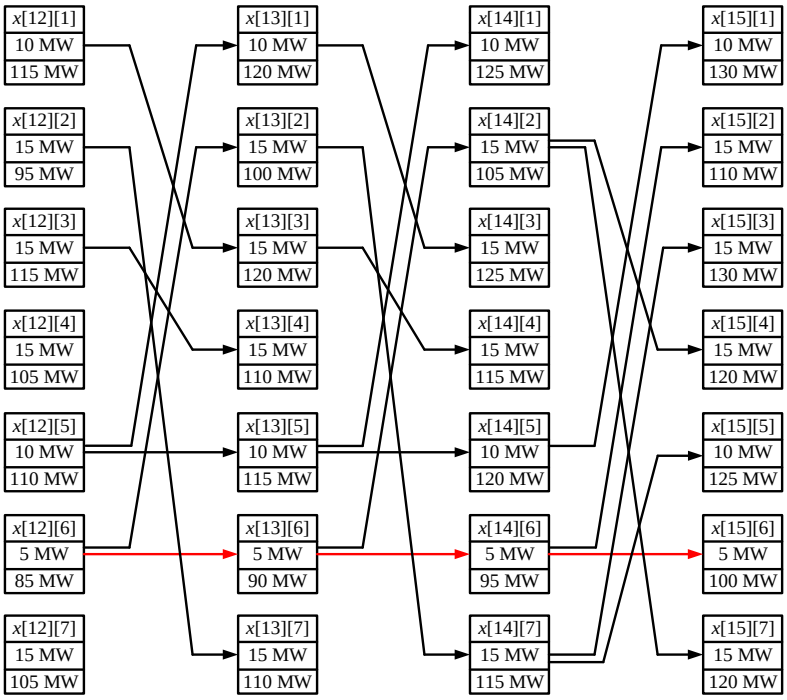

Figure 12 DP computations for the example system from stage 12 to 15 (optimal trajectory marked by red).

4.2 Test System 2

The following example is used as a second test case to evaluate and demonstrate the algorithm in a more realistic setting. The distribution system with nine buses and nine switches is shown below.

4.2.1 System Modeling

The one-line diagram of the test distribution system is shown in Figure 13. For the system, we assume the feeder head is rated 110 kV, buses 2-9 have voltage ratings of 13.8 kV and the loadings are 5 MW+j2 MVAr. The system base MVA is 100 MVA. The distribution lines have impedance 0.1524 + j0.2095 Ω between adjacent buses. Switches S1 and S9 are circuit breakers with current upper limit of 20 kA, S2 and S5 are reclosers with current upper limit of 10 kA, S3, S6, and S8 are load break switches and their current upper limits are 800 A. S4 and S7 are sectionalizers, which can only make or break at no-load, so their current upper limit is 0 A. Suppose a fault occurs between S4 and S5. In response to the fault, recloser S2 opens automatically to isolate buses 3 – 8.

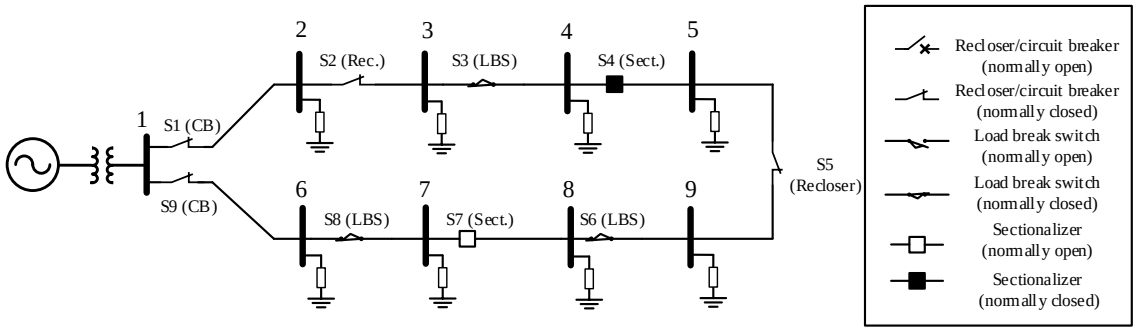

Figure 13 One-line diagram of the test distribution system with nine switches.

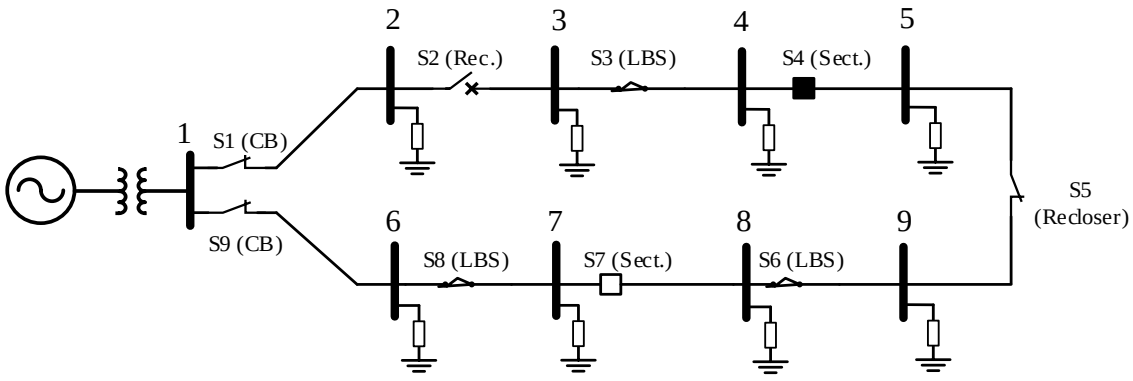

Figure 14 One-line diagram of the test distribution system when a fault occurs between S4 and S5. Recloser S2 opens automatically.

The DP-based service restoration algorithm will be initiated at this moment to restore the interrupted loads. Therefore, the control variable $u(0)$ at stage 0 is [1, 0 ,1, 1, 1, 1, 0, 1, 1]. By definition, the cost of operation and total cost in this state are both 0.

4.2.2 Initialization

In DP formulation for service restoration, the states are initialized at the beginning of the algorithm. That is, for stage i, we need to specify the control variable $u(i)$ and cost of operation Cost[i][j] for all states j. Since there are 9 switches, the total number of states at one stage is 2^9 = 512. Among the 512 states, 47 of them are not feasible. After eliminating them, the resulting DP formulation has 465 states at each stage.

4.2.3 Forward Computation and Stopping Criterion

The computation and stopping criterion are the same as those for the first example system in Section 4.1. Based on the stopping criterion, the algorithm stops at stage 15, and the optimal state is 450. Figure 15 to Figure 18 show the DP computation for states

from stage 0 to 15. Note that the algorithm does not stop until stage 15 based on the stopping criterion but the optimal state stays the same after stage 7. Table 4 below shows the optimal state at each stage and the associated optimal total cost:

Table 4 State number with minimum OptimalTotalCost and associated OptimalTotalCost for stages 1 to 15

Stage number	State number with minimum OptimalTotalCost	Minimum OptimalTotalCost (MW)
1	1, 307, 338, 353, 361	25
2	462	40
3	446, 454, 462	55
4	438, 446, 454, 462	75
5	438, 446, 454, 462	95
6	438, 446, 450, 454, 462	100
7	450	105
8	450	110
9	450	115
10	450	120
11	450	125
12	450	130
13	450	135
14	450	140
15	450	145

Particularly, the figures show the optimal trajectory in red by backtracking from the optimal state in stage 15. The optimal trajectory is 1 – 338 – 462 – 446 – 444 – 448 – 450 – 450 – 450 – 450 – 450 – 450 – 450 – 450 – 450 – 450. After eliminating the transitions from a state to itself, the optimal switching sequence is 1 – 338 – 462 – 446 – 444 – 448 – 450, which corresponds to the following switching actions: open S4, close S2, open S5, open S8, close S7, and close S8.

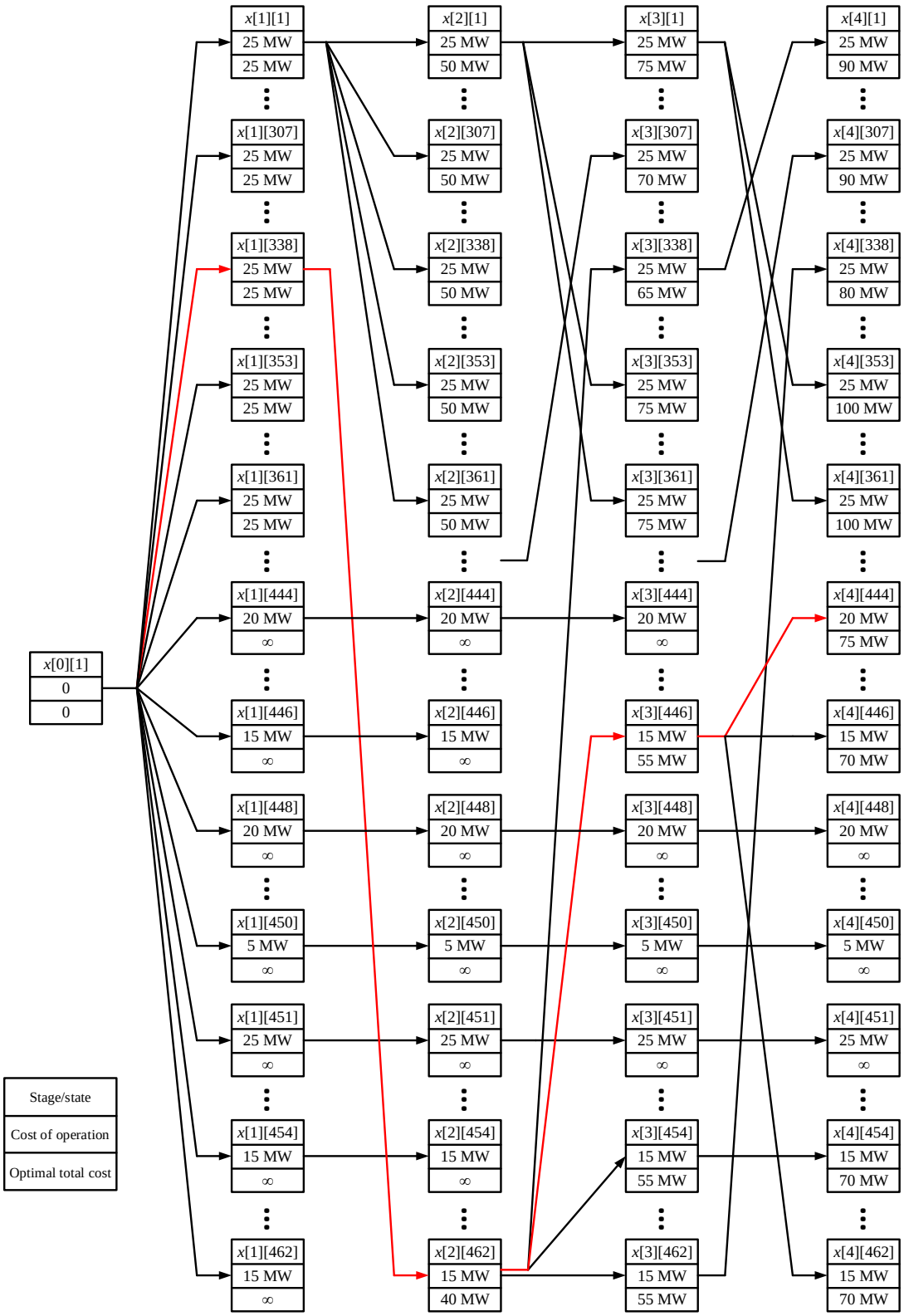

Figure 15 DP computations for the example system from stage 0 to 4 (optimal trajectory marked by red).

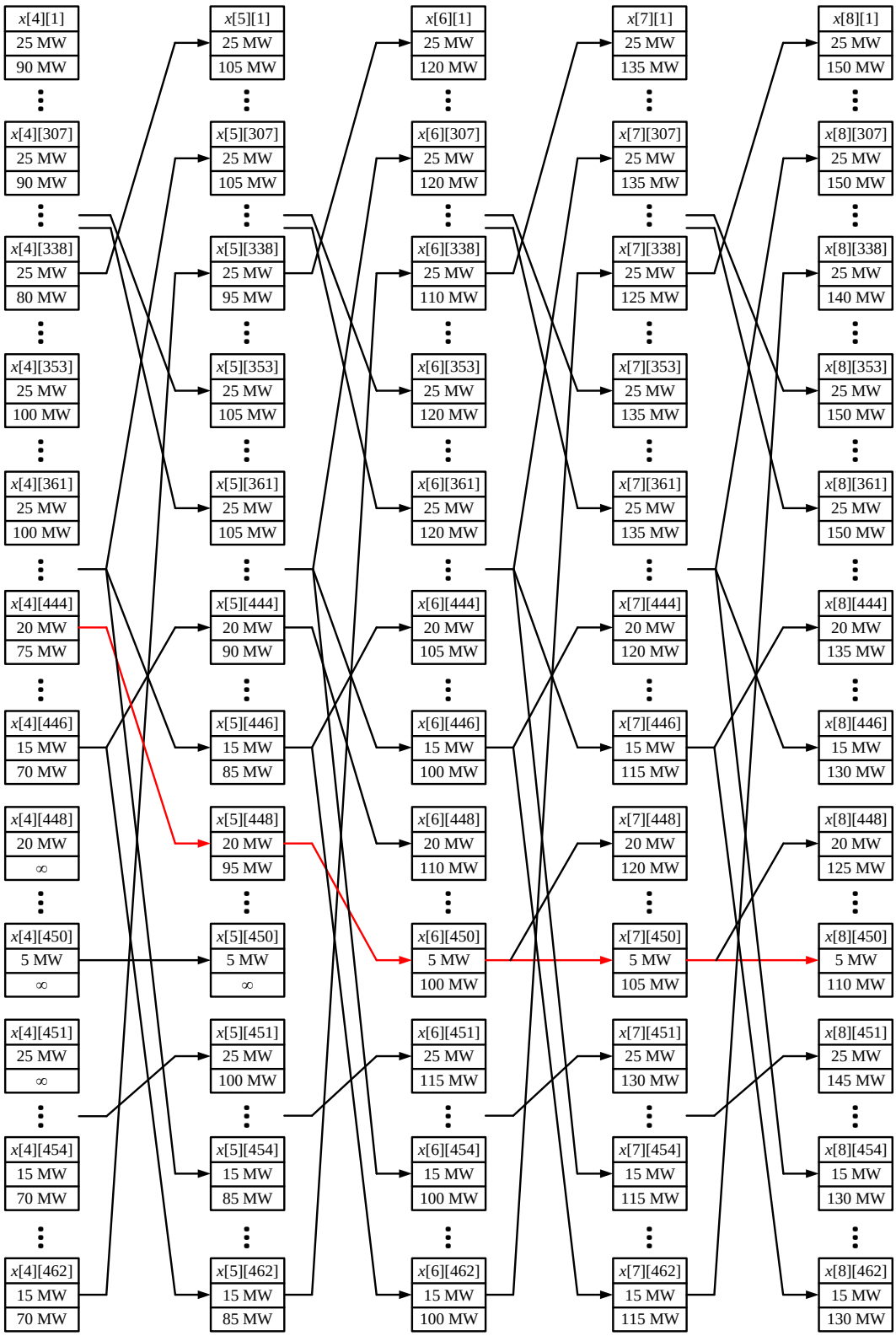

Figure 16 DP computations for the example system from stage 4 to 8 (optimal trajectory marked by red).

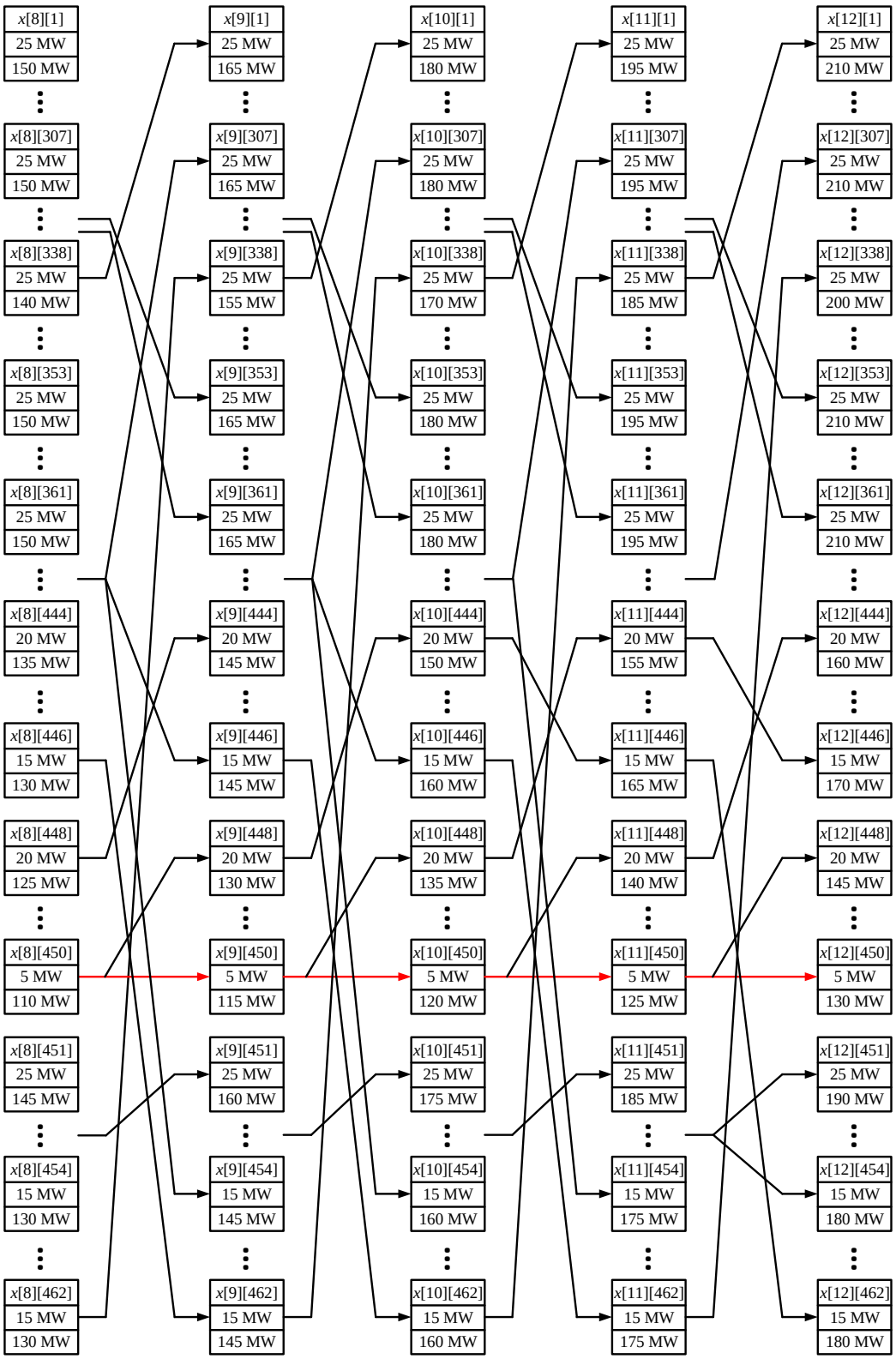

Figure 17 DP computations for the example system from stage 8 to 12 (optimal trajectory marked by red).

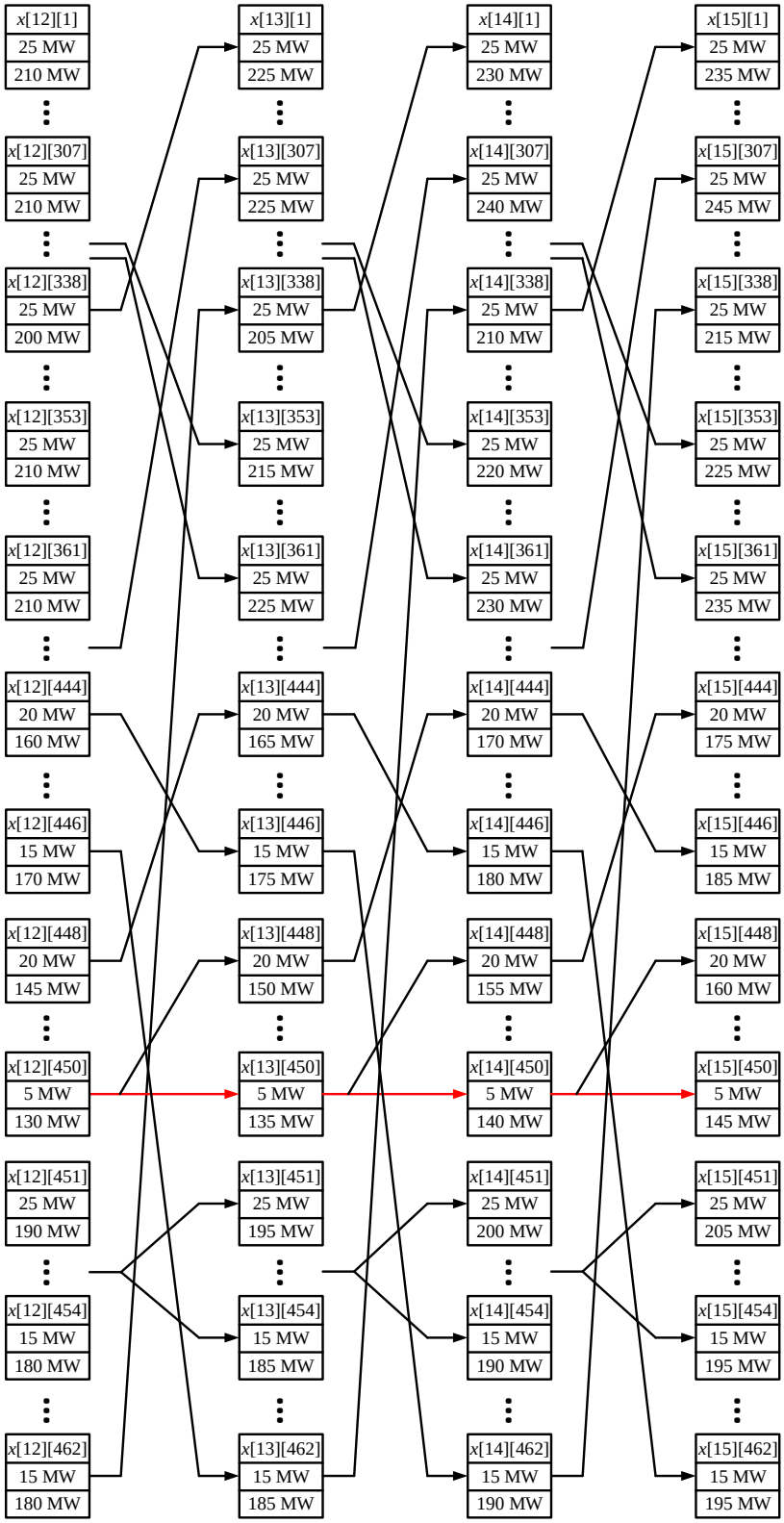

Figure 18 DP computation for the example system from stage 12 to 15 (optimal trajectory marked by red).

CHAPTER 5. SERVICE RESTORATION WITH OPERATIONAL CONSTRAINTS

It is well known that distribution systems are always operated with tight operational constraints during normal operating conditions. Many devices and end users in distribution systems are sensitive to small disturbances of nominal voltages/currents, which necessitate the tight regulation of operational constraints even during service restoration stage. The basic dynamic programming formulation for service restoration has been introduced in the last chapters where no operational constraints other than switch current upper bound are considered. As a flexible and versatile solution technique, dynamic programming lends itself to easy incorporation of operational constraints with only minor changes to the main algorithm. Specifically, the operational constraints other than switch current upper bounds will be modeled as soft constraints, the violations of which are penalized, but not forbidden. For a minimization problem, a positive weighted sum modeling different constraint violations can be added to the cost of operation to reflect the relative significance of constraints. Violation of critical constraints may incur very high marginal cost while constraints of lesser importance results in less cost increase.

In the remainder of the chapter, three operational constraints are introduced and incorporated in the dynamic programming formulation, which are bus voltage, distribution line current, and feeder capacity constraints. The effect of operational constraints incorporation will be demonstrated by an example system.

5.1 Modeling System Operational Constraints

Every bus *i* has voltage lower and upper bounds specified as

$$V_i^{\min} \le |V_i| \le V_i^{\max}. \tag{12}$$

Every line section between bus *i* and *j* has upper bound on current magnitude specified as

$$| I_{ij} | \le I_{ij}^{\max} \tag{13}$$

To account for operational constraints, two penalty terms are added to every state's cost of operation which capture the severities of voltage magnitude and line flow constraint violation, respectively. To ensure consistency, the units of unserved load real power, voltage magnitude and line current magnitude are all converted to per unit such that the physical interpretation is valid. The penalty terms for bus voltage and line current constraint violations are defined as:

$$h_1^i = \begin{cases} \alpha\left(V_i^{\min} - |V_i|\right), & |V_i| < V_i^{\min} \\ 0, & V_i^{\min} \le |V_i| \le V_i^{\max} \\ \alpha\left(|V_i| - V_i^{\max}\right), & |V_i| > V_i^{\max} \end{cases} \tag{14}$$

and

$$h_2^{ij} = \begin{cases} 0, & |I_{ij}| \le I_{ij}^{\max} \\ \beta\left(|I_{ij}| - I_{ij}^{\max}\right), & |I_{ij}| > I_{ij}^{\max} \end{cases} \tag{15}$$

These piecewise linear penalty functions are shown pictorially in Figure 19 and Figure 20.

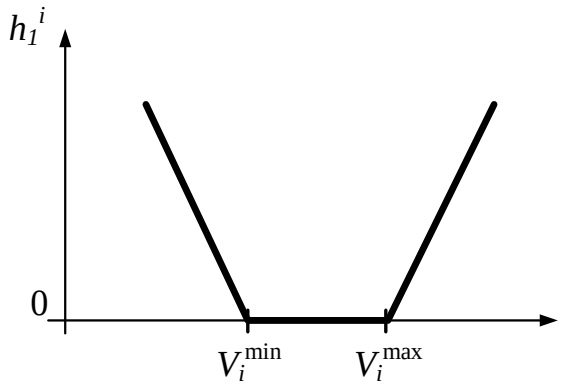

Figure 19 Piecewise linear penalty function for bus voltage magnitude constraint

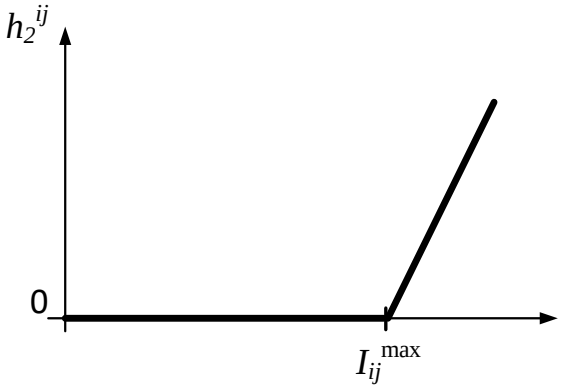

Figure 20 Piecewise linear penalty function for line current magnitude constraint

The penalty terms are then added to the cost of operation in Equation (4), which becomes

$$\text{Cost}[k+1][i] = \begin{cases} U(x[k+1][i]) + \sum_{i \in B} h_1^i + \sum_{(i,j) \in E} h_2^{ij}, & \text{State } i \text{ is feasible} \\ \infty, & \text{Otherwise} \end{cases} \quad (16)$$

where B and E are the set of buses and line sections, respectively, U is the total real power of unserved loads, and all quantities are in per unit.

Other relevant constraints can be considered in this way as well, such as radiality constraint.

5.2 Example

The following example is used as a test case to demonstrate the effect of incorporating soft operational constraints in deriving optimal switching sequence for service restoration. The test distribution system with three feeders, fourteen buses, and twelve switches is shown below. In the first computational experiment, no operational constraints are imposed. The constraints are subsequently imposed in Section 5.2.4 and the DP algorithm is executed again, and the comparison between the two cases are made.

5.2.1 System Modeling

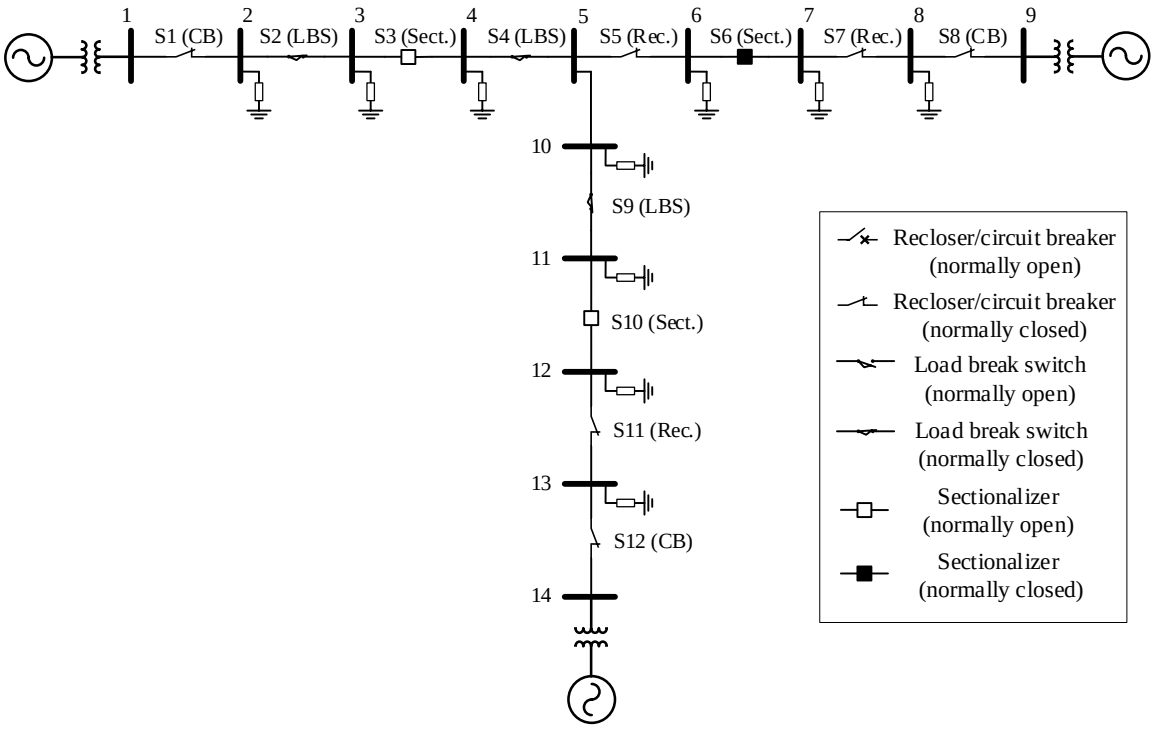

Figure 21 One-line diagram of the 14-bus distribution system with twelve switches.

The one-line diagram of the test distribution system is shown in Figure 21. For the system, we assume the feeder heads are rated 110 kV, buses 1-14 have voltage ratings of 13.8 kV. Buses 2 – 4, 6 – 8, and 10 – 14 are load buses where buses 2, 3, 7, 8, 12, and 13 have loading of 5 MW + j2 MVAr and buses 4, 6, 10, and 11 have loading of 3 MW +

j1MVAr. The system base power is 100 MVA. The distribution lines have impedance 0.1524 + j0.2095 Ω between adjacent buses. Switches S1, S8, and S12 are circuit breakers with current upper limit of 20 kA, S5, S7, and S11 are reclosers with current upper limit of 10 kA, S2, S4, and S9 are load break switches and their current upper limits are 800 A. S3, S6, and S10 are sectionalizers, which can only make or break at no-load, so their current upper limit is 0 A. Suppose a fault occurs between S5 and S6. In response to the fault, recloser S7 opens automatically, which interrupts services to load buses 4 – 7, 10, and 11 (shown in Figure 22 enclosed by red dashed lines).

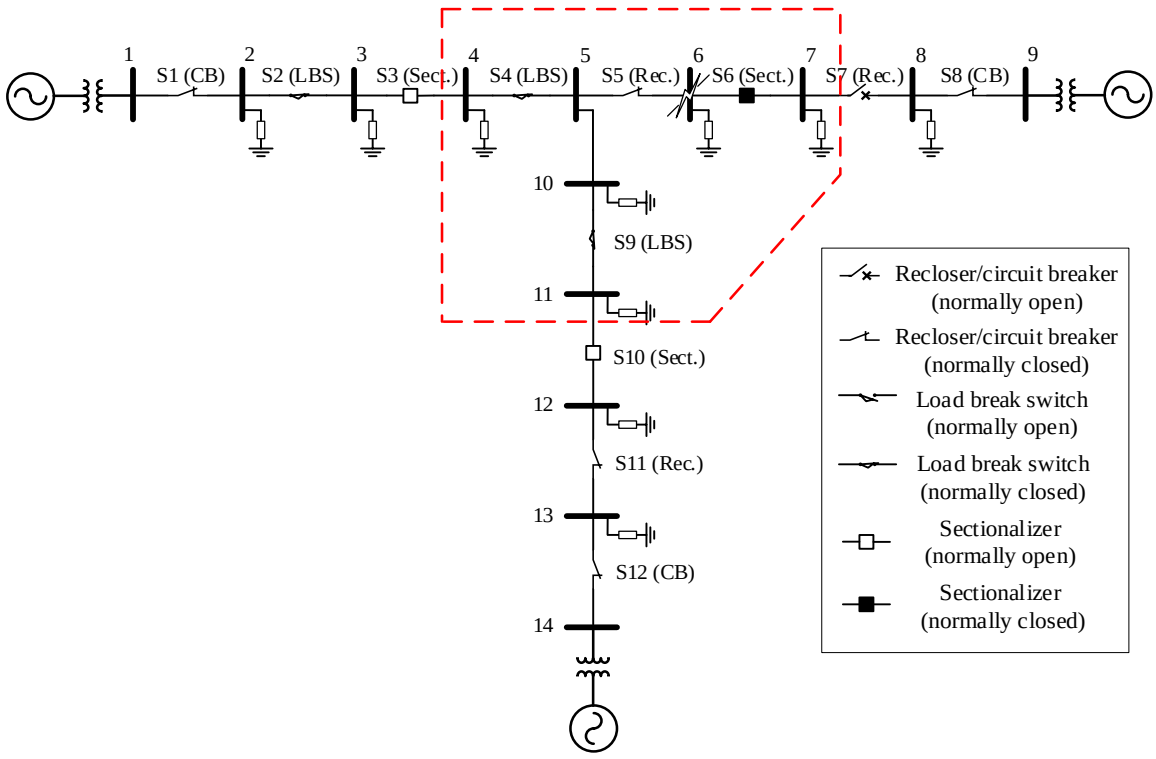

Figure 22 The 14-bus test system after a fault occurs between S5 and S6 (isolated region enclosed by red dashed lines).

The DP-based service restoration algorithm will be initiated at this moment to restore the interrupted loads. Therefore, the control variable $u(0)$ at stage 0 is [1, 1, 0, 1,

1, 1, 0, 1, 1, 0, 1, 1]. By definition, the cost of operation and total cost in this state are both 0.

5.2.2 Initialization

In DP formulation for service restoration, the states are initialized at the beginning of the algorithm. That is, for stage *i*, we need to specify the control variable *u*(*i*) and cost of operation Cost[*i*][*j*] for all states *j*. Since there are 12 switches, the total number of states at one stage is 2^{12} = 4096. Among the 4096 states, 729 of them are not feasible. After eliminating them, the resulting DP formulation has 3367 states at each stage.

Table 5 State number with minimum OptimalTotalCost and associated OptimalTotalCost for stages 1 to 15

Stage number	State number with minimum OptimalTotalCost	Minimum OptimalTotalCost (pu)
1	1, 2803, 2913, 2960, 3012	0.15
2	2990	0.27
3	2773, 2881, 2982, 2990	0.39
4	2664, 2765, 2773, 2873, 2881, 2982, 2990	0.51
5	2656, 2664, 2765, 2773, 2873, 2881, 2982, 2990	0.63
6	2885, 3315	0.70
7	2885, 3315	0.73
8	2885, 3315	0.76
9	2885, 3315	0.79
10	2885, 3315	0.82
11	2885, 3315	0.85
12	2885, 3315	0.88
13	2885, 3315	0.91
14	2885, 3315	0.94
15	2885, 3315	0.97

5.2.3 Forward Computation and Stopping Criterion

The stopping criterion is that the optimal state does not change for 10 stages. Based on the stopping criterion, the algorithm stops at stage 15, and the optimal states are 2885 and 3315. Figure 25 to Figure 28 show the DP computation for states from stage 0 to 15. Note that the algorithm does not stop until stage 15 based on the stopping criterion but the optimal states stay the same after stage 6. Table 5 shows the optimal states at each stage and the associated optimal total cost:

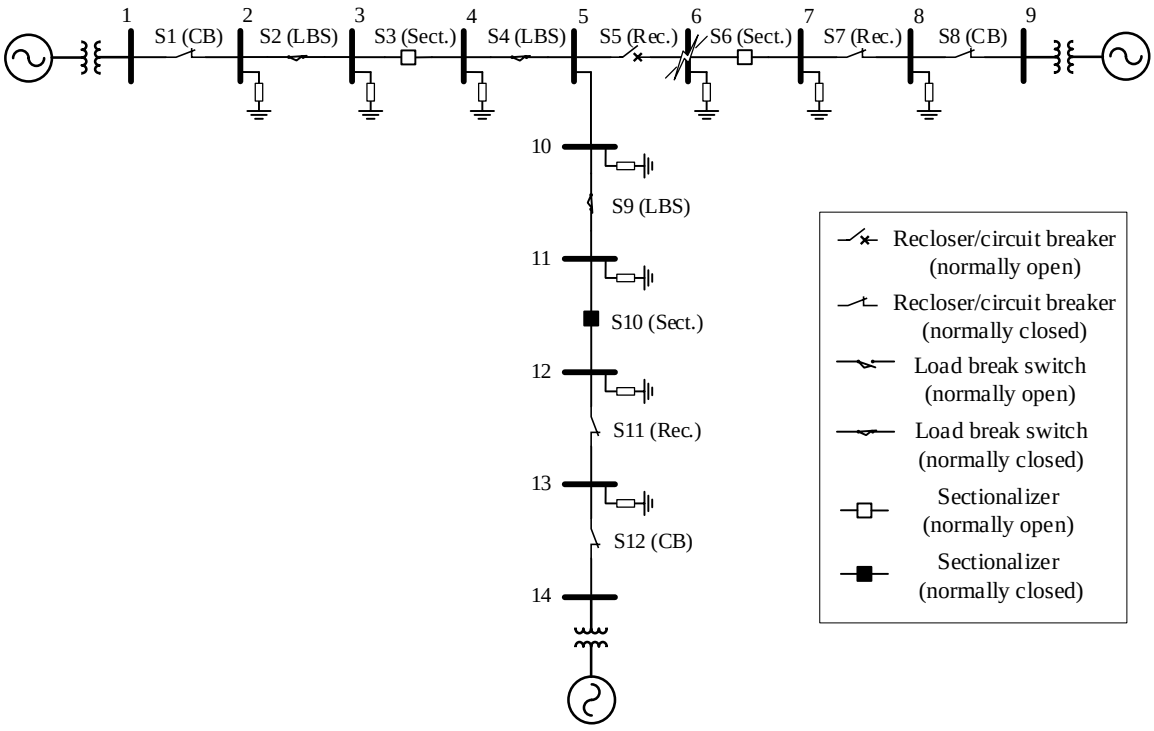

Figure 23 Optimal final topology of the 14-bus system.

Particularly, Figure 25 to Figure 28 show the optimal trajectory in red by backtracking from the optimal state 2885 in stage 15. The optimal trajectory is 1 – 2913 – 2911 – 2915 – 2917 – 2853 – 2885 – 2885 – 2885 – 2885 – 2885 – 2885 – 2885 – 2885 – 2885. After eliminating the transitions from a state to itself, the optimal switching sequence is 1-2913-2911-2915-2917-2853-2885, which corresponds to the following

switching operations: open S5, open S11, close S10, close S11, open S6, and close S7. These switching operations accomplish the following tasks: 1) isolate the faulted bus by opening S5 and S6; 2) restore loads at buses 4, 10, and 11 through the third feeder originating at bus 14 by closing S10; 3) restore load at bus 7 through the second feeder originating at bus 9 by closing S7. The final topology is shown in Figure 23. It is seen from Table 5 that there is an alternative optimal final topology (state 3315). The alternative topology is shown in Figure 24:

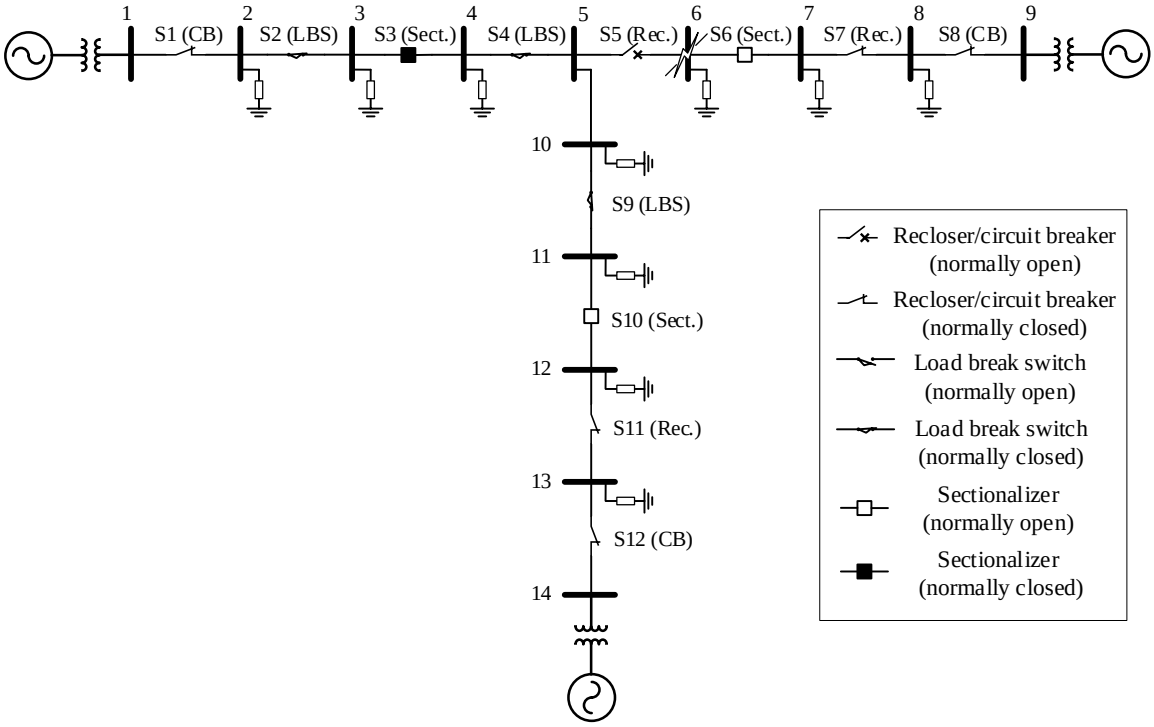

Figure 24 Alternative optimal final topology of the 14-bus system.

The only difference between the optimal topology in Figure 24 and the one in Figure 23 is that S3 is closed instead of S10 so that the isolated section is transferred to the left feeder originating at bus 1 instead of the bottom one originating at bus 14.

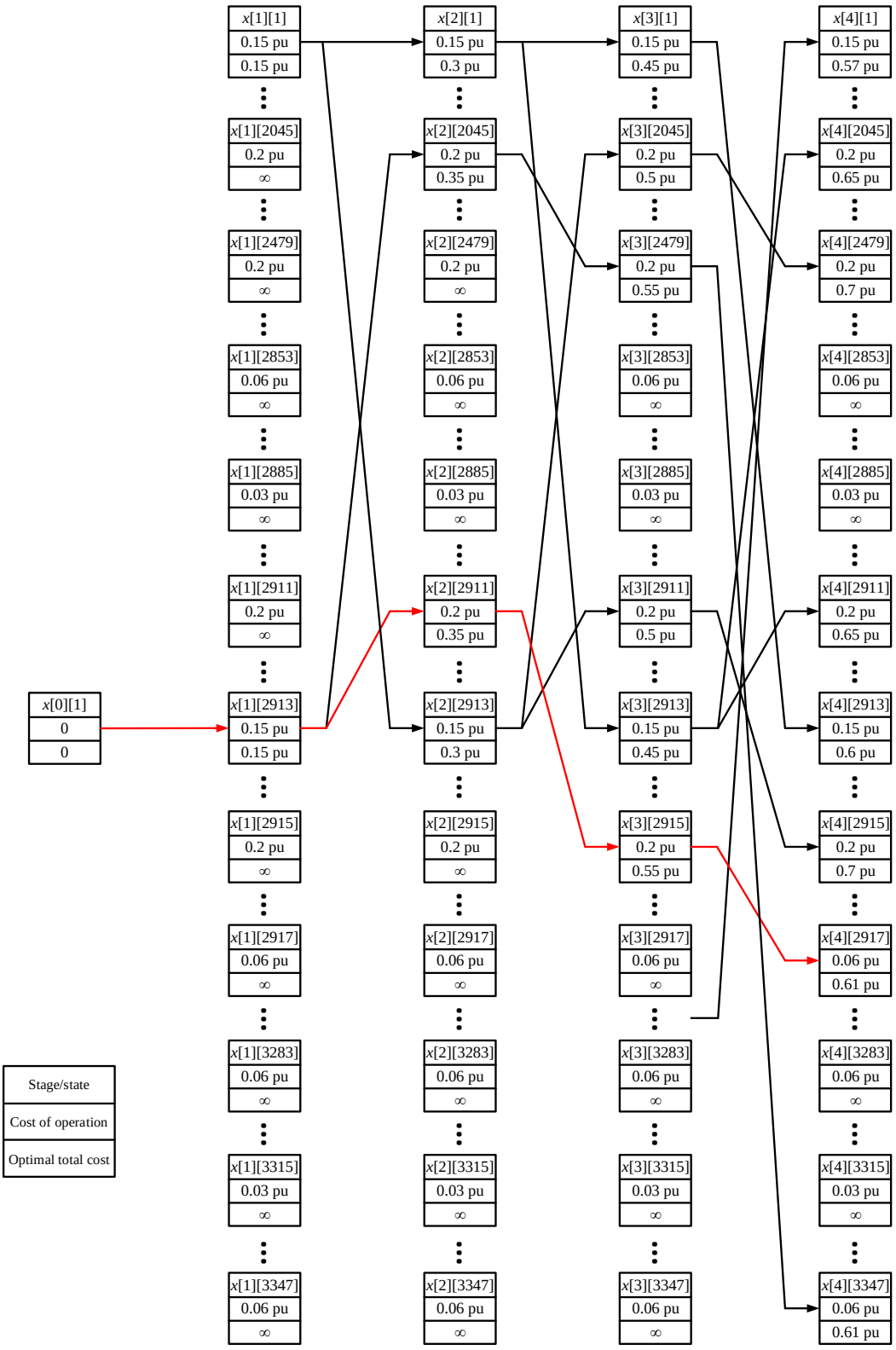

Figure 25 DP computations for the example system from stage 0 to 4 (optimal trajectory marked by red).

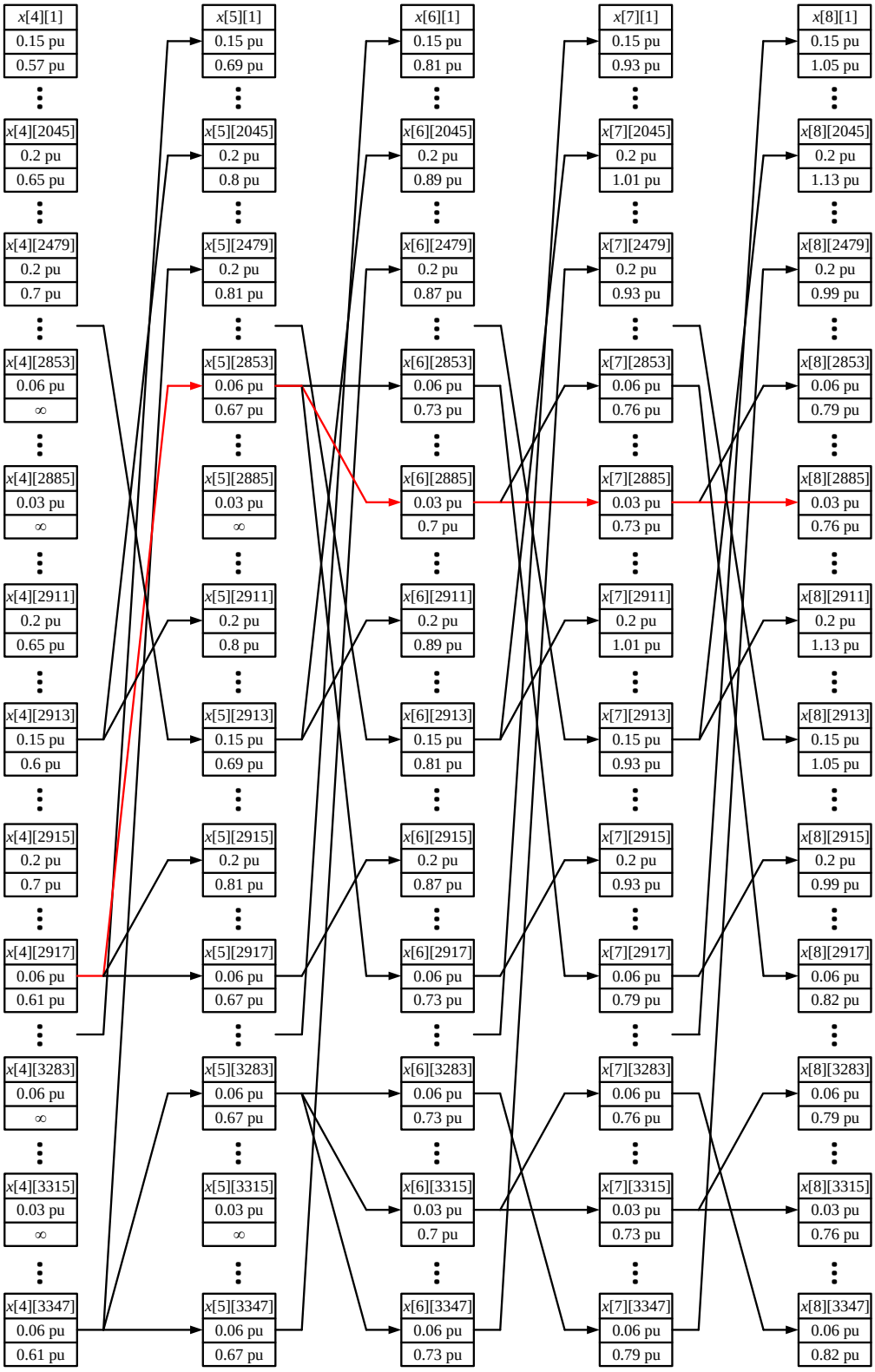

Figure 26 DP computations for the example system from stage 4 to 8 (optimal trajectory marked by red).

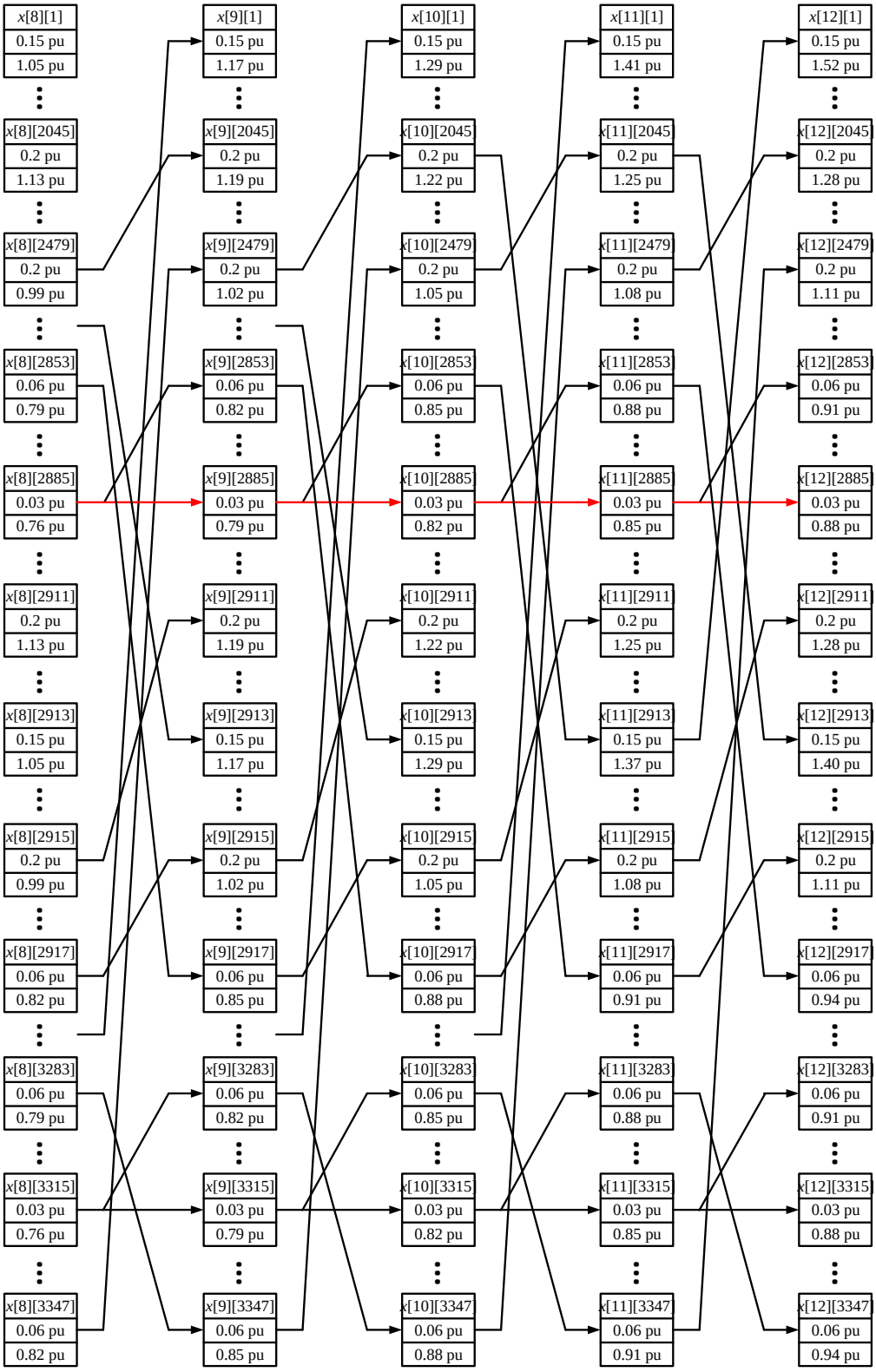

Figure 27 DP computations for the example system from stage 8 to 12 (optimal trajectory marked by red).

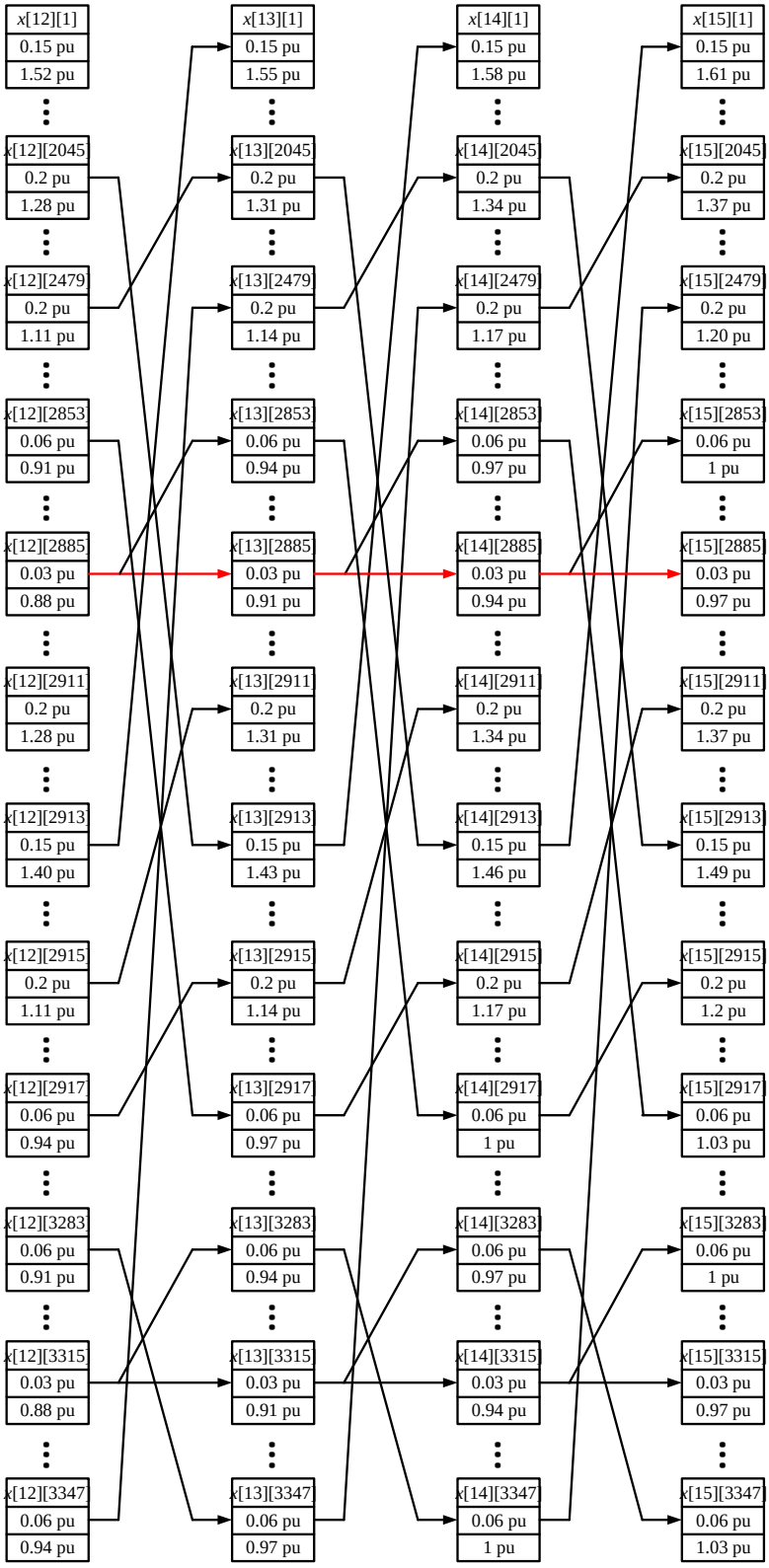

Figure 28 DP computations for the example system from stage 12 to 15 (optimal trajectory marked by red).

5.2.4 Imposing Operational Constraints

When operational constraints are present, the optimal switching sequence as well as the optimal final topology may be different. For the specific test system, we now impose the following constraints: 1) **voltage magnitude constraint**: for every bus, the voltage magnitude should be between 0.95 and 1.05 pu; 2) **line flow constraints**: line sections between buses (12, 13) and (13, 14) have capacity of 0.1673 pu (700 A) and all other line sections have capacity of 0.2390 pu (1 kA). With these constraints, we examine the optimal final topology obtained above. The power flow result of the topology is tabulated in Table 6:

Table 6 Power flow result of optimal final topology for 14-bus system without operational constraints (constraint violations marked by red-colored font)

Bus voltage magnitude		Line flow		
Bus No.	Voltage mag. (pu)	'From' bus	'To' bus	Current mag. (pu)
1	1	1	2	0.1094
2	0.9874	2	3	0.0549
3	0.9810	3	4	—
4	0.9315	4	5	0.0339
5	0.9352	5	6	—
6	—	6	7	—
7	0.9894	7	8	0.0320
8	0.9929	8	9	0.0638
9	1	5	10	0.0339
10	0.9390	10	11	0.0676
11	0.9465	11	12	0.1010
12	0.9578	12	13	0.1572
13	0.9756	13	14	0.2124
14	1			

It can be seen from Table 6 that the topology induces both voltage magnitude and line flow constraint violations. To account for these constraints, we impose the following penalty term for each constraint violation to the state's cost of operation:

$$\text{penalty} = \begin{cases} 10 \mid v_{\text{actual}} - v_{\text{critical}} \mid, & \text{if } v_{\text{actual}} \text{ violates the constraint} \\ 0, & \text{otherwise} \end{cases} \quad (17)$$

where v can be either bus voltage magnitude or line current magnitude, and the subscripts 'actual' and 'critical' refer to the actual and critical (minimum or maximum bus voltage magnitude, or maximum line current magnitude) per unit values, respectively. It is expected after imposing operational constraints, the DP algorithm may converge to an alternative topology which complies better with the constraints through different switching operations.

It can be inferred from Figure 22 that such topology does exist. Instead of transferring all interrupted loads (loads on buses 4, 10, and 11) to a single feeder, the loads can be distributed between both feeders originating at bus 1 and bus 14, thus alleviating system stress.

5.2.5 Computation Results

The DP algorithm is rerun with the penalty term in Equation (17) incorporated in the cost of operation. The stopping criterion is the same as the last one without considering operational constraints (optimal state doesn't change for 10 stages). Based on the stopping criterion, the algorithm stops at stage 22, and the optimal states are 2885 and 3315. Figure 25 to Figure 28 show the DP computation for states from stage 0 to 15. Note that the algorithm does not stop until stage 15 based on the stopping criterion but the optimal states stay the same after stage 6. Table 7 below shows the optimal states at each stage and the associated optimal total cost:

Table 7 State number with minimum OptimalTotalCost and associated OptimalTotalCost for stages 1 to 22

Stage number	State number with minimum OptimalTotalCost	Minimum OptimalTotalCost (pu)
1	1, 2803, 2913, 2960, 3012	0.15
2	2990	0.27
3	2773, 2881, 2982, 2990	0.39
4	2664, 2765, 2773, 2873, 2881, 2982, 2990	0.51
5	2656, 2664, 2765, 2773, 2873, 2881, 2982, 2990	0.63
6	2656, 2664, 2765, 2773, 2873, 2881, 2982, 2990	0.75
7	2656, 2664, 2765, 2773, 2873, 2881, 2982, 2990	0.87
8	3307	0.97
9	3307	1.03
10	3307	1.09
11	3307	1.15
12	3307	1.21
13	3311, 3319	1.25
14	3311, 3319	1.28
15	3311, 3319	1.31
16	3311, 3319	1.34
17	3311, 3319	1.37
18	3311, 3319	1.40
19	3311, 3319	1.43
20	3311, 3319	1.46
21	3311, 3319	1.49
22	3311, 3319	1.52

In particular, Figure 30 to Figure 35 show the optimal trajectory in red by backtracking from the optimal state 3311 in stage 22. The optimal trajectory is 1 – 2960 – 2990 – 2881 – 2873 – 2005 – 2439 – 3307 – 3305 – 3309 – 3311 – 3311 – 3311 – 3311 – 3311 – 3311 – 3311 – 3311 – 3311 – 3311 – 3311. After eliminating the transitions from a state to itself, the optimal switching sequence is 1 – 2960 – 2990 – 2881 – 2873 – 2005 – 2439 – 3307 – 3305 – 3309 – 3311, which corresponds to the following switching operations: open S6, close S7, open S5, open S9, open S2, close S3,

close S2, open S11, close S10, and close S11. These switching operations accomplish the following five tasks: 1) isolate the faulted bus by opening S5 and S6; 2) divide the isolated section into two parts by opening S9; 3) restore loads at buses 4 and 10 through the first feeder originating at bus 1 by closing S3; 4) restore load at bus 7 through the second feeder originating at bus 9 by closing S7; 5) restore load at bus 11 through the third feeder originating at bus 14 by closing S10. The final topology is shown in Figure 23.

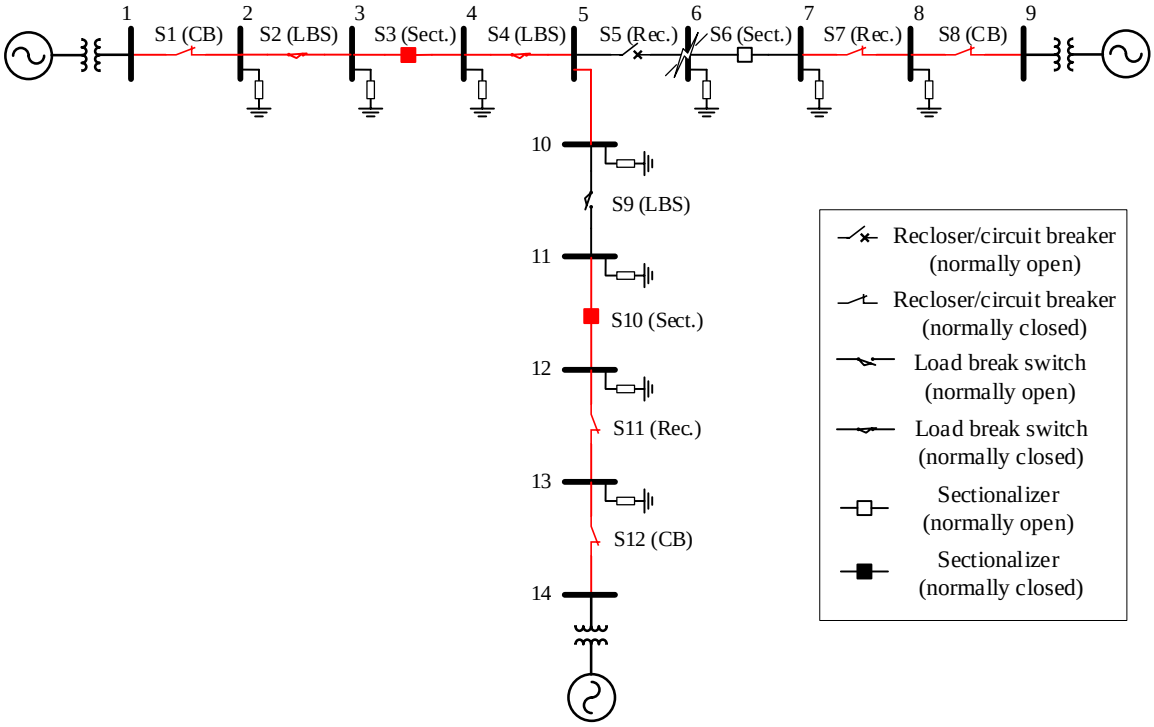

Figure 29 Optimal final topology of the 14-bus system considering operational constraints (feeders marked by red lines).

It is seen from Figure 29 that instead of transferring all transferrable loads in the isolated section to one feeder through less switching operations, a different set of switching actions with slightly more operations is devised due to the imposed constraints which distribute loads in the isolated region to two distinct feeders, which alleviates the

system stress. To verify this, we present the power flow results for the optimal final topology in Table 8:

Table 8 Power flow result of optimal final topology for 14-bus system with operational constraints

Bus voltage magnitude		Line flow		
Bus No.	Voltage mag. (pu)	'From' bus	'To' bus	Current mag. (pu)
1	1	1	2	0.1769
2	0.9797	2	3	0.1220
3	0.9659	3	4	0.0662
4	0.9585	4	5	0.0332
5	0.9548	5	6	—
6	—	6	7	—
7	0.9894	7	8	0.0320
8	0.9929	8	9	0.0638
9	1	5	10	0.0332
10	0.9511	10	11	—
11	0.9700	11	12	0.0326
12	0.9736	12	13	0.0879
13	0.9836	13	14	0.1426
14	1			

It can be readily verified that no constraints are violated for this topology. Another observation is that more switching operations are performed compared with the one without operational constraints in Section 5.2.3. As a result, the OptimalTotalCost is higher when the optimal topology is first reached (1.16 compared to 0.7 without operational constraints). However, it should be noted that the lower optimal cost obtained by ignoring operational constraints comes at a price of constraint violation, which has adverse effect on system operation.

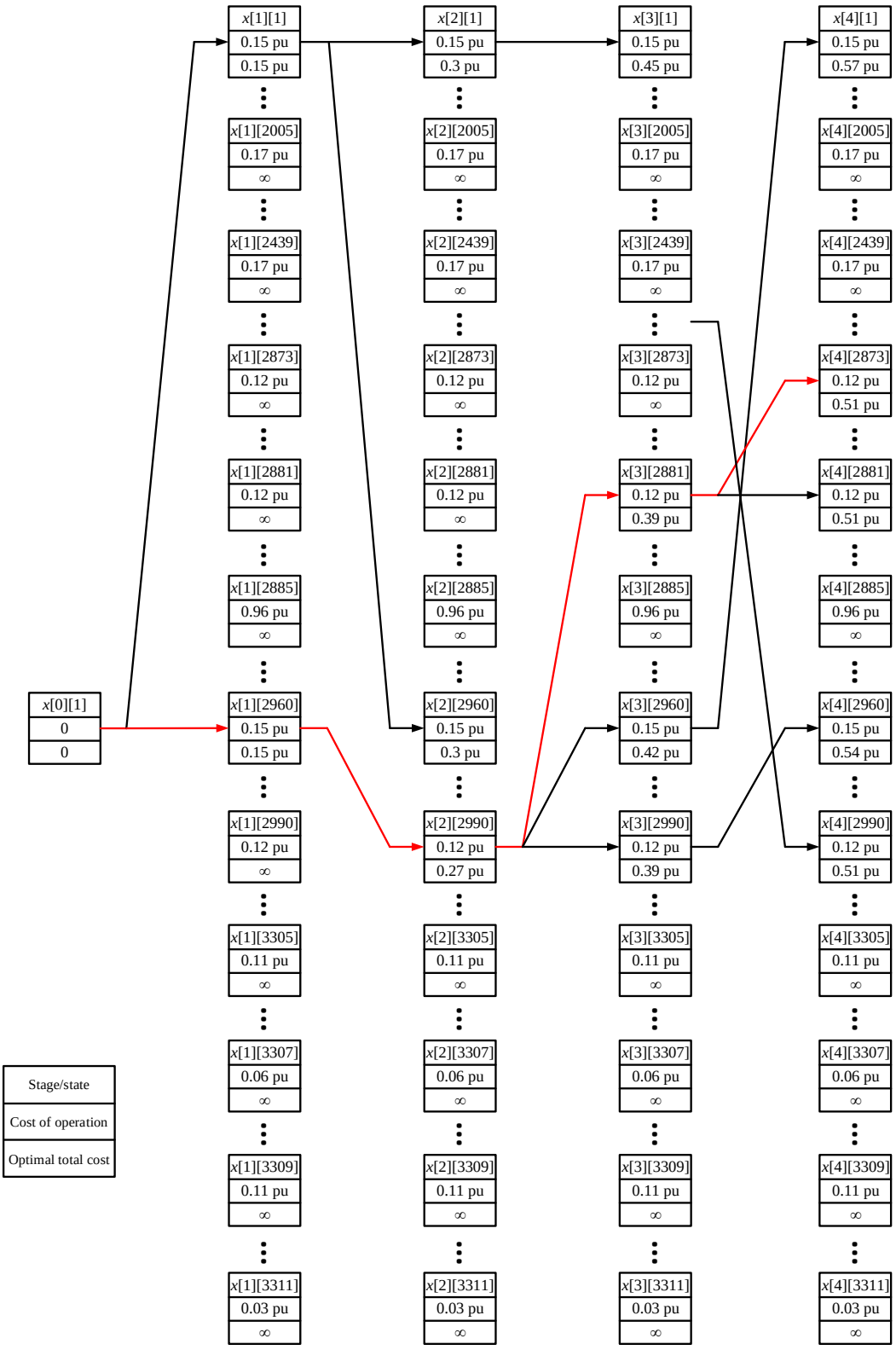

Figure 30 DP computation for the example system from stage 0 to 4 (optimal trajectory marked by red).

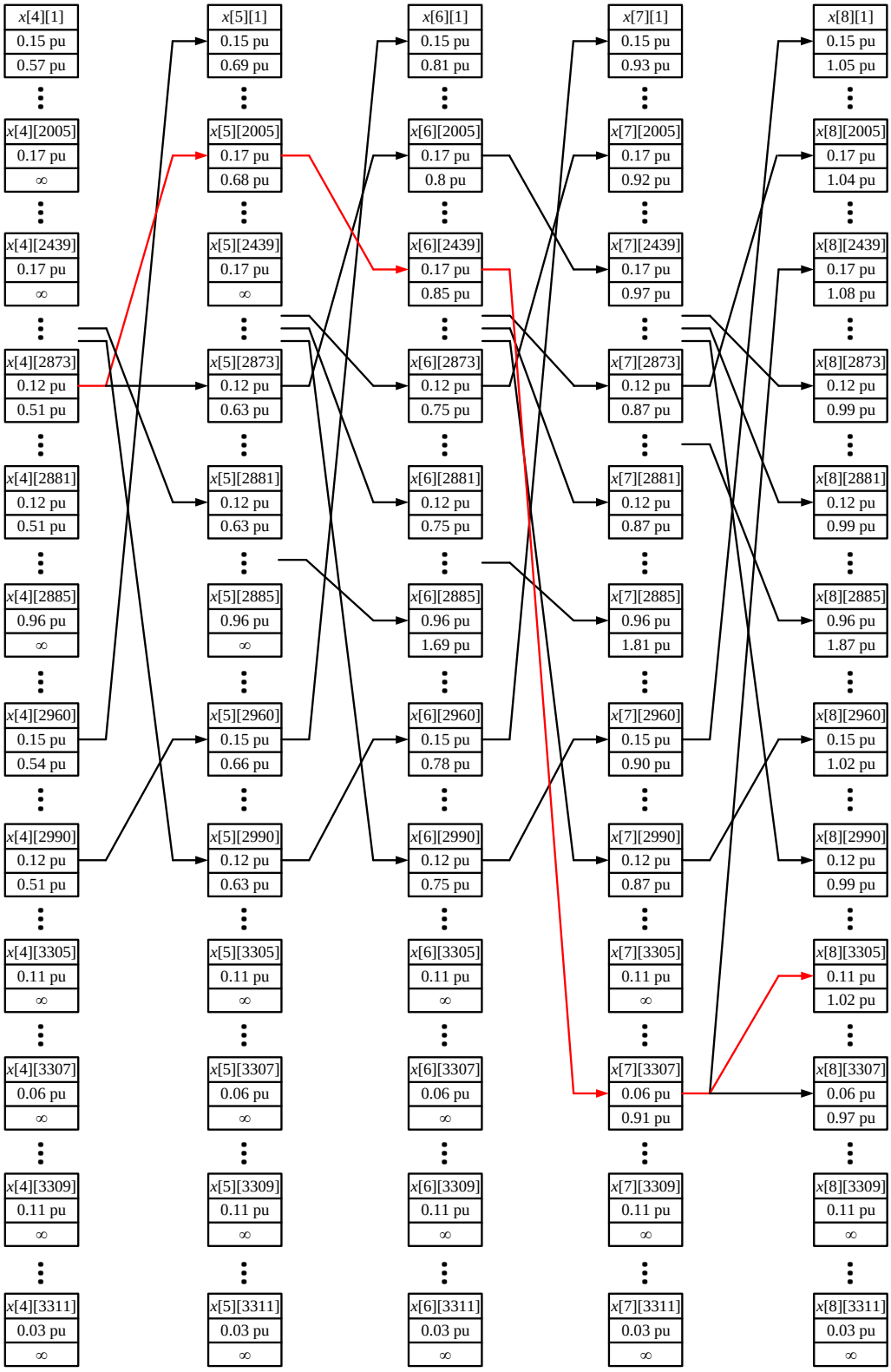

Figure 31 DP computation for the example system from stage 4 to 8 (optimal trajectory marked by red).

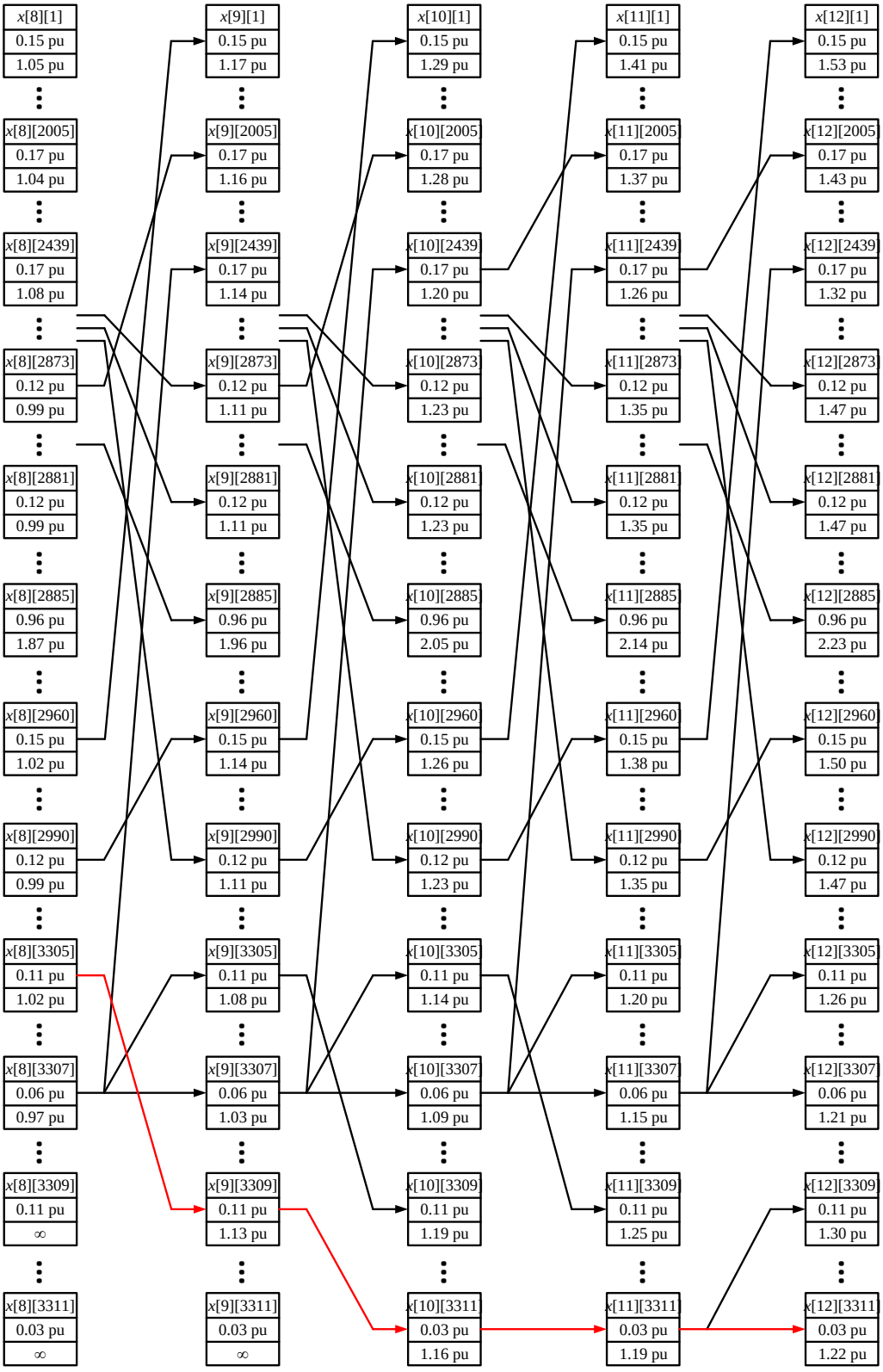

Figure 32 DP computation for the example system from stage 8 to 12 (optimal trajectory marked by red).

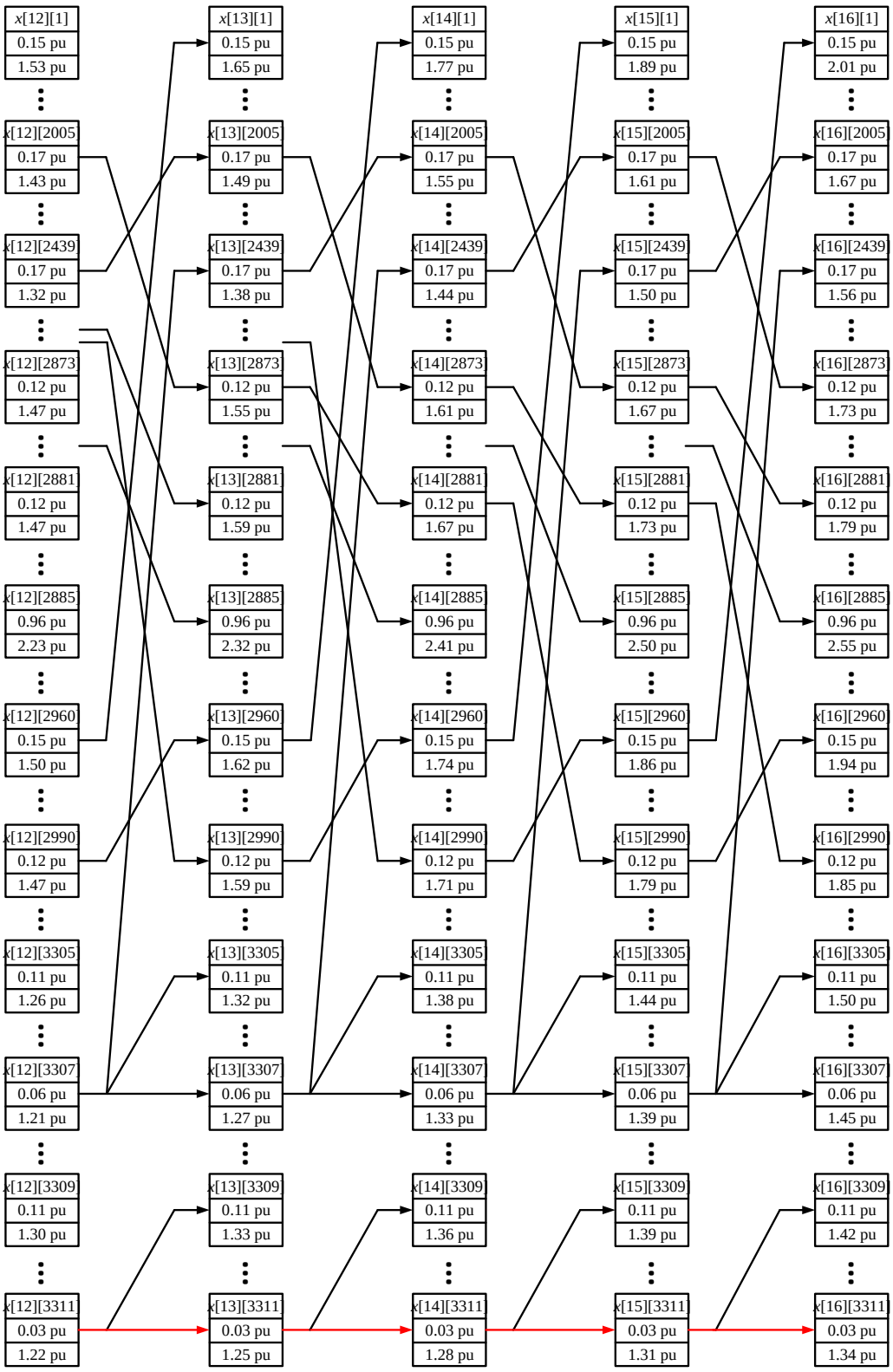

Figure 33 DP computation for the example system from stage 12 to 16 (optimal trajectory marked by red).

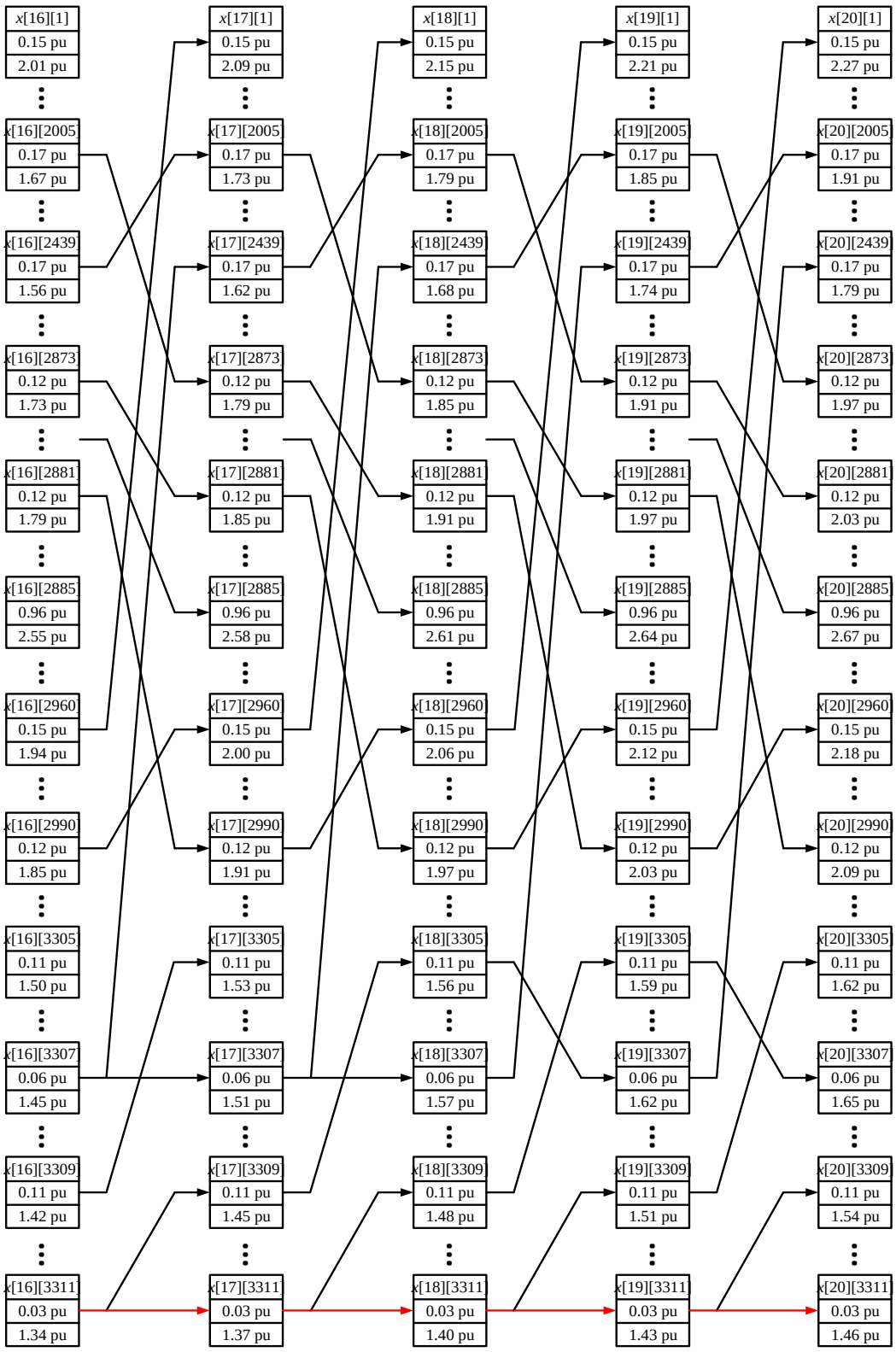

Figure 34 DP computation for the example system from stage 16 to 20 (optimal trajectory marked by red).

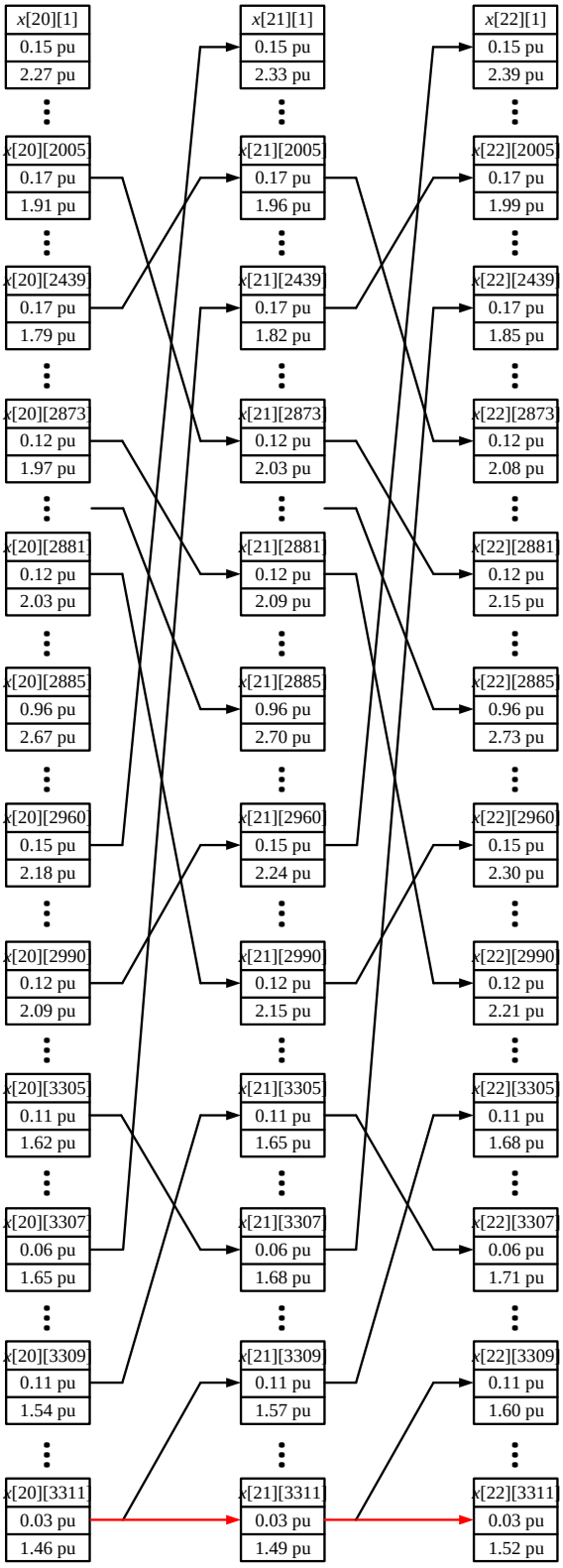

Figure 35 DP computation for the example system from stage 20 to 22 (optimal trajectory marked by red).

CHAPTER 6. DISTRIBUTION SYSTEM STATE ESTIMATION BY SWITCH MEASUREMENTS

6.1 Introduction

State estimation is the method to determine system state variables based on system measurements. The resulting state variables estimated by the method can then be used to determine system parameters such as system loading conditions and power flow, which is essential for system operations such as network reconfiguration. For our problem, the state variables are the voltage magnitudes and angles at all but the reference bus. For distribution systems considered in the project, the measurements are taken from switches installed on distribution lines. These switches are capable of measuring voltage magnitude, line current magnitude, as well as line power factor. Of the three measurements, line current magnitude can be measured with high accuracy while the accuracies of voltage magnitude and line power factor measurements are lower. Instead of directly formulating the system equations using voltage, current, and power factor measurements, we use line power flow which can be calculated from the measurements due to numerical issues with current and angle measurements [62]. In this chapter, we discuss how to cast the state estimation problem using weighted least square formulation and then solve it using Newton-Raphson method. The output data of the state estimation algorithm are the best estimate of state variables in the weighted least square fashion, recognizing that the imperfection comes from errors in the measured quantities.

6.2 System Modeling

We consider a radial distribution feeder with $n+1$ buses where buses 1 to n are load buses and bus 0 is the slack bus representing the busbar located in the substation with regulated voltage magnitude and reference phase angle. Since the feeder is radial, there are n line sections between buses. Suppose there is a switch installed at the midpoint of every line section and these switches have measurement capabilities to measure voltage magnitude, current magnitude, and the power factor of line power flow. The switches can be regarded as virtual load buses with zero load consumption and we number these buses from $n+1$ to $2n$. For ease of exposition, we establish the one-to-one correspondence between the switch number and endpoints of line section as follows: by assuming all actual load buses have positive load demand, the direction of a line section can be determined by the direction of the power flow. The receiving end of a line section defined this way is unique for a radial network. We number the virtual load bus of the switch on line section (i,k) by $n+k$. This number convention is illustrated in the one-line diagram in Figure 36 below:

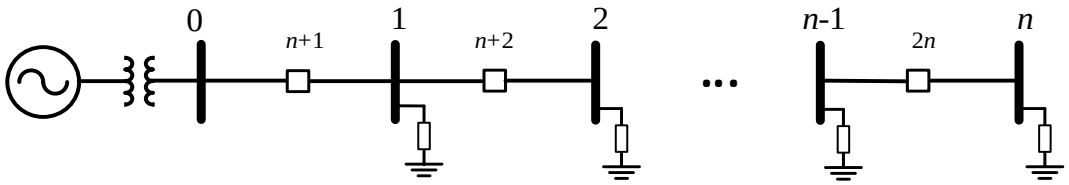

Figure 36 Illustration of virtual load bus numbering.

Every switch $n+k$ provides three measurements: voltage magnitude V_{n+k}, current magnitude $I_{n+k,k}$, and power factor $\mathrm{pf}_{n+k,k}$. Based on these measurements, the real and reactive power flow from bus $n+k$ to bus k at the sending end (bus $n+k$) can be calculated:

$$
\begin{aligned}
P_{n+k,k} &= V_{n+k} I_{n+k,k} \mathrm{pf}_{n+k,k}, \\
Q_{n+k,k} &= V_{n+k} I_{n+k,k} \sqrt{1-\mathrm{pf}_{n+k,k}^2}.
\end{aligned} \tag{18}
$$

There are also two virtual measurements that the load at switch $n+k$ always satisfy: $P_{n+k} = Q_{n+k} = 0$.

To set up the state estimation problem, define state variables to be the voltage magnitudes and phase angles at all buses except the reference bus as

$$
x = [\theta_1, \theta_2, \ldots, \theta_{2n}, V_1, V_2, \ldots, V_{2n}]^T. \tag{19}
$$

Then for switch bus $n+k$ on line section (i,k), the measurements can be represented by the state variables as

$$
\begin{aligned}
P_{n+k,k} &= \mathrm{f}_k(x) = G^f_{k,n+k} V^2_{n+k} + V_{n+k} V_k (G^f_{k,k} \cos\theta_{n+k,k} + B^f_{k,k} \sin\theta_{n+k,k}), \\
Q_{n+k,k} &= \mathrm{f}_{n+k}(x) = -B^f_{k,n+k} V^2_{n+k} + V_{n+k} V_k (G^f_{k,k} \sin\theta_{n+k,k} - B^f_{k,k} \cos\theta_{n+k,k}), \\
P_{n+k} &= \mathrm{f}_{2n+k}(x) = -G_{n+k,n+k} V^2_{n+k} - \textstyle\sum_{j=i,k} V_j V_{n+k} (G_{n+k,j} \cos\theta_{n+k,j} + B_{n+k,j} \sin\theta_{n+k,j}), \\
Q_{n+k} &= \mathrm{f}_{3n+k}(x) = B_{n+k,n+k} V^2_{n+k} - \textstyle\sum_{j=i,k} V_j V_{n+k} (G_{n+k,j} \sin\theta_{n+k,j} - B_{n+k,j} \cos\theta_{n+k,j}), \\
V_{n+k} &= \mathrm{f}_{4n+k}(x) = V_{n+k},
\end{aligned} \tag{20}
$$

where $G_{ik} + \mathrm{j} B_{ik} = Y_{ik}$ is the (i,k)-th element of the system bus admittance matrix; the superscript "f" denotes the branch admittance matrix at the sending ends of the lines; $\theta_{ik} := \theta_i - \theta_k$ is the phase angle difference between buses i and k. Let the measurement vector $z = [P^f, Q^f, P, Q, V]^T$ consists of the vectors of line real and reactive power

flows, virtual real and reactive power injections, and switch voltage magnitudes. It follows the *i*-th measurement error can be represented as $|z_i - f_i(x)|$.

6.3 Formulation and Solution Method

We apply weighted least-squares (WLS) method for state estimation. The goal is to minimize the sum of measurement errors:

$$J(x) = \sum_{i=1}^{5n} \frac{[z_i - f_i(x)]^2}{\sigma_i^2} \tag{21}$$

where 5*n* is the number of independent measurements (5 measurements for each switch), z_i is the actual value of the *i*-th measurement, $f_i(x)$ is the estimated value of the *i*-th measurement based on the state variable vector *x*, and σ_i^2 is the variance of the *i*-th measurement.

Since $f_i(x)$ is generally a nonlinear function of the state variables *x*, we must resort to an iterative technique to minimize *J(x)*. A commonly used technique for power system state estimation is to calculate the gradient of *J(x)* and then force it to zero using Newton-Raphson method.

The state estimation problem is an unconstrained minimization problem of the following form

$$\min_x \; J(x) = \sum_{i=1}^{5n} \frac{[z_i - \mathrm{f}_i(x)]^2}{\sigma_i^2}. \tag{22}$$

The gradient of *J(x)* is defined as

$$\nabla_x J(x) = \left[\frac{\partial J(x)}{\partial x_1} \quad \frac{\partial J(x)}{\partial x_2} \quad \cdots \quad \frac{\partial J(x)}{\partial x_{4n}} \right]^T, \tag{23}$$

which can then be expanded as

$$\nabla_x J(x) = -2 \begin{bmatrix} \frac{\partial \mathrm{f}_1}{\partial x_1} & \frac{\partial \mathrm{f}_2}{\partial x_1} & \cdots & \frac{\partial \mathrm{f}_{5n}}{\partial x_1} \\ \frac{\partial \mathrm{f}_1}{\partial x_2} & \frac{\partial \mathrm{f}_2}{\partial x_2} & \cdots & \frac{\partial \mathrm{f}_{5n}}{\partial x_2} \\ \vdots & \vdots & \ddots & \vdots \\ \frac{\partial \mathrm{f}_1}{\partial x_{4n}} & \frac{\partial \mathrm{f}_2}{\partial x_{4n}} & \cdots & \frac{\partial \mathrm{f}_{5n}}{\partial x_{4n}} \end{bmatrix} \begin{bmatrix} \frac{1}{\sigma_1^2} & & & \\ & \frac{1}{\sigma_2^2} & & \\ & & \ddots & \\ & & & \frac{1}{\sigma_{5n}^2} \end{bmatrix} \begin{bmatrix} z_1 - \mathrm{f}_1(x) \\ z_2 - \mathrm{f}_2(x) \\ \vdots \\ z_{5n} - \mathrm{f}_{5n}(x) \end{bmatrix}. \tag{24}$$

For brevity, define

$$H = \begin{bmatrix} \frac{\partial \mathrm{f}_1}{\partial x_1} & \frac{\partial \mathrm{f}_2}{\partial x_1} & \cdots & \frac{\partial \mathrm{f}_{5n}}{\partial x_1} \\ \frac{\partial \mathrm{f}_1}{\partial x_2} & \frac{\partial \mathrm{f}_2}{\partial x_2} & \cdots & \frac{\partial \mathrm{f}_{5n}}{\partial x_2} \\ \vdots & \vdots & \ddots & \vdots \\ \frac{\partial \mathrm{f}_1}{\partial x_{4n}} & \frac{\partial \mathrm{f}_2}{\partial x_{4n}} & \cdots & \frac{\partial \mathrm{f}_{5n}}{\partial x_{4n}} \end{bmatrix}, \tag{25}$$

and

$$R = \begin{bmatrix} \sigma_1^2 & & & \\ & \sigma_2^2 & & \\ & & \ddots & \\ & & & \sigma_{5n}^2 \end{bmatrix}. \tag{26}$$

Then Equation (24) can be written as

$$\nabla_x J(x) = -2H^T R^{-1} \begin{bmatrix} z_1 - \mathrm{f}_1(x) \\ z_2 - \mathrm{f}_2(x) \\ \vdots \\ z_{5n} - \mathrm{f}_{5n}(x) \end{bmatrix}. \tag{27}$$

To make $\nabla_x J(x)$ equal to zero, we apply Newton-Raphson method, then the state mismatch is given as

$$\Delta x = \left(\frac{\partial \nabla_x J(x)}{\partial x} \right)^{-1} \left(-\nabla_x J(x) \right). \tag{28}$$

Then Jacobian of $\nabla_x J(x)$ is calculated as

$$\begin{aligned} \frac{\partial \nabla_x J(x)}{\partial x} &= \frac{\partial}{\partial x} \left\{ -2H^T R^{-1} \begin{bmatrix} z_1 - \mathrm{f}_1(x) \\ z_2 - \mathrm{f}_2(x) \\ \vdots \\ z_{5n} - \mathrm{f}_{5n}(x) \end{bmatrix} \right\} \\ &= -2H^T R^{-1}(-H) \\ &= 2H^T R^{-1} H. \end{aligned} \tag{29}$$

Then

$$\Delta x = \left(H^T R^{-1} H \right)^{-1} H^T R^{-1} \begin{bmatrix} z_1 - \mathrm{f}_1(x) \\ z_2 - \mathrm{f}_2(x) \\ \vdots \\ z_{5n} - \mathrm{f}_{5n}(x) \end{bmatrix}. \tag{30}$$

6.4 Test Results

The algorithm is tested on the 33-bus system [6] with switch on the midpoint of each distribution line section. To demonstrate the state estimation algorithm on these measurements, under initial normal loading condition given in Appendix A, the calculated line power flow data as well as switch voltage magnitudes are used together with a random number-generating algorithm to produce measurements with random errors. The measurements are obtained by adding Gaussian noise to the exact line flow and voltage magnitude. The errors are generated from a normal distribution with mean set at the exact value, and standard deviation $\sigma = 5 \times 10^{-3}$ p.u. for line power and switch voltage measurements. While the switch power injections are virtual measurements that don't need to be physically measured or generated, the standard deviation is set to $\sigma = 1 \times 10^{-5}$ p.u.. The generated measurements for line power flow and switch voltage magnitude are shown in Table 9.

The state estimation algorithm is executed to obtain estimates for bus voltage magnitudes and phase angles given the measurements shown in Table 9. The stopping criterion is $\max \left| \Delta x_i \right| < 10^{-8}$. The procedure took four iterations to converge, with the initial state vector x^0 set to 1 p.u. and 0 rad for the voltage magnitudes and phase angles

at all buses, respectively. The sum of the measurement residual, *J(x)*, is calculated and displayed in Table 10.

Table 9 Line power flow measurements under initial operating conditions (powers in p.u.).

From Bus	To Bus	Actual 'from' bus injection		Measured 'from' bus injection		Actual voltage magnitudes on switches	Measured voltage magnitudes on switches
		P	*Q*	*P*	*Q*	*V*	*V*
S1	1	3.9127	2.4328	3.9138	2.4371	0.9985	1.0024
S2	2	3.4191	2.1951	3.4121	2.1954	0.9898	1.0020
S3	3	2.3533	1.6762	2.3542	1.6710	0.9789	0.9804
S4	4	2.2138	1.5892	2.2185	1.5771	0.9714	0.9716
S5	5	2.1253	1.5380	2.1247	1.5366	0.9585	0.9556
S6	6	1.0943	0.5248	1.1021	0.5305	0.9475	0.9465
S7	7	0.8909	0.4208	0.8937	0.4217	0.9433	0.9431
S8	8	0.6864	0.3184	0.6843	0.3187	0.9378	0.9290
S9	9	0.6226	0.2957	0.6218	0.2991	0.9318	0.9305
S10	10	0.5605	0.2743	0.5591	0.2674	0.9284	0.9322
S11	11	0.5148	0.2441	0.5160	0.2512	0.9273	0.9244
S12	12	0.4530	0.2079	0.4568	0.2034	0.9235	0.9259
S13	13	0.3913	0.1714	0.3899	0.1716	0.9193	0.9242
S14	14	0.2708	0.0907	0.2731	0.0889	0.9174	0.9228
S15	15	0.2104	0.0805	0.2192	0.0812	0.9160	0.9199
S16	16	0.1502	0.0602	0.1548	0.0505	0.9143	0.9030
S17	17	0.0900	0.0400	0.0942	0.0476	0.9130	0.9102
S18	18	0.3611	0.1610	0.3570	0.1637	0.9967	1.0012
S19	19	0.2706	0.1206	0.2679	0.1306	0.9946	0.9966
S20	20	0.1801	0.0801	0.1813	0.0872	0.9924	0.9925
S21	21	0.0900	0.0400	0.0895	0.0401	0.9918	0.9940
S22	22	0.9380	0.4561	0.9299	0.4514	0.9809	0.9865
S23	23	0.8439	0.4030	0.8363	0.3943	0.9758	0.9765
S24	24	0.4206	0.2005	0.4258	0.2006	0.9708	0.9670
S25	25	0.9496	0.9729	0.9458	0.9740	0.9483	0.9474
S26	26	0.8866	0.9465	0.8970	0.9517	0.9461	0.9450
S27	27	0.8192	0.9157	0.8081	0.9109	0.9391	0.9435
S28	28	0.7497	0.8873	0.7519	0.8912	0.9292	0.9313
S29	29	0.6238	0.8128	0.6238	0.8132	0.9233	0.9261
S30	30	0.4210	0.2111	0.4172	0.2072	0.9195	0.9202
S31	31	0.2701	0.1401	0.2721	0.1440	0.9169	0.9151
S32	32	0.0600	0.0400	0.0560	0.0413	0.9163	0.9166

Table 10 Measurement residual of state estimation solution (residuals in p.u.)

Iteration	Sum of residual ($J(x)$)
1	3.02×10^{6}
2	8.48×10^{5}
3	68.42
4	23.99

The state estimation algorithm obtains the estimated bus voltage values, which are shown in Table 11. Notice that the estimated values are close to the true values from which the measurements are made.

Table 11 State estimation solution (voltages in p.u., angles in rad)

State estimation solution					State estimation solution				
Bus No.	Actual mag	Est. mag	Actual angle	Est. angle	Bus No.	Actual mag	Est. mag	Actual angle	Est. angle
1	0.9969	0.9969	0.0164	0.0166	33	0.9985	0.9985	0.0082	0.0083
2	0.9827	0.9827	0.0945	0.0953	34	0.9898	0.9898	0.0552	0.0557
3	0.9751	0.9751	0.1565	0.1562	35	0.9789	0.9789	0.1254	0.1256
4	0.9676	0.9677	0.2268	0.2244	36	0.9714	0.9714	0.1916	0.1902
5	0.9493	0.9493	0.1328	0.1300	37	0.9585	0.9585	0.1803	0.1777
6	0.9457	0.9457	-0.0994	-0.1036	38	0.9475	0.9475	0.0169	0.0134
7	0.9409	0.9409	-0.0662	-0.0705	39	0.9433	0.9433	-0.0828	-0.0871
8	0.9347	0.9347	-0.1391	-0.1427	40	0.9378	0.9378	-0.1026	-0.1065
9	0.9289	0.9288	-0.2013	-0.2031	41	0.9318	0.9318	-0.1701	-0.1728
10	0.9280	0.9280	-0.1943	-0.1967	42	0.9284	0.9284	-0.1978	-0.1999
11	0.9265	0.9265	-0.1844	-0.1857	43	0.9273	0.9273	-0.1893	-0.1912
12	0.9204	0.9204	-0.2750	-0.2809	44	0.9235	0.9234	-0.2295	-0.2331
13	0.9181	0.9181	-0.3522	-0.3577	45	0.9193	0.9192	-0.3136	-0.3192
14	0.9167	0.9167	-0.3902	-0.3966	46	0.9174	0.9174	-0.3712	-0.3771
15	0.9153	0.9153	-0.4132	-0.4214	47	0.9160	0.9160	-0.4017	-0.4090
16	0.9133	0.9133	-0.4904	-0.5073	48	0.9143	0.9143	-0.4518	-0.4643
17	0.9127	0.9127	-0.5000	-0.5155	49	0.9130	0.9130	-0.4952	-0.5114
18	0.9964	0.9964	0.0049	0.0054	50	0.9967	0.9967	0.0107	0.0110
19	0.9928	0.9927	-0.0627	-0.0554	51	0.9946	0.9946	-0.0288	-0.0249
20	0.9921	0.9920	-0.0820	-0.0738	52	0.9924	0.9924	-0.0723	-0.0646
21	0.9915	0.9914	-0.1021	-0.0938	53	0.9918	0.9917	-0.0921	-0.0838
22	0.9791	0.9792	0.0644	0.0653	54	0.9809	0.9809	0.0795	0.0804

23	0.9724	0.9726	-0.0232	-0.0232	55	0.9758	0.9759	0.0207	0.0213
24	0.9691	0.9692	-0.0675	-0.0687	56	0.9708	0.9709	-0.0453	-0.0459
25	0.9474	0.9474	0.1771	0.1746	57	0.9483	0.9484	0.1549	0.1523
26	0.9448	0.9448	0.2351	0.2325	58	0.9461	0.9461	0.2060	0.2035
27	0.9334	0.9335	0.3190	0.3186	59	0.9391	0.9391	0.2768	0.2753
28	0.9251	0.9252	0.3945	0.3948	60	0.9292	0.9294	0.3566	0.3565
29	0.9215	0.9216	0.5022	0.5025	61	0.9233	0.9234	0.4483	0.4485
30	0.9174	0.9175	0.4183	0.4186	62	0.9195	0.9196	0.4604	0.4606
31	0.9165	0.9166	0.3941	0.3946	63	0.9169	0.9171	0.4062	0.4066
32	0.9162	0.9163	0.3863	0.3879	64	0.9163	0.9165	0.3902	0.3912

The state estimation solution can then be used to calculate load power injections. The next table presents the calculated power injection along with the actual ones under normal loading condition.

Table 12 Comparison of estimated power injections and actual ones (powers in p.u.)

Bus power injection					Bus power injection				
Bus No.	Actual *P*	Est. *P*	Actual *Q*	Est. *Q*	Bus No.	Actual *P*	Est. *P*	Actual *Q*	Est. *Q*
0	3.9177	3.9202	2.4351	2.4403	33	0	0.0000	0	0.0000
1	-0.1000	-0.1122	-0.0600	-0.0613	34	0	0.0000	0	0.0000
2	-0.0900	-0.0903	-0.0400	-0.0533	35	0	0.0000	0	0.0000
3	-0.1200	-0.1163	-0.0800	-0.0840	36	0	0.0000	0	0.0000
4	-0.0600	-0.0652	-0.0300	-0.0193	37	0	0.0000	0	0.0000
5	-0.0600	-0.0554	-0.0200	-0.0117	38	0	0.0000	0	0.0000
6	-0.2000	-0.2050	-0.1000	-0.1048	39	0	0.0000	0	0.0000
7	-0.2000	-0.2049	-0.1000	-0.1006	40	0	0.0000	0	0.0000
8	-0.0600	-0.0587	-0.0200	-0.0169	41	0	0.0000	0	0.0000
9	-0.0600	-0.0606	-0.0200	-0.0304	42	0	0.0000	0	0.0000
10	-0.0450	-0.0424	-0.0300	-0.0159	43	0	0.0000	0	0.0000
11	-0.0600	-0.0574	-0.0350	-0.0466	44	0	0.0000	0	0.0000
12	-0.0600	-0.0652	-0.0350	-0.0303	45	0	0.0000	0	0.0000
13	-0.1200	-0.1162	-0.0800	-0.0820	46	0	0.0000	0	0.0000
14	-0.0600	-0.0535	-0.0100	-0.0074	47	0	0.0000	0	0.0000
15	-0.0600	-0.0641	-0.0200	-0.0304	48	0	0.0000	0	0.0000
16	-0.0600	-0.0606	-0.0200	-0.0027	49	0	0.0000	0	0.0000
17	-0.0900	-0.0941	-0.0400	-0.0476	50	0	0.0000	0	0.0000
18	-0.0900	-0.0886	-0.0400	-0.0327	51	0	0.0000	0	0.0000
19	-0.0900	-0.0861	-0.0400	-0.0429	52	0	0.0000	0	0.0000
20	-0.0900	-0.0917	-0.0400	-0.0470	53	0	0.0000	0	0.0000
21	-0.0900	-0.0895	-0.0400	-0.0401	54	0	0.0000	0	0.0000

22	-0.0900	-0.0895	-0.0500	-0.0540	55	0	0.0000	0	0.0000
23	-0.4200	-0.4074	-0.2000	-0.1913	56	0	0.0000	0	0.0000
24	-0.4200	-0.4251	-0.2000	-0.2001	57	0	0.0000	0	0.0000
25	-0.0600	-0.0458	-0.0250	-0.0209	58	0	0.0000	0	0.0000
26	-0.0600	-0.0816	-0.0250	-0.0351	59	0	0.0000	0	0.0000
27	-0.0600	-0.0467	-0.0200	-0.0113	60	0	0.0000	0	0.0000
28	-0.1200	-0.1222	-0.0700	-0.0736	61	0	0.0000	0	0.0000
29	-0.2000	-0.2038	-0.6000	-0.6042	62	0	0.0000	0	0.0000
30	-0.1500	-0.1442	-0.0700	-0.0623	63	0	0.0000	0	0.0000
31	-0.2100	-0.2160	-0.1000	-0.1025	64	0	0.0000	0	0.0000
32	-0.0600	-0.0560	-0.0400	-0.0413					

CHAPTER 7. COMPARATIVE STUDY WITH BENCHMARK EXHAUSTIVE SEARCH ALGORITHM ON LARGE DISTRIBUTION SYSTEM

7.1 Introduction

Due to tradeoff between computational speed and optimality, metaheuristic algorithms and MIP solvers discussed in CHAPTER 2 have gained certain popularity for distribution reconfiguration applications including service restoration. Despite the proposal and successful application of these optimization approaches, exhaustive search-based methods remain viable approaches for reconfiguration problems. This is partly because exhaustive search methods are intuitive and easy to maintain by distribution system operators, and partly due to the reason that the service restoration task can often be performed on a small section of the entire distribution system, thus making the size of the problem manageable for exhaustive search.

In this chapter, we describe an exhaustive search method developed for Korea Electric Power Corporation (KEPCO) for service restoration. The first step of the method identifies the subsystem of interest for service restoration; it then divides the subsystem into two levels according to layers of feeders; exhaustive search of possible radial topologies is then performed sequentially on the two subsystems; the topologies are ranked based on multi-objective cost functions. The details of the algorithm will be presented in the remainder of the chapter.

After introducing the exhaustive search method, we compare it with the proposed dynamic programming-based service restoration method. By benchmarking with the solution obtained by the exhaustive search method, the capability of the dynamic programming method in obtaining good final topology can be examined. However, it should be noted that the dynamic programming-based approach focuses on minimizing the cumulative cost as opposed to the final cost alone, and the cost functions are defined differently, so the final topologies do not necessarily coincide. It should be noted that a major advantage of the proposed DP-based method over exhaustive search method lies in the capability of deriving the switching sequence. When the system size and number of switches is too large to perform DP effectively, the exhaustive method can be used to pre-screen the most relevant subsystem on which switching sequence can be obtained based on DP, which will be demonstrated in Sections 7.3 – 7.4.

7.2 Exhaustive Search Method for Service Restoration

7.2.1 Introduction

First, we introduce some terms and definitions. After system fault occurs and is isolated, the outage area can be identified. The outage area is the subsystem where the loads are disconnected from the rest of the system and are not energized by any feeder. The level 1 backup feeders are defined to be the feeders that can be connected to the outage area by closing one open tie switch. Open tie switches between the outage area and level 1 backup feeders are called level 1 boundary switches. Similarly, level 2 backup feeders are defined to be the feeders that can be connected to level 1 feeders by closing

one open tie switch. Open tie switches between level 1 and level 2 backup feeders are called level 2 boundary switches.

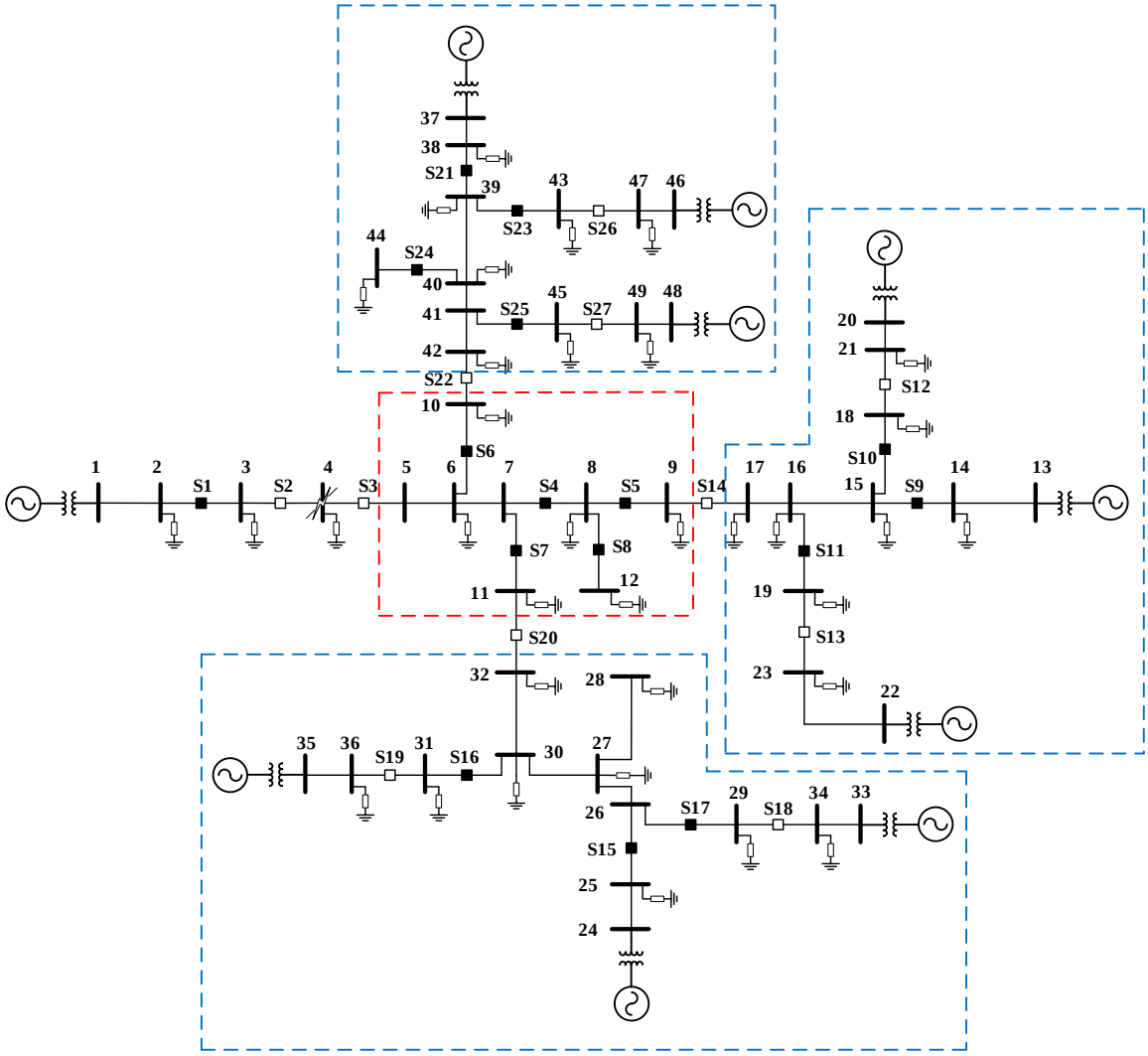

Figure 37 One line diagram of the 49-bus system with 10 feeders and 27 switches.

As an illustration, see the example system with 10 feeders, 49 buses and 27 switches shown in Figure 37. Given the fact that a fault occurs between S2 and S3 and suppose the fault has been isolated by opening switches S2 and S3. The outage area consisting of buses 5 – 12 is thus de-energized (enclosed by red dashed lines). The three feeders starting at buses 13, 24, and 37 are level 1 backup feeders; and the six feeders

starting at buses 20, 22, 33, 35, 46, and 48 are level 2 backup feeders. The three level 1 backup feeders and neighboring level 2 backup feeders form three distinct areas enclosed by blue dashed lines, for which reconfiguration can be performed separately. There are three level 1 boundary switches: S14, S20, and S22; and six level 2 boundary switches: S12, S13, S18, S19, S26, and S27.

To limit the problem size, the subsystem considered by the exhaustive search algorithm is restricted to the outage area, level 1 backup feeders, and level 2 backup feeders. The rest of the system is not considered for service restoration by the algorithm. To further reduce the search space, switches in level 2 backup feeders are not considered. That is, only switches in the outage area, level 1 backup feeders, as well as level 1 and level 2 boundary switches can be operated. By introducing a parameter called maximum number of level 2 load transfers (max_nL2LT), which is the maximum number of level 2 backup feeders picking up loads originally fed by level 1 backup feeders (for instance, if S12 is closed and S10 is open, number of level 2 load transfer is 1 since the level 2 backup feeder originating at bus 20 picks up load at bus 18, which is originally fed by the level 1 backup feeder starting at bus 13), number of possible topologies can be further reduced by limiting level 2 load transfers, which will be discussed in detail in the sequel.

7.2.2 Sequential Exhaustive Search

After the subsystem of interest for service restoration has been determined, a spanning tree generation algorithm will be employed to find all radial topologies that both isolate the fault and restore services to the outage area. For the example system in

Figure 37, we want to find all radial topologies such that the fault is isolated by opening S2 and S3, and that services to buses 5 – 12 are restored.

It is noted that the task of generating all radial topologies amounts to performing switching operations in two sets of switches: 1) switches in the outage area and level 1 boundary switches (which are called level 1 switching operations), and 2) switches in level 1 backup feeders and level 2 boundary switches (which are called level 2 switching operations). Since the two subsystems where the switches lie are disjoint, any radial topology can be generated sequentially by first generating a radial topology considering only level 2 switching operations (level 2 reconfiguration), and then generating a radial topology considering only level 1 switching operations (level 1 reconfiguration). Another simple observation is that level 2 switching operations can be performed for each level 1 backup feeder separately. Take the test system in Figure 37 for example: level 2 switching operations can be performed on three sets of feeders enclosed in blue dashed lines separately.

The overall reconfigurations can be performed by first performing level 2 reconfigurations for each level 1 backup feeder, and then performing level 1 reconfiguration for the outage area. For example, a potential service restoration strategy for the example system is to 1) close S14 and S20 and open S4; 2) open S10 and close S12; and 3) open S16 and close S19. Switching operations in item 1 constitute level 1 switching operations, which restore services to the outage area. Switching operations in items 2 and 3 constitute level 2 switching operations, which aim to ensure a balanced load sharing among backup feeders such that all feeders have similar load margins and no feeders are overloaded.

Suppose there are *m* level 1 backup feeders where the *i*-th level 1 backup feeder and neighboring level 2 backup feeders has n_i possible radial topologies, the total number of possible level 2 topologies is thus $\prod_{i=1}^{m} n_i$. Suppose also that there are *N* level 1 reconfigurations, then the total number of radial topologies for the entire system is $N\prod_{i=1}^{m} n_i$. To reduce computational burden, instead of evaluating all $N\prod_{i=1}^{m} n_i$ topologies, the possible level 2 reconfigurations for each level 1 backup feeder and neighboring level 2 backup feeders is grouped based on their number of level 2 load transfer and ranked within each group, only the best topology in each group is kept and all other topologies are ignored. In this way, the total number of possible radial topologies can be greatly reduced while most preferable topologies are kept. Specifically, each level 1 backup feeder only keeps one topology for each number of level 2 load transfer. The maximum total number of level 2 load transfer is passed to the algorithm to control the search space. For example, when at most one level 2 load transfer is allowed, the total number of potential topologies reduces to $N(m+1)$ since the level 2 load transfer can be made among any of the *m* level 1 backup feeders, or no level 2 load transfer is performed.

7.2.3 Level 2 Switching Operations Evaluation

For each level 2 switching operation, the overall cost function is evaluated as a weighted sum of seven individual cost functions. The individual cost functions are: 1) number of level 2 switching operations (NS), 2) level 1 backup feeder margin (MG), 3) load balance (LB), 4) maximum voltage deviation (VD), 5) switch reliability (SR), 6) total number of level 2 load transfers (nL2LT), and 7) total real power loss (LOSS). To normalize different cost functions, we define all of them in a way such that they lie

between 0 and 1. Additionally, all cost functions are defined such that smaller values indicate more desirable operations. Specifically, these cost functions are defined as follows:

- Let N be the total number of level 2 switching operations, the normalized cost of NS is

$$f_1 = 1 - \frac{1}{N} \tag{31}$$

- Let the total load of the level 1 backup feeder be S MVA and the maximum load capacity of this feeder be $\overline{S}$ MVA, the normalized cost of MG is

$$f_2 = \frac{S}{\overline{S}} \tag{32}$$

- Let there be m' backup feeders including the level 1 backup feeder and the neighboring level 2 backup feeders, and the average total load of all backup feeders be S_{avg} MVA, the normalized cost of LB is

$$f_3 = \frac{\sqrt{\sum_{i=1}^{m'} (S_i - S_{avg})^2 / m'}}{S_{avg}\sqrt{m'-1}} \tag{33}$$

- Let the maximum voltage deviation for buses in the i-th backup feeder be δV_i, and the maximum allowable voltage deviation for all backup feeders be ΔV, the normalized cost of VD is

$$f_4 = \frac{\max_{1 \le i \le m} \{\delta V_i\}}{\Delta V} \tag{34}$$

- Each switch has a reliability index which is an integral value between 1 and 4. Smaller value represents higher reliability. Let there be *p* operated switches, and the reliability of the *i*-th operated switch be σ_i, the normalized cost of SR is

$$f_5 = 1 - \frac{1}{\sum_{i=1}^{p} \sigma_i} \tag{35}$$

- Let the total number of level 2 load transfers be *M*, the normalized cost of nL2LT is

$$f_6 = 1 - \frac{1}{M + 1} \tag{36}$$

- The system loss of the level 1 backup feeder and all related level 2 backup feeders are ranked for all possible radial topologies. Let the loss of this specific topology be the *r*-th smallest, the normalized cost of LOSS is

$$f_7 = 1 - \frac{1}{r} \tag{37}$$

Each function is also associated with a nonnegative weight $0 \le w_i \le 1$. The sum of all weight is 1: $\sum_{i=1}^{7} w_i = 1$. Then the overall cost of a specific topology is evaluated as

$$\text{cost} = \sum_{i=1}^{m} w_i \, \mathrm{f}_i \tag{38}$$

Example: consider the following level 2 service restoration scheme:

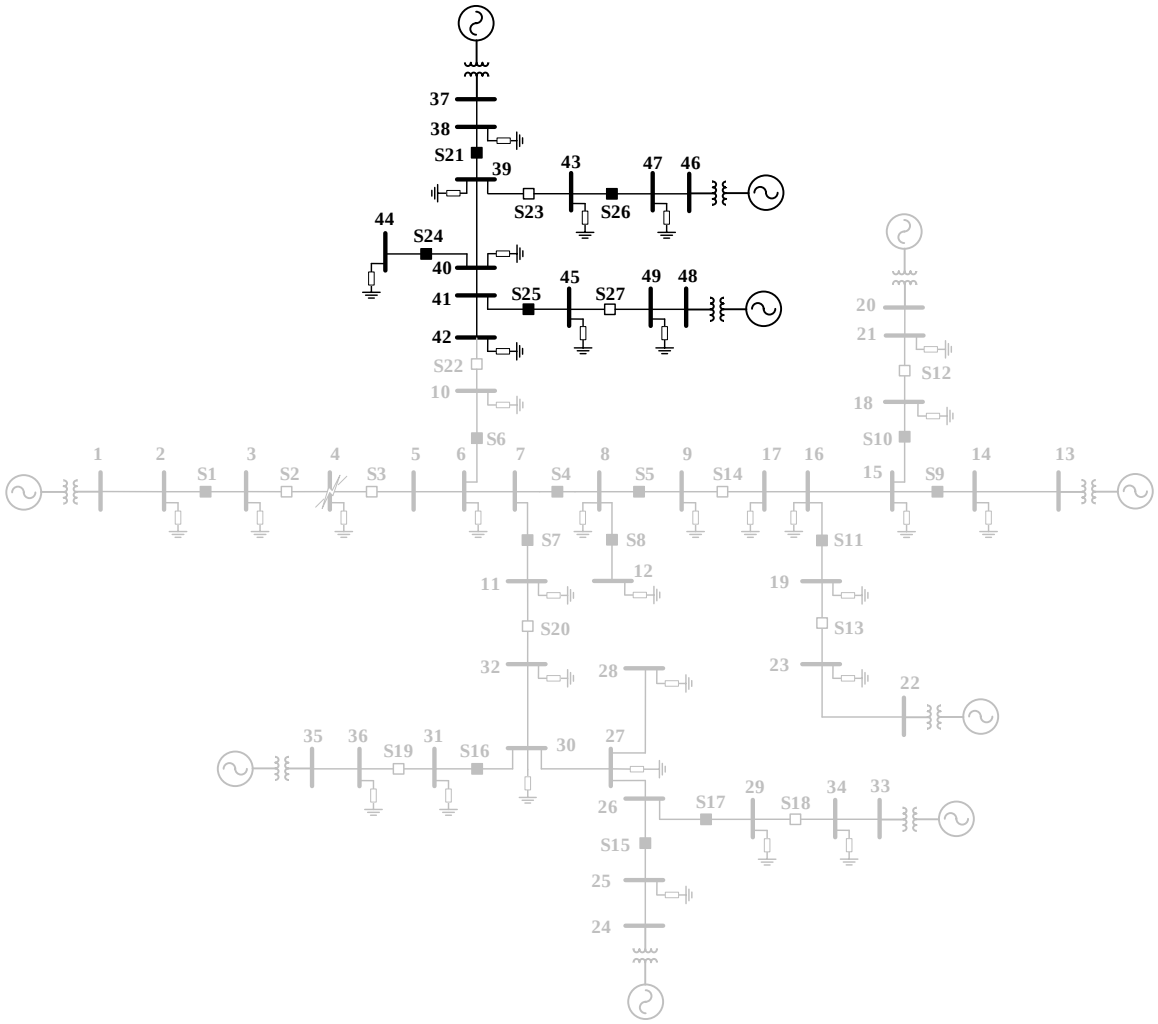

Figure 38 Example partial level 2 reconfiguration of the 49-bus system.

This is part of level 2 service restoration where only one of the three level 1 backup feeders (from bus 37) is considered. For this specific example, one switch is opened: S23, and one switch is closed: S26. So, the number of switching operations is 2.

To evaluate the overall cost, we first evaluate the individual cost functions given by Equations (31) to (37) one by one. Since the number of switching operations is 2, the cost of NS (Equation (31)) is $f_1 = 1 - 1/2 = 0.5$. Let the maximum capacity of the level 1 backup feeder BF1 be 10 MVA and suppose the actual load on the feeder is 5 MVA, then the load margin is 10 – 5 = 5 MVA, so the cost of LIMG (Equation (32)) is $f_2 = 1 - 5/10 = 0.5$. Let the loads on the two level 2 backup feeders BF11 and BF12 be 8 MVA for both of them, since the average load of all three feeders is (5 + 8 + 8) / 3 = 7, the cost of LB (Equation (33)) is $f_3 = \sqrt{((5-7)^2 + (8-7)^2 + (8-7)^2)/3} / (7\sqrt{3-1}) = 0.1429$. Let the maximum voltage deviation be 5% and suppose the maximum voltage deviation at the three feeders are 2%, 3%, and 3%, respectively, then the cost of VD (Equation (34)) is $f_4 = \max\{0.02, 0.03, 0.03\}/0.05 = 0.6$. Suppose both of the two operated switches have reliability index 1, then the cost of SR (Equation (35)) is $f_5 = 1 - 1/(1+1) = 0.5$. Since the number of level 2 load transfer is 1 (part of loads on feeder at bus 37 is transferred to feeder at bus 46 by closing S26 and opening S23), the cost of nL2LT (Equation (36)) is $f_6 = 1 - 1/(1+1) = 0.5$. Suppose among all candidate level 2 reconfigurations for the set of feeders, the loss of the specific topology is ranked 2nd lowest, then the cost of LOSS (Equation (37)) is $f_7 = 1 - 1/2 = 0.5$. Let the weights (w_i) of the seven cost functions be 0.3, 0.2, 0.1, 0.1, 0.1, 0.1, 0.1, then the overall cost is $\sum_{i=1}^{7} w_i f_i = 0.4643$.

7.2.4 Level 1 Switching Operations and Overall Topology Evaluation

Every overall topology is obtained by combining a level 1 reconfiguration and a level 2 reconfiguration. The overall cost function of an overall topology is evaluated as a weighted sum of seven individual cost functions as well. The individual cost functions

are: 1) number of level 1 switching operations (NS), 2) total margin (MG), 3) load balance (LB), 4) voltage drop (VD), 5) switch reliability (SR), 6) total number of level 2 load transfer (nL2LT), and 7) total ohmic real power loss (LOSS). To normalize different cost functions, we define all of them in a way such that they lie between 0 and 1. Additionally, all cost functions are defined such that smaller values indicate more desirable operations. Specifically, these cost functions are defined as follows:

- Let N be the total number of level 1 switching operations, the normalized cost of NS is

$$\mathrm{f}_1 = 1 - \frac{1}{N} \tag{39}$$

- Let there be m level 1 backup feeders and let the total load of the i-th level 1 backup feeder be S_i and the maximum load capacity of this feeder be $\overline{S_i}$, the normalized cost of MG is

$$\mathrm{f}_2 = \frac{\sum_{i=1}^{m} S_i}{\sum_{i=1}^{m} \overline{S_i}} \tag{40}$$

- Let the average total load of all level 1 backup feeders be S_{avg}, the normalized cost of LB is

$$\mathrm{f}_3 = \frac{\sqrt{\sum_{i=1}^{m} (S_i - S_{avg})^2 / m}}{S_{avg}\sqrt{m-1}} \tag{41}$$

- Let the maximum voltage deviation for buses in the *i*-th level 1 backup feeder be δV_i, and the system-wide maximum allowable voltage deviation be ΔV, the normalized cost of VD is

$$f_4 = \frac{\max_{1 \le i \le m}\{\delta V_i\}}{\Delta V} \tag{42}$$

- Each switch has a reliability index which is an integral value between 1 and 4. Smaller value represents higher reliability. Let there be *p* operated switches and the reliability of the *i*-th operated switch be σ_i, the normalized cost of SR is

$$f_5 = 1 - \frac{1}{\sum_{i=1}^{p} \sigma_i} \tag{43}$$

- Let the total number of level 2 load transfer be *M*, the normalized cost of nL2LT is

$$f_6 = 1 - \frac{1}{M+1} \tag{44}$$

- The system loss for restored outage area and level 1 backup feeders are ranked for all possible radial topologies. Let the loss of a specific topology be the *r*-th smallest, the normalized cost of LOSS is

$$f_7 = 1 - \frac{1}{r} \tag{45}$$

Each function is also associated with a nonnegative weight $0 \le w_i \le 1$. The sum of all weight is 1: $\sum_{i=1}^{7} w_i = 1$. Then the overall cost of a specific topology is evaluated as

$$\text{cost} = \sum_{i=1}^{m} w_i \, \mathrm{f}_i \tag{46}$$

Example: Consider the overall service restoration topology in Figure 41 obtained by combining level 1 reconfiguration in Figure 39 and level 2 reconfiguration in Figure 40:

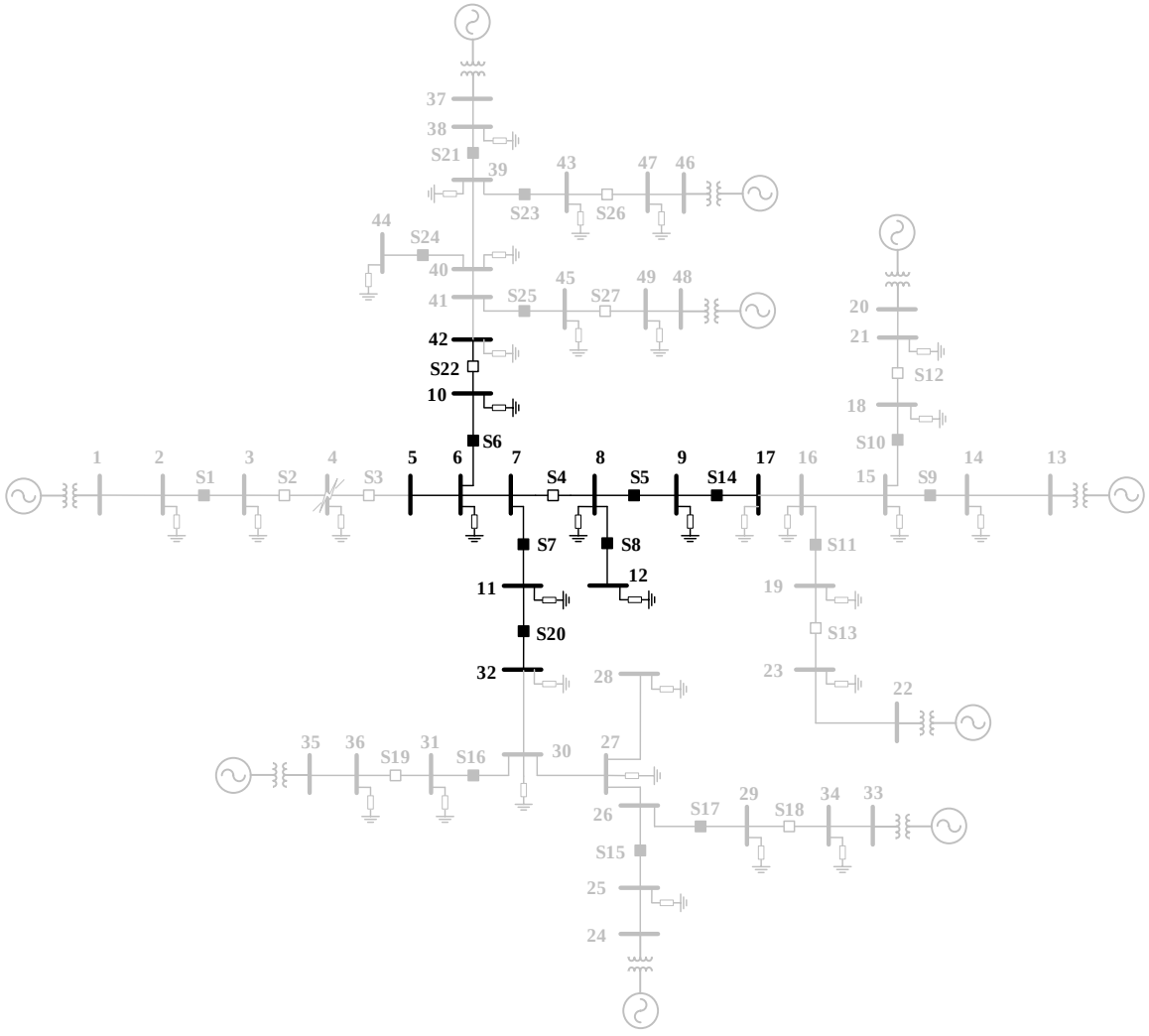

Figure 39 Example level 1 reconfiguration of the 49-bus system.

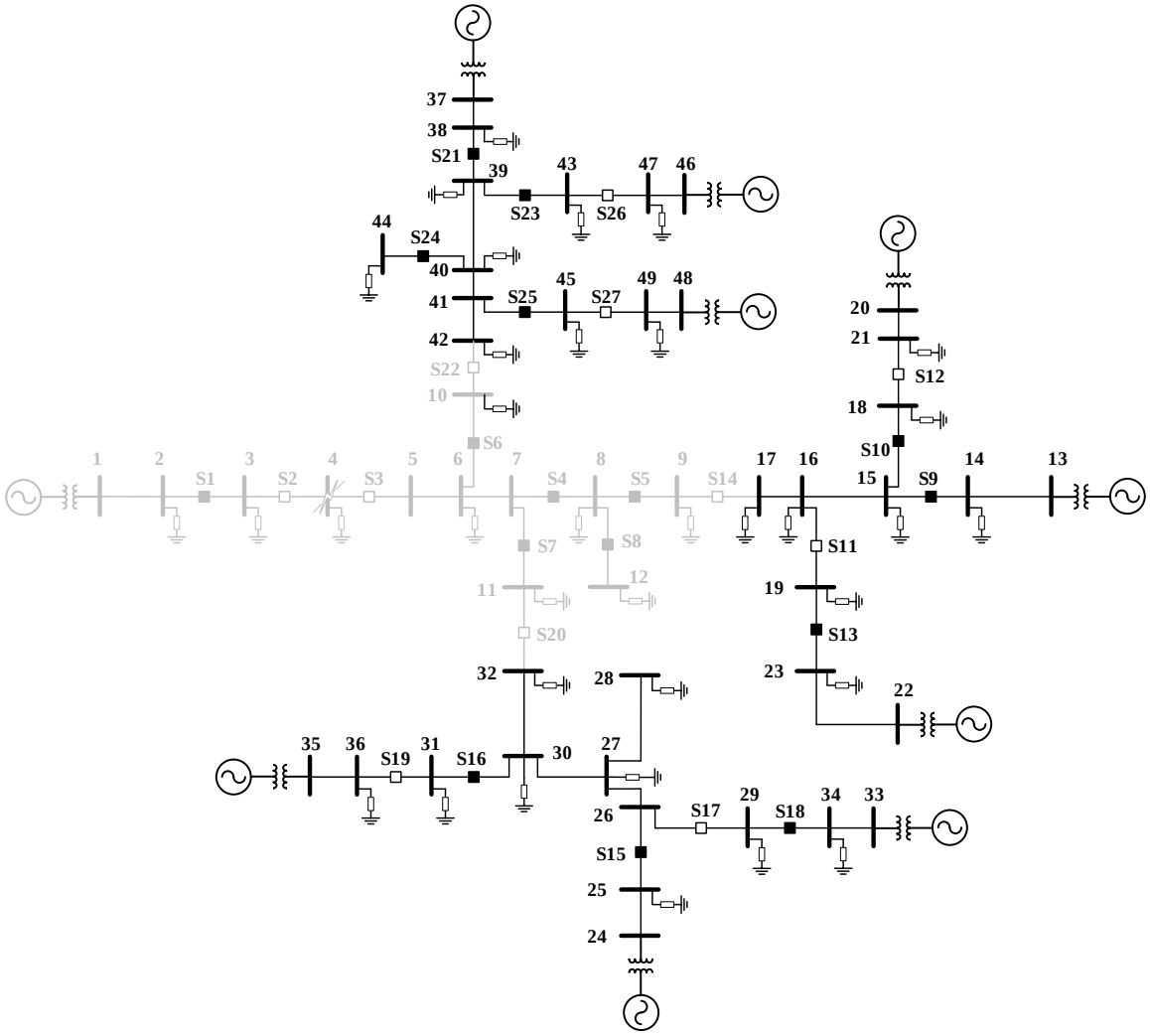

Figure 40 Example level 2 reconfiguration of the 49-bus system.

For this specific example, three switches are opened: S4 (in level 1), S11 and S17 (in level 2); four switches are closed: S14, S20 (in level 1), S13, and S18 (in level 2). So, the number of switching operations is 7.

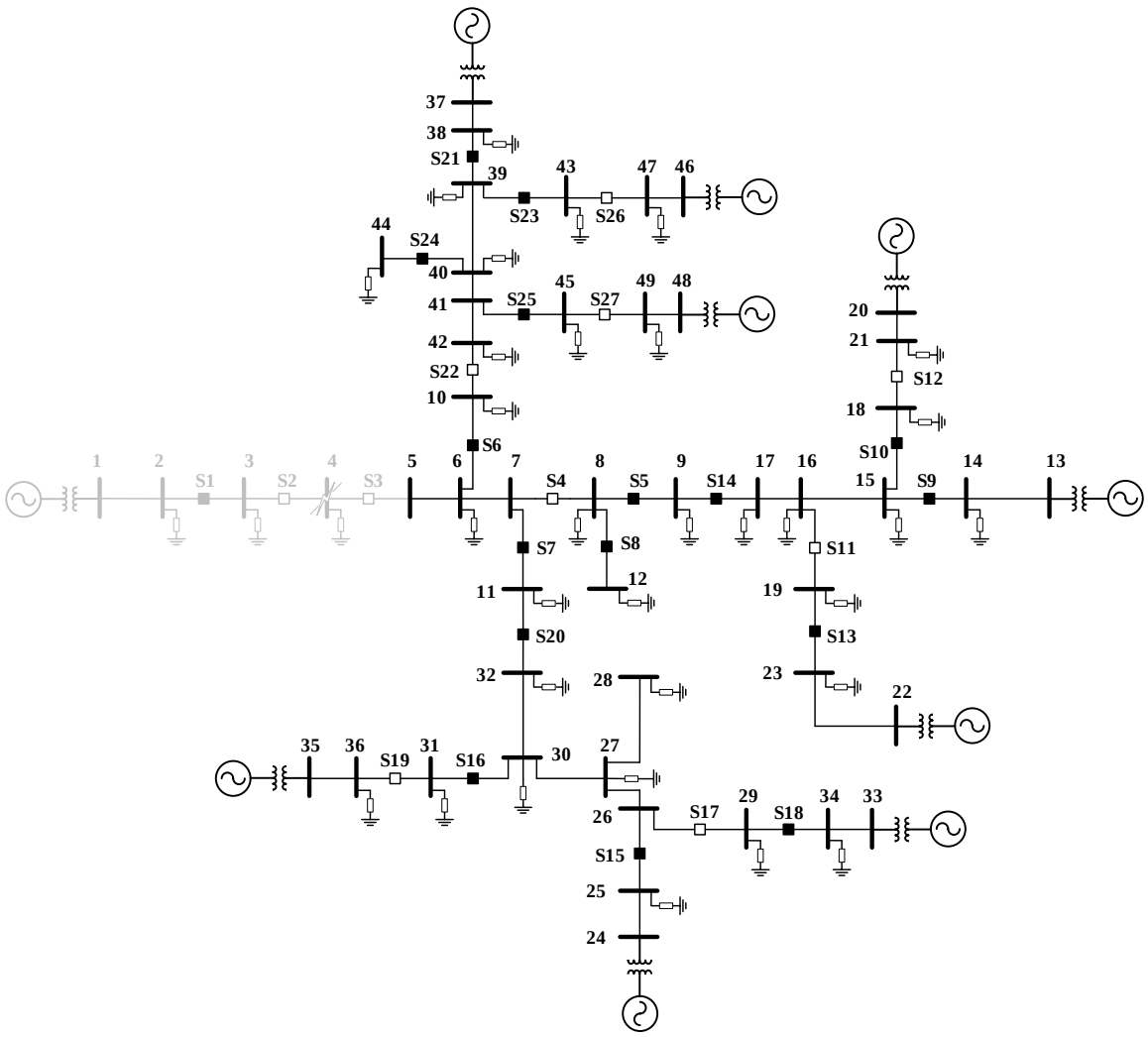

Figure 41 Example overall reconfiguration of the 49-bus system.

To evaluate the overall cost, we first evaluate the individual cost functions given by Equations (39) to (45) one by one. Since the number of switching operations is 7, the cost of NS (Equation (39)) is $f_1 = 1 - 1/7 = 0.8571$. Let the maximum capacity of level 1 backup feeders at buses 13, 24, and 37 be 10 MVA and suppose the load on the three feeders are 9, 10, and 8 MVA, then the cost of MG (Equation (40)) is $f_2 = (9^2 + 10^2 + 8^2) / (10^2 + 10^2 + 10^2) = 0.8167$. Since the average feeder load is (9 + 10 + 8) / 3 = 9, the cost of LB (Equation (41)) is $f_3 = \sqrt{((9-9)^2 + (8-9)^2 + (10-9)^2)/3} / (9\sqrt{3-1}) = 0.0642$. Let

the maximum voltage deviation be 5% and suppose the maximum voltage deviation at the three feeders are 3%, 4%, and 2%, respectively, then the cost of VD (Equation (42)) is $f_4 = \max\{0.03, 0.04, 0.02\}/0.05 = 0.8$. Suppose the seven operated switches have the following reliability index:

Switch ID	S4	S11	S13	S14	S17	S18	S20
Reliability	1	1	3	3	1	2	1

Then the cost of SR (Equation (43)) is $f_5 = 1 - 1/(1+1+3+3+1+2+1) = 0.9167$. Since the number of level 2 load transfer is 2 (part of loads on feeder at bus 22 is transferred to the feeder at bus 13 and part of loads on feeder at bus 33 is transferred to the feeder at bus 24), the cost of nL2LT (Equation (44)) is $f_6 = 1 - 1/(1+2) = 0.6667$. Suppose among all feasible candidate overall reconfigurations, the loss of the specific topology is ranked 3rd lowest, then the cost of LOSS (Equation (45)) is $f_7 = 1 - 1/3 = 0.6667$. Let the weights (w_i) of the seven cost functions be 0.3, 0.2, 0.1, 0.1, 0.1, 0.1, 0.1, then the overall cost can be calculated as $\sum_{i=1}^{7} w_i f_i = 0.7319$.

7.2.5 Overall Algorithm

The overall algorithm of the sequential exhaustive search algorithm can be summarized by the following steps:

Step 1 (outage area identification and initialization): Identify outage area, level 1 backup feeders, and level 2 backup feeders. Obtain maximum allowable number of level 2 load transfers (max_nL2LT). Isolate the fault by opening all switches adjacent to the fault location.

Step 2 (level 2 exhaustive search): For each area composed of a level 1 backup feeder and the neighbouring level 2 backup feeders, perform exhaustive search to find all radial topologies. This may involve switching operations on switches in the specific level 1 backup feeder and open tie switches connecting the level 1 backup feeder and neighbouring level 2 backup feeders. Group the topologies based on their respective number of level 2 load transfers and discard all topologies whose number of level 2 load transfers are greater than max_nL2LT. For each topology, evaluate its cost function. For each group of topologies, save the topology with optimal cost and discard the rest. For example, for a system with 3 level 1 backup feeders and max_nL2LT = 3, the algorithm saves at most 12 topologies:

nL2LT / level 1 backup feeder	nL2LT = 0	nL2LT = 1	nL2LT = 2	nL2LT = 3
Backup feeder 1	Topology 1	Topology 2	Topology 3	Topology 4
Backup feeder 2	Topology 5	Topology 6	Topology 7	Topology 8
Backup feeder 3	Topology 9	Topology 10	Topology 11	Topology 12

Step 3 (level 1 exhaustive search): This step deals with the actual restoration of the outage area: sectionalize the outage area and transfer the sections to level 1 backup feeder. Specifically, exhaustive search is performed to find all radial topologies for the outage area. This involves switching operations on switches in the outage area and open tie switches connecting outage area and level 1 backup feeder. Store all such radial topologies.

Step 4 (Overall topology evaluation): Evaluate all possible radial topologies that restore the outage area by combining topologies obtained in step 2 and step 3. Specifically, evaluate all combinations of radial topologies in outage area (obtained in step 3) and level 1 backup feeders (obtained in step 2) and make sure the total number of

level 2 load transfer is no more than max_nL2LT. Evaluate the topologies based on cost function in Equation (46) and find the optimal one among all candidates.

7.3 Computation Results

The computation results of the exhaustive method on the test system in Figure 37 are presented in this section. The system parameters of the test system can be found in Appendix B. Bus voltage and line current capacity constraints are enforced. Feeder capacity is the capacity of the line which is incident to the feeder head bus. The weights for both level 1 and level 2 cost functions are defined as 0.3, 0.2, 0.1, 0.1, 0.1, 0.1, and 0.1. The maximum number of level 2 load transfers max_nL2LT = 2.

7.3.1 Level 2 and Level 1 Exhaustive Search

All level 2 reconfigurations are identified and the corresponding costs are evaluated. There are three level 1 backup feeders, the reconfigurations as well as the costs for each one of them are listed below:

Table 13 Level 2 reconfigurations and costs for feeder at bus 37

No.	Switches to close	Switches to open	Number of level 2 load transfers	Cost
1	S26, S27	S23, S25	2	0.5467
2	S26, S27	S21, S25	2	Infeasible
3	S26, S27	S21, S23	2	Infeasible
4	S27	S21	1	Infeasible
5	S27	S25	1	0.5463
6	—	—	0	0.2628
7	S26	S21	1	Infeasible
8	S26	S23	1	0.5561

Table 14 Level 2 reconfigurations and costs for feeder at bus 13

No.	Switches to close	Switches to open	Number of level 2 load transfers	Cost
1	S12	S10	1	0.5749
2	S12, S13	S10, S11	2	0.5338
3	S12, S13	S9, S10	2	Infeasible
4	S12, S13	S9, S11	2	0.5837
5	S12	S9	1	Infeasible
6	S13	S9	1	Infeasible
7	—	—	0	0.2998
8	S13	S11	1	0.5385

Table 15 Level 2 reconfigurations and costs for feeder at bus 24

No.	Switches to close	Switches to open	Number of level 2 load transfers	Cost
1	S18, S19	S17, S16	2	0.5234
2	S18, S19	S15, S16	2	Infeasible
3	S18, S19	S15, S17	2	Infeasible
4	S19	S15	1	Infeasible
5	S19	S16	1	0.5611
6	—	—	0	0.2688
7	S18	S15	1	Infeasible
8	S18	S17	1	0.5161

Remember that for every feeder, only the optimal topology for each number of level 2 load transfers is used. So, the resulting candidate topologies for the three feeders are shown in Tables 16 – 18.

Table 16 Optimal level 2 reconfigurations for feeder at bus 37

No.	Switches to close	Switches to open	Number of level 2 load transfers
1	—	—	0
2	S27	S25	1
3	S26, S27	S23, S25	2

Table 17 Optimal level 2 reconfigurations and costs for feeder at bus 13

No.	Switches to close	Switches to open	Number of level 2 load transfers
1	—	—	0
2	S13	S11	1
3	S12, S13	S10, S11	2

Table 18 Optimal level 2 reconfigurations and costs for feeder at bus 24

No.	Switches to close	Switches to open	Number of level 2 load transfers
1	—	—	0
2	S18	S17	1
3	S18, S19	S16, S17	2

For the outage area, 16 radial topologies are found, which are shown in **Error! Not a valid bookmark self-reference.**. These topologies will be combined with level 2 candidate topologies to yield the overall system topologies.

Table 19 Switching operations for all level 1 reconfigurations for the test system

No.	Switches to close	Switches to open
1	S14, S20	S5
2	S14, S20	S4
3	S22, S14, S20	S4, S6
4	S22, S14, S20	S5, S6
5	S22, S14, S20	S6, S7
6	S22, S14, S20	S5, S7
7	S22, S14, S20	S4, S7
8	S14, S20	S7
9	S14	—
10	S22, S14	S4
11	S22, S14	S5
12	S22, S14	S6
13	S22, S20	S6
14	S22	—
15	S20	—
16	S22, S20	S7

7.3.2 Overall Topology Evaluation

The level 2 and level 1 reconfigurations found in the last section are combined to form overall system reconfiguration. There are 18 feasible reconfigurations with at most 2 level 2 load transfers. The reconfigurations are listed in Table 20 and Table 21 below. Specifically, Table 20 shows the individual and overall cost functions of all feasible reconfigurations and Table 21 shows the switching operations to achieve these topologies from the initial topology given in Figure 37. It is noted that the last two columns of the table use feeder head bus number to designate the respective feeder.

Table 20 All overall system reconfigurations ranked based on overall cost

Rank	NS	MG	LB	VD	SR	nL2LT	Loss	Sum
1	0.89	0.82	0.05	0.48	0.93	0.67	0.00	0.64
2	0.89	0.83	0.09	0.48	0.93	0.67	0.50	0.70
3	0.89	0.87	0.03	0.48	0.94	0.67	0.67	0.72
4	0.86	0.82	0.05	0.57	0.92	0.67	0.80	0.72
5	0.86	0.94	0.03	0.48	0.92	0.50	0.90	0.73
6	0.86	0.94	0.03	0.48	0.92	0.50	0.91	0.73
7	0.89	0.88	0.06	0.48	0.94	0.67	0.75	0.73
8	0.89	0.87	0.03	0.47	0.93	0.67	0.83	0.73
9	0.89	0.87	0.03	0.47	0.93	0.67	0.86	0.74
10	0.86	0.88	0.06	0.57	0.93	0.67	0.88	0.74
11	0.89	0.87	0.03	0.59	0.93	0.67	0.89	0.75
12	0.86	0.94	0.03	0.72	0.91	0.50	0.94	0.75
13	0.89	0.82	0.05	0.72	0.93	0.67	0.92	0.76
14	0.89	0.87	0.03	0.67	0.93	0.67	0.92	0.76
15	0.86	0.87	0.03	0.83	0.91	0.67	0.94	0.77
16	0.86	0.88	0.06	0.80	0.92	0.67	0.94	0.77
17	0.89	0.88	0.06	0.72	0.93	0.67	0.93	0.77
18	0.89	0.94	0.03	0.72	0.93	0.67	0.93	0.78

Table 21 Switching operations and related backup feeders used of all system reconfigurations

Rank	Switches to close	Switches to open	Level 1 backup feeders	Level 2 backup feeders
1	S14, S20, S22, S13, S18	S4, S6, S11, S17	13, 24, 37	22, 33
2	S14, S20, S22, S13, S18	S4, S7, S11, S17	13, 24, 37	22, 33

Table 21 (continued)

3	S14, S20, S22, S13, S27	S4, S7, S11, S25	13, 24, 37	22, 48
4	S14, S20, S13, S18	S4, S11, S17	13, 24	22, 33
5	S14, S20, S22, S13	S4, S6, S11	13, 24, 37	22
6	S14, S20, S22, S13	S4, S7, S11	13, 24, 37	22
7	S14, S20, S22, S13, S27	S4, S6, S11, S25	13, 24, 37	22, 48
8	S14, S20, S22, S12, S13	S4, S6, S10, S11	13, 24, 37	20, 22
9	S14, S20, S22, S12, S13	S4, S7, S10, S11	13, 24, 37	20, 22
10	S14, S22, S13, S27	S4, S11, S25	13, 37	22, 48
11	S14, S20, S22, S12, S13	S6, S7, S10, S11	13, 24, 37	20, 22
12	S14, S20, S22, S18	S5, S6, S17	13, 24, 37	33
13	S14, S20, S22, S13, S18	S5, S6, S11, S17	13, 24, 37	22, 33
14	S14, S20, S22, S18, S19	S5, S6, S16, S17	13, 24, 37	33, 35
15	S20, S22, S18, S19	S6, S16, S17	24, 37	33, 35
16	S14, S20, S18, S19	S5, S16, S17	13, 24	33, 35
17	S14, S20, S22, S18, S27	S5, S6, S17, S25	13, 24, 37	33, 48
18	S14, S20, S22, S26, S27	S5, S7, S23, S25	13, 24, 37	46, 48

7.4 Computation Results by Dynamic Programming

In this section, we examine the proposed DP-based DSR algorithm on the large system studied in this chapter. Since the system contains 27 switches, and it would be impractical to evaluate all 2^{27} potential topologies, a proper subsystem should be selected. This is a relevant problem for large distribution system where the outage area may be small but there exist many neighboring feeders where the de-energized loads can be transferred to. Picking the most appropriate feeders under this scenario is crucial for the successful implementation of the DSR problem.

It is noted that the exhaustive search results in Table 21 provides a way to obtain the subsystem. We check the candidate reconfigurations that only involve a subset of level 1 backup feeders. It can be seen from the table that the first three candidate topologies all use all three level 1 backup feeders, and the best reconfiguration that uses only two out of all three level 1 backup feeders is the fourth reconfiguration. To this end,

we select the subsystem of the entire system as shown in Figure 42, which excludes the level 1 backup feeder and neighboring level 2 backup feeders that are not used in the reconfiguration. It is hoped that the switching sequence generated by the DP-based algorithm leads to a favorable final topology. As will be verified, the proposed DP-based algorithm does generate a switching sequence that leads to the fourth reconfiguration shown in Table 21.

7.4.1 System Modeling

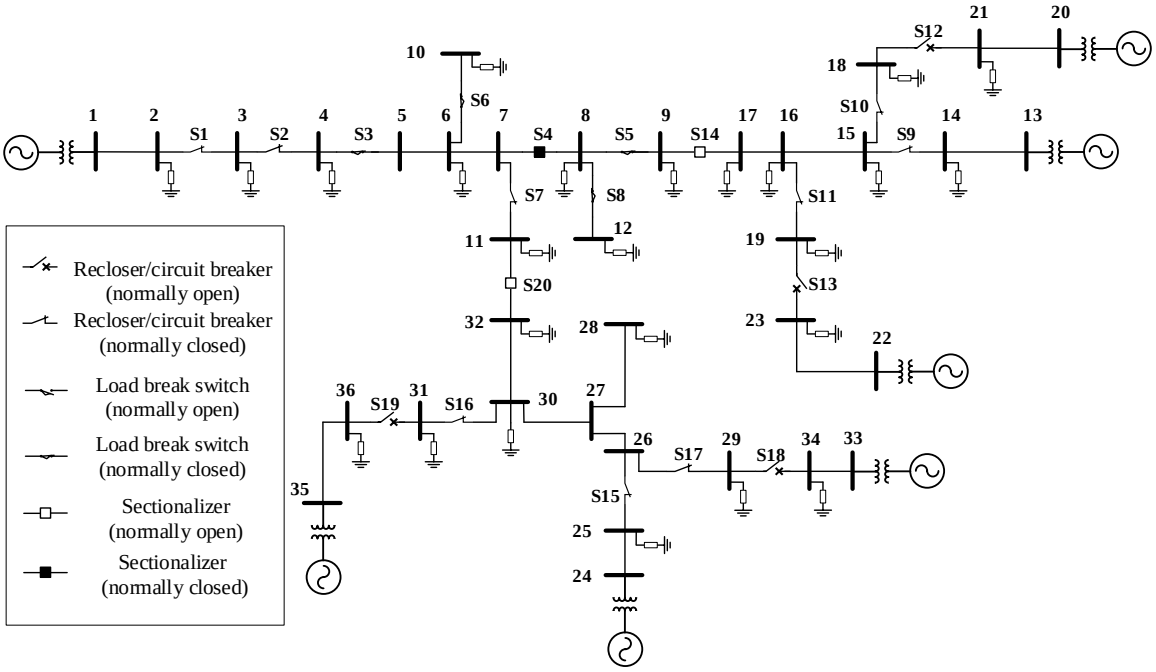

Figure 42 One-line diagram of the 36-bus-20-switch test distribution.

The one-line diagram of the test distribution system is shown in Figure 42. The detailed system parameters can be found in Appendix B. The system base MVA is 100 MVA. Switches S1, S9, S12, S13, S15, S18, and S19 are circuit breakers with current upper limit of 20 kA, S2, S7, S10, S11, S16, and S17 are reclosers with current upper

limit of 10 kA, S3, S5, S6, and S8 are load break switches and their current upper limits are 800 A. Switches S4, S14, and S20 are sectionalizers, which can only make or break at no-load, so their current upper limit is 0 A.

To account for the system operational constraints, we impose the following penalty term for each bus voltage and line current constraint violation which will be added to the state's cost of operation:

$$\text{penalty} = \begin{cases} 10 \mid v_{\text{actual}} - v_{\text{critical}} \mid, & \text{if } v_{\text{actual}} \text{ violates the constraint} \\ 0, & \text{otherwise} \end{cases} \tag{47}$$

where v can be either bus voltage magnitude or line current magnitude, and the subscripts 'actual' and 'critical' refer to the actual and critical (minimum or maximum bus voltage magnitude, or maximum line current magnitude) per unit values, respectively. The radiality constraint is also imposed for each state: a penalty term of 0.1 p.u. is added to the cost of operation if the topology is not radial.

Suppose a fault occurs between S2 and S3. In response to the fault, recloser S2 opens automatically to isolate buses 5 – 12. The initial post-fault topology is shown in Figure 43. The DP-based service restoration algorithm will be initiated at this moment to restore the interrupted loads. Therefore, the control variable $u(0)$ at stage 0 is [1, 0 ,1, 1, 1, 1, 1, 1, 1, 1, 1, 0, 0, 0, 1, 1, 1, 0, 0, 0]. By definition, the cost of operation and total cost in this state are both 0.

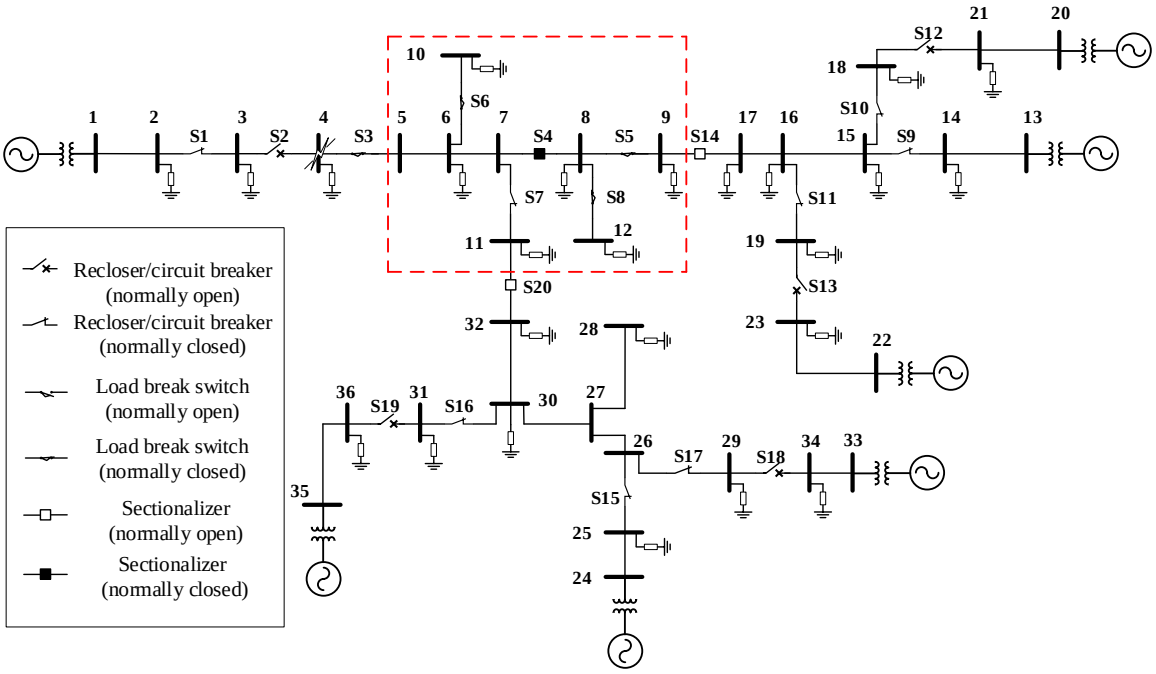

Figure 43 One-line diagram of the test distribution system when a fault occurs between S2 and S3. Recloser S2 opens automatically.

7.4.2 Initialization

For each stage i, we need to specify the control variable $u(i)$ and cost of operation Cost[i][j] for all states j. Since there are 20 switches, the total number of states at one stage is 2^{20} = 1048576. Among the 1048576 states, 361780 of them are not feasible either due to failure of fault isolation or power flow divergence. After eliminating them, the resulting DP formulation has 686796 states at each stage.

For this system, the initialization is the most time-consuming part of the algorithm due to the large number of switches. A full-fledged power flow algorithm needs to be performed for each candidate topology whose fault is isolated in order to check for power flow convergence and potential constraint violation. For this system, 686796 power flows

need to be performed, which takes 1722.4 seconds (= 28.7 minutes) using MATLAB on a 64-bit computer with Intel Core i7 CPU 2.60GHz processor and 4 GB RAM.

There are ways to improve the computation speed of the algorithm. For instance, the costs of operation don't have to be evaluated for all states at once during the initialization stage. Instead, they can be evaluated incrementally during the forward computation stage when they are reached by neighboring states for the first time. Some states with high cost of operation can be disregarded in the process and subsequently the power flow evaluation can be omitted. Another approach is to apply faster power flow routines at the price of slightly lower computational accuracy. The above acceleration strategies will be pursued as a future research direction and also discussed in more detail at the end the thesis in CHAPTER 8.

7.4.3 Forward Computation and Stopping Criterion

Since the system is large, the stopping criterion is adjusted so that the algorithm stops when the optimal state (the state with the minimum total cost among all states in the stage) does not change for 15 stages. Based on the stopping criterion, the algorithm stops at stage 35, and the optimal state is 1.05.

Compared to the initialization step, the forward computation is computationally friendlier, which takes 238.4 seconds.

Figure 45 to Figure 53 show the DP computation for states from stage 0 to 35. Note that the algorithm does not stop until stage 35 based on the stopping criterion but

the algorithm converges to the optimal state relatively fast (at stage 12). Table 22 below shows the optimal state at each stage and the associated optimal total cost:

Table 22 State number with minimum OptimalTotalCost and associated OptimalTotalCost for stages 1 to 35

Stage number	State number with minimum OptimalTotalCost	Minimum OptimalTotalCost (p.u.)
1	1, 588481, 642406, 669286, 678060, 683235, 684989	0.07
2	1, 522945, 555713, 572097, 580289, …, 684989 (22 states)	0.14
3	1, 490177, 506561, 514753, 518849, …, 684989 (42 states)	0.21
4	1, 473793, 481985, 486081, 490177, …, 684989 (57 states)	0.28
5	1, 465601, 469697, 473793, 477889, …, 684989 (63 states)	0.35
6	1, 461505, 465601, 469697, 473793, …, 684989 (64 states)	0.42
7	1, 461505, 465601, 469697, 473793, …, 684989 (64 states)	0.49
8	1, 461505, 465601, 469697, 473793, …, 684989 (64 states)	0.56
9	498049, 506241, 514433, 522625, 623233, 628761, 636673, 642201	0.61
10	498049, 506241, 514433, 522625, 623233, 628761, 636673, 642201	0.65
11	498049, 506241, 514433, 522625, 623233, 628761, 636673, 642201	0.69
12	555696, 572080, 584368	0.73
13	555696, 572080, 584368	0.75
14	555696, 572080, 584368	0.77
15	555696, 572080, 584368	0.79
16	555696, 572080, 584368	0.81
17	555696, 572080, 584368	0.83
18	555696, 572080, 584368	0.85
19	555696, 572080, 584368	0.87
20	555696, 572080, 584368	0.89
21	522622	0.91
22	522622	0.92
23	522622	0.93
24	522622	0.94

Table 22 (continued)

25	522622	0.95
26	522622	0.96
27	522622	0.97
28	522622	0.98
29	522622	0.99
30	522622	1.00
31	522622	1.01
32	522622	1.02
33	522622	1.03
34	522622	1.04
35	522622	1.05

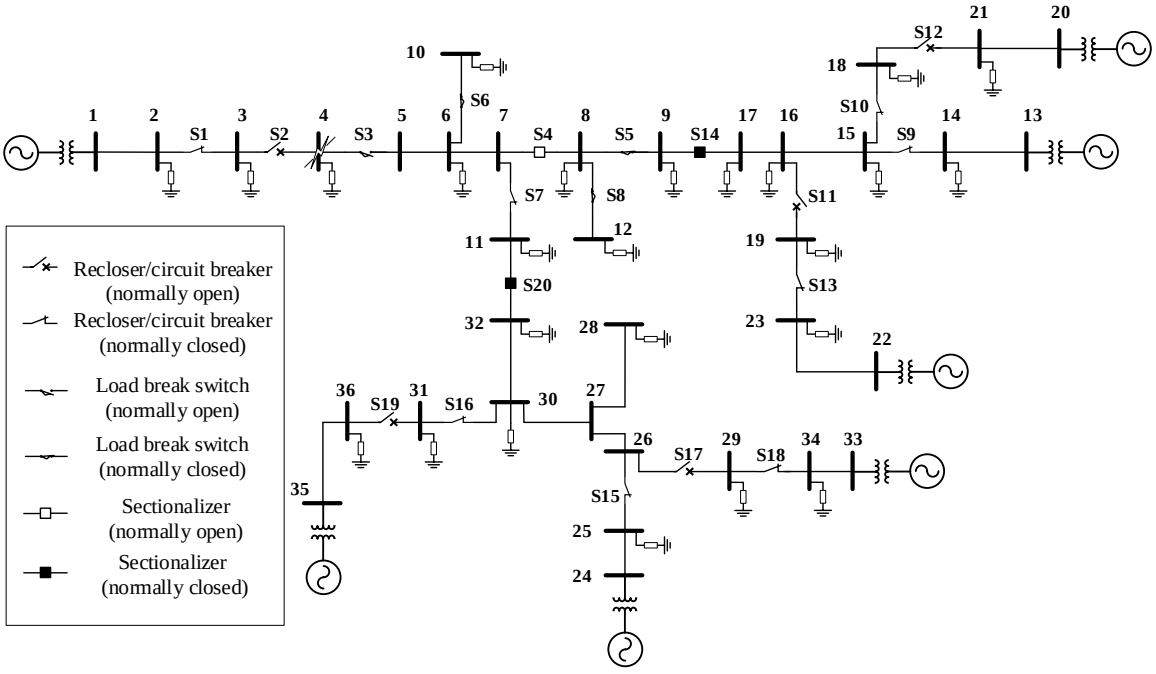

Figure 44 One-line diagram of the final topology for the test distribution system using DP-based DSR algorithm.

Particularly, the figures show the optimal trajectory in red by backtracking from the optimal state in stage 35. The optimal trajectory is 1 – 642406 – 642078 – 642160 – 640848 – 640889 – 640201 – 522625 – 522617 – 522621 – 522589 – 522590 – 522622 – 522622 – 522622 – 522622 – 522622 – 522622 – 522622 – 522622 – 522622 – 522622 –

522622 – 522622 – 522622 – 522622 – 522622 – 522622 – 522622 – 522622 – 522622 – 522622 – 522622 – 522622 – 522622 – 522622. After eliminating the transitions from a state to itself, the optimal switching sequence is 1 – 642406 – 642078 – 642160 – 640848 – 640889 – 640201 – 522625 – 522617 – 522621 – 522589 – 522590 – 522622, which corresponds to the following switching actions: open S4, open S11, close S13, open S9, close S14, close S9, open S3, open S17, close S18, open S15, close S20, and close S15. The final topology is shown in Figure 44.

It is seen that the final topology is the same as the fourth topology obtained by exhaustive search in Table 21.

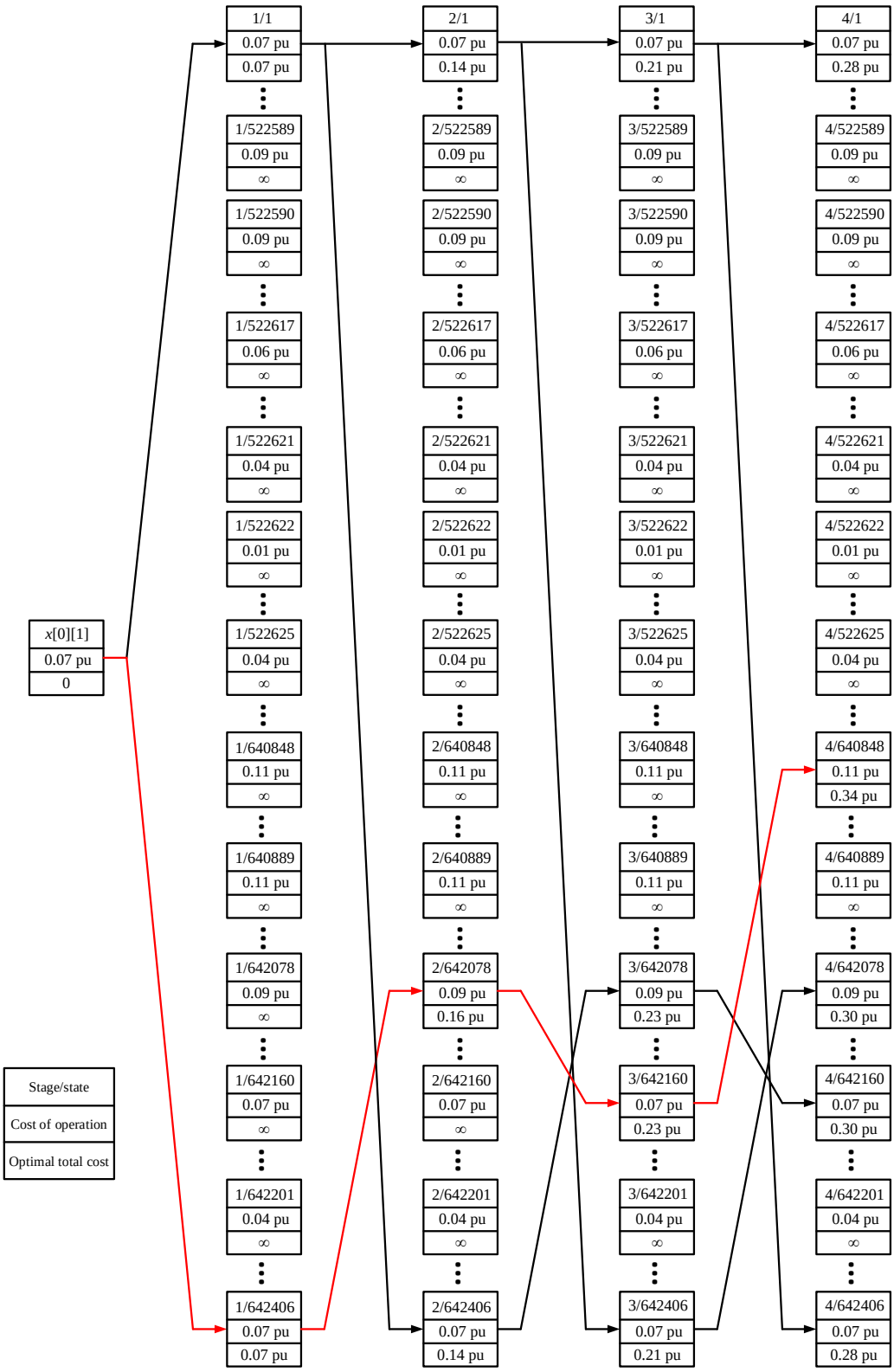

Figure 45 DP computation for the example system from stage 0 to 4 (optimal trajectory marked by red).

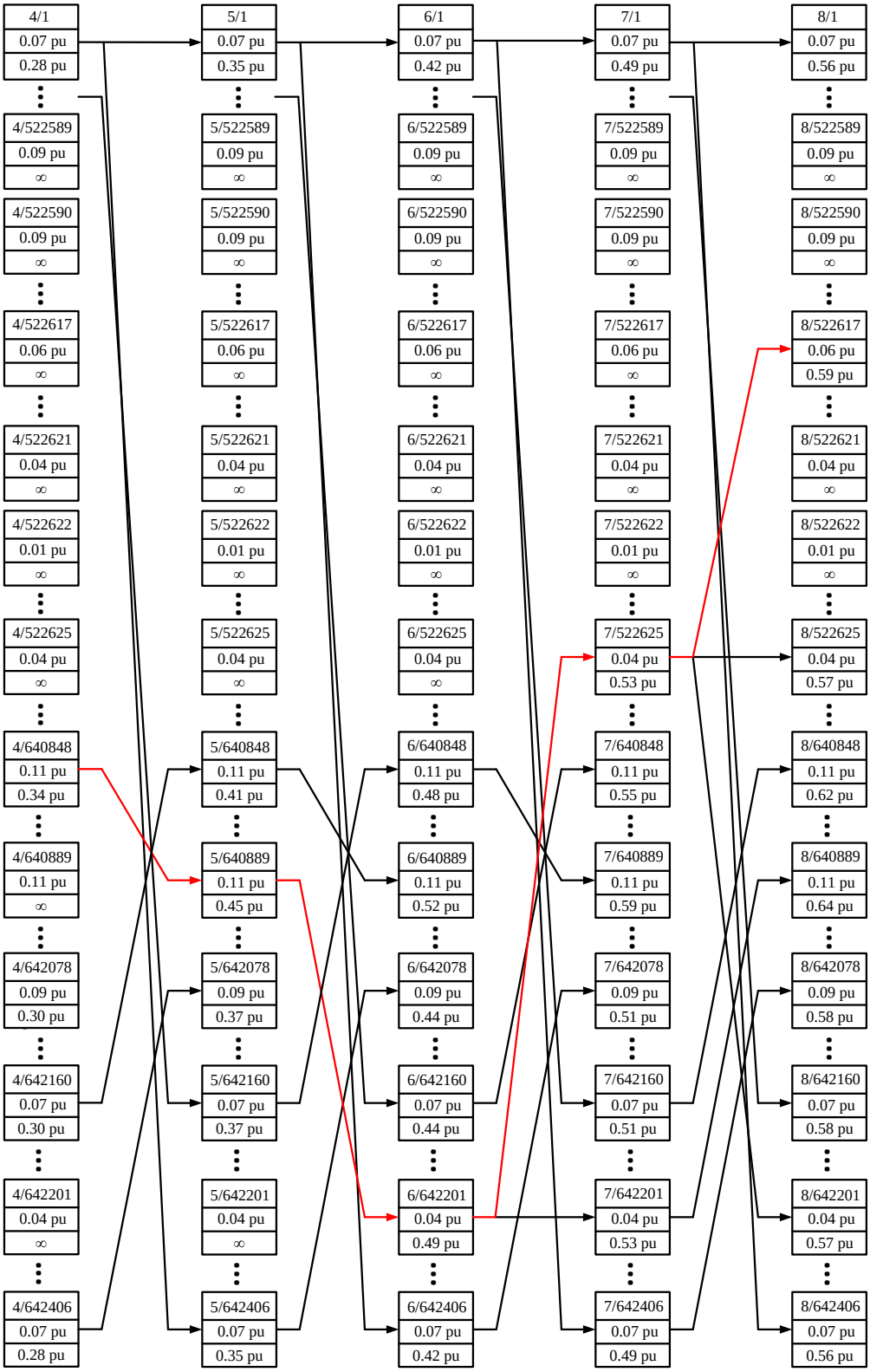

Figure 46 DP computation for the example system from stage 4 to 8 (optimal trajectory marked by red).

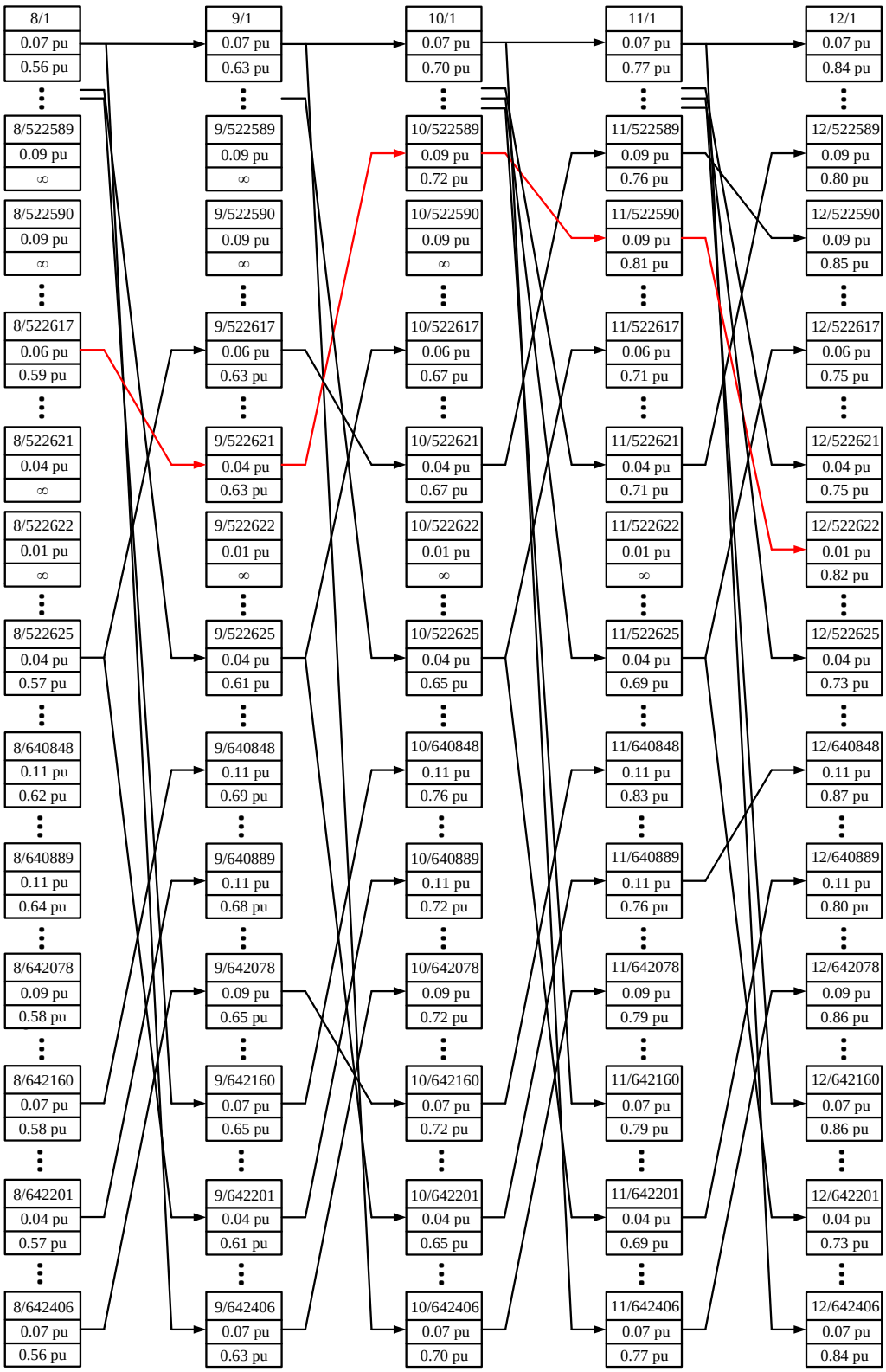

Figure 47 DP computation for the example system from stage 8 to 12 (optimal trajectory marked by red).

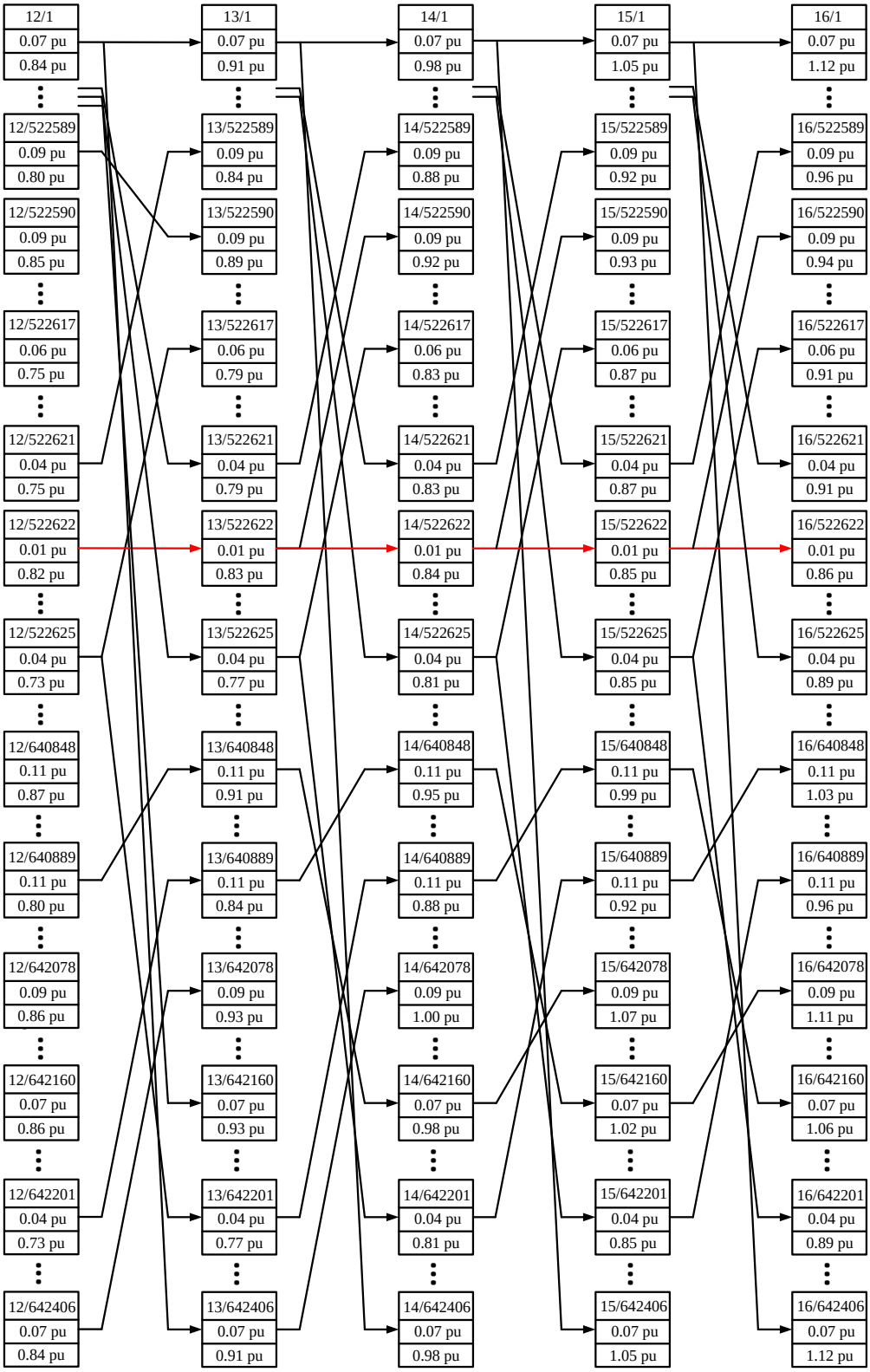

Figure 48 DP computation for the example system from stage 12 to 16 (optimal trajectory marked by red).

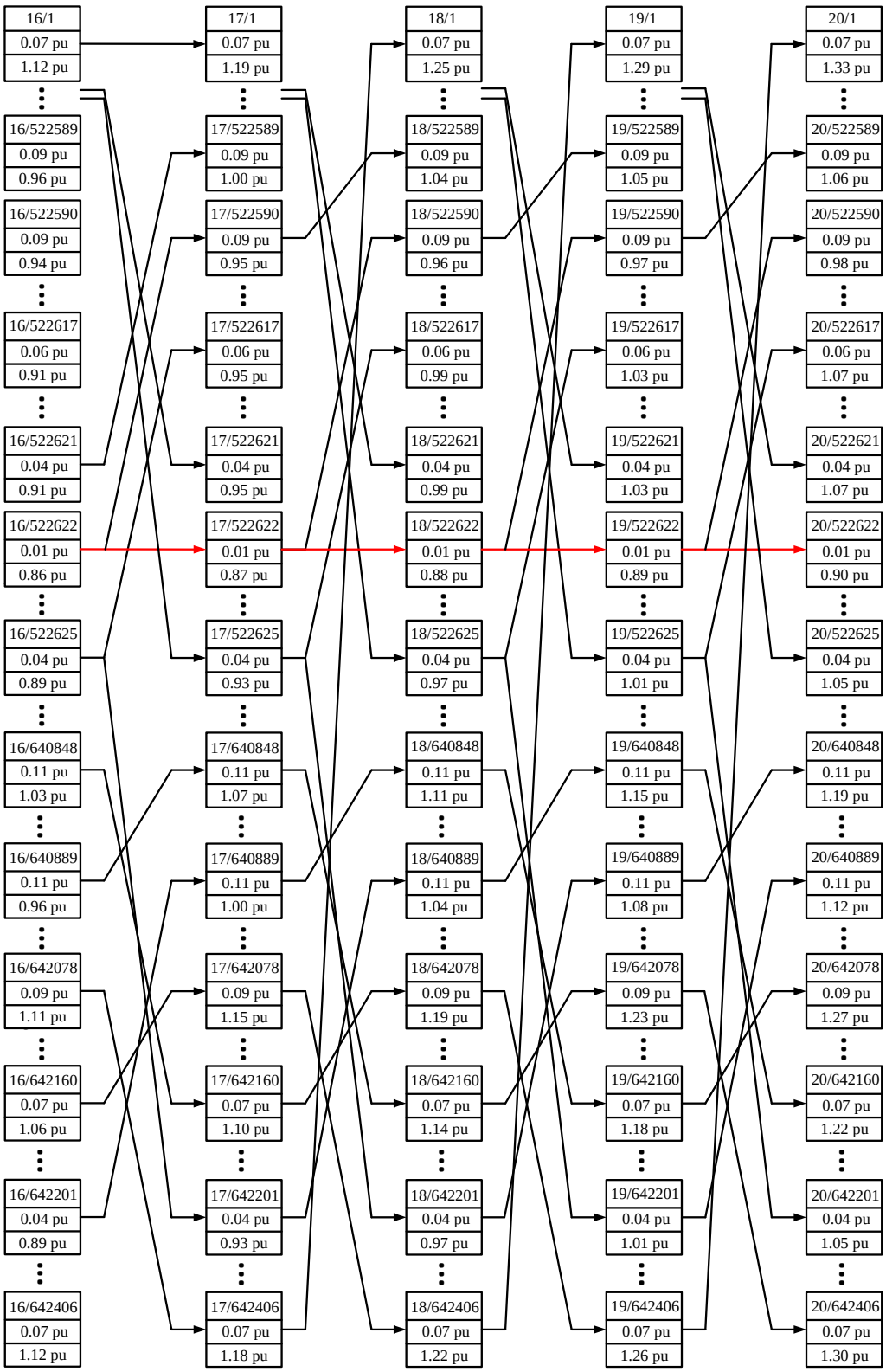

Figure 49 DP computation for the example system from stage 16 to 20 (optimal trajectory marked by red).

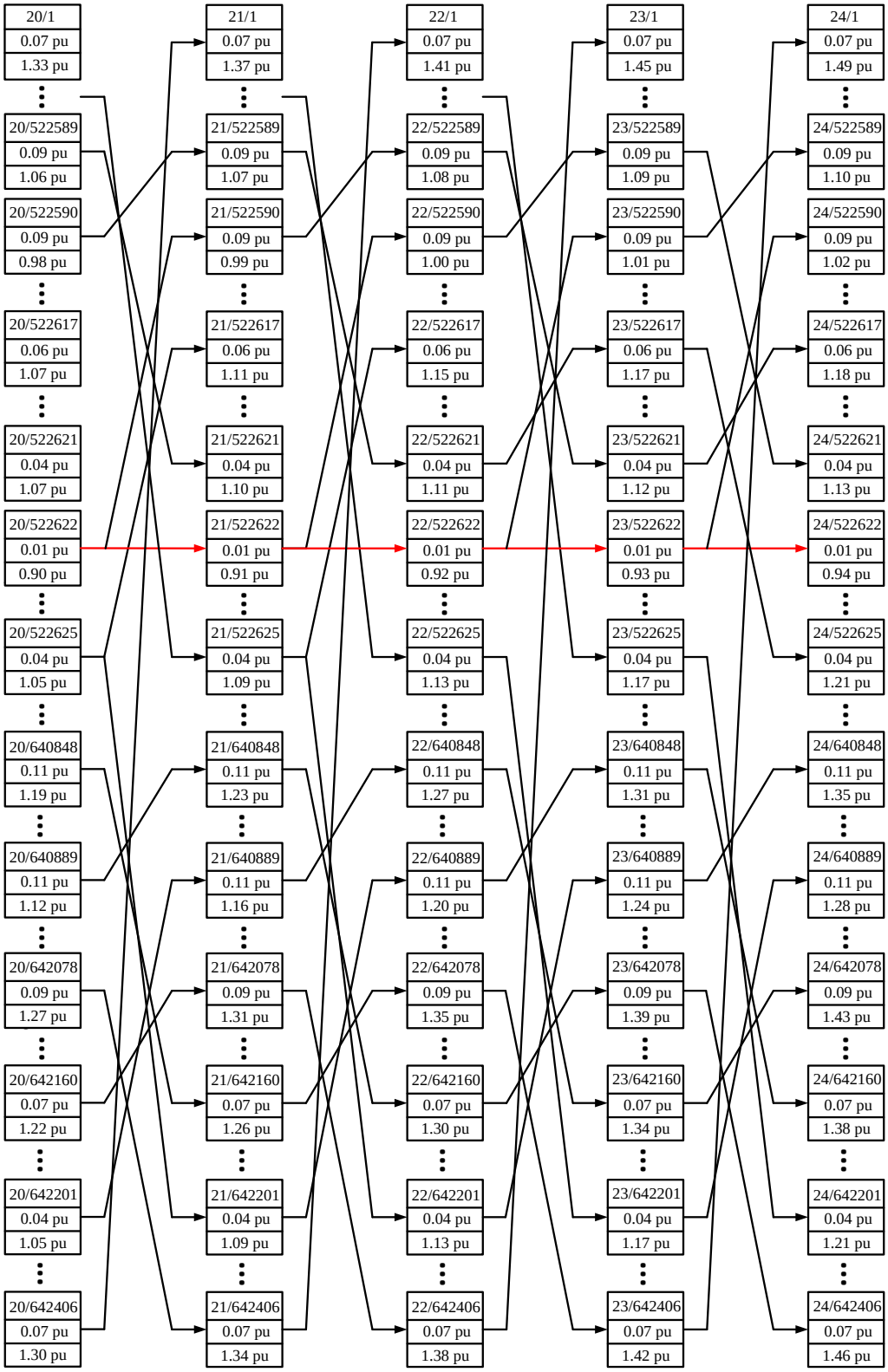

Figure 50 DP computation for the example system from stage 20 to 24 (optimal trajectory marked by red).

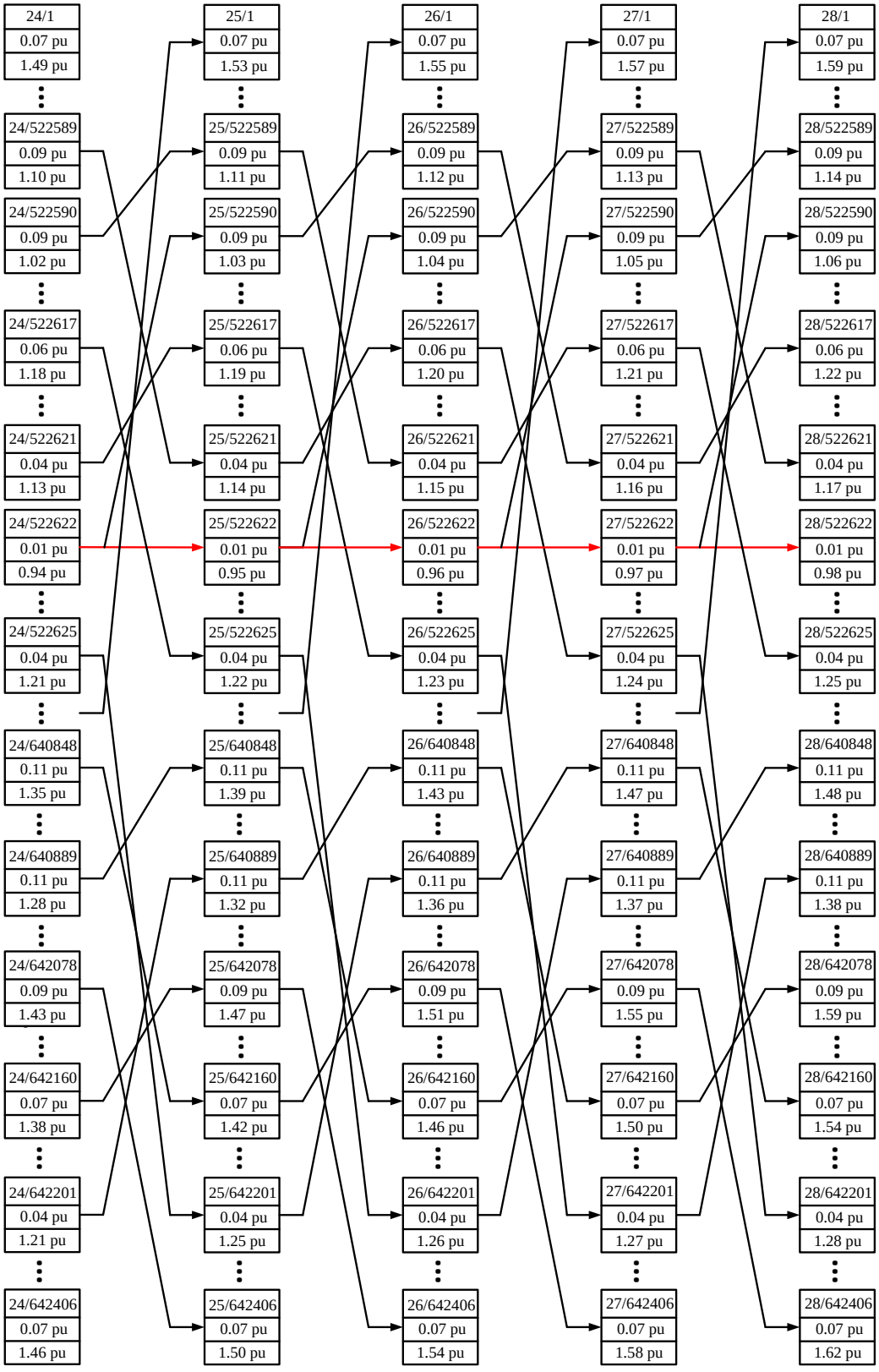

Figure 51 DP computation for the example system from stage 24 to 28 (optimal trajectory marked by red).

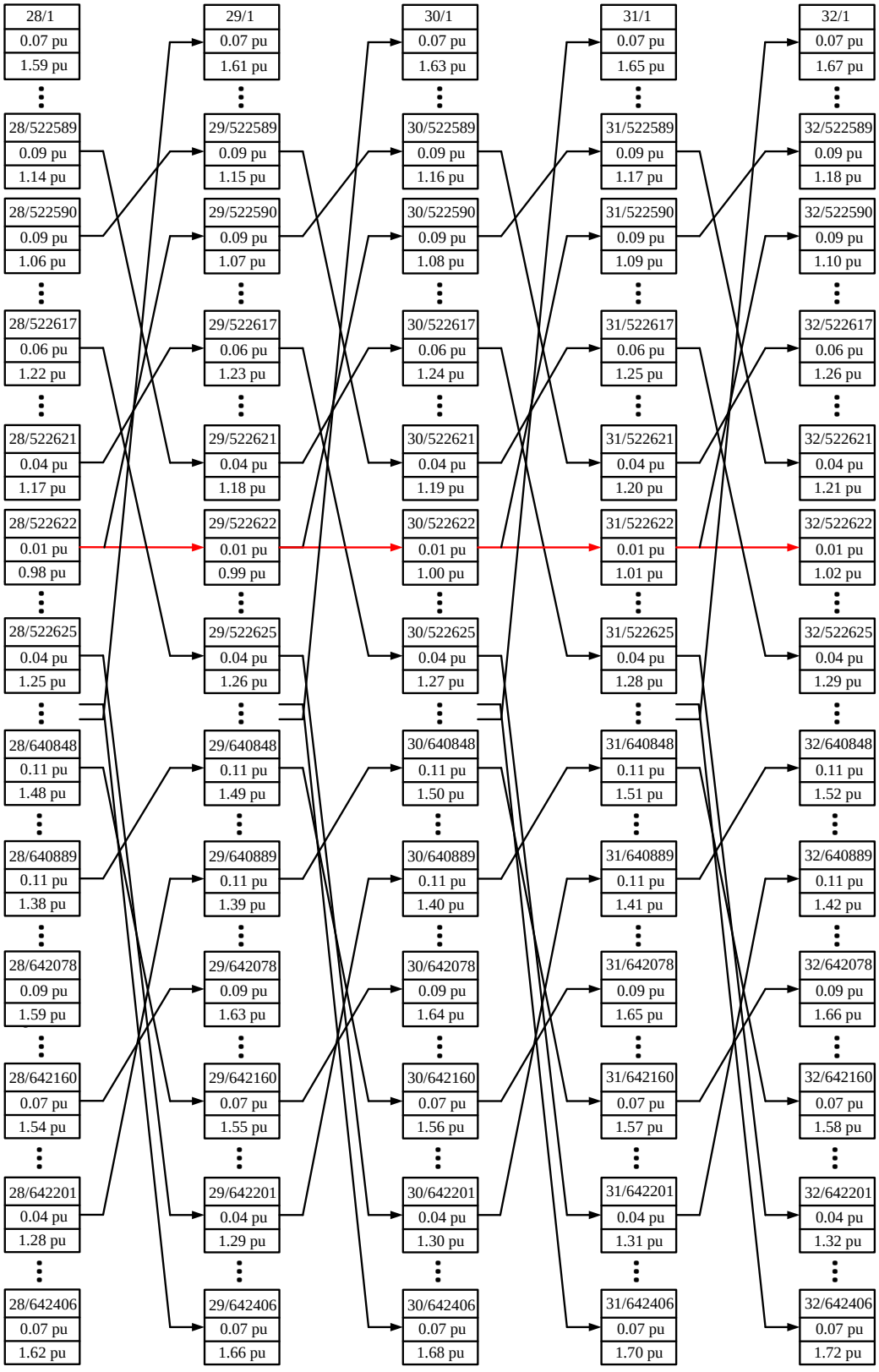

Figure 52 DP computation for the example system from stage 28 to 32 (optimal trajectory marked by red).

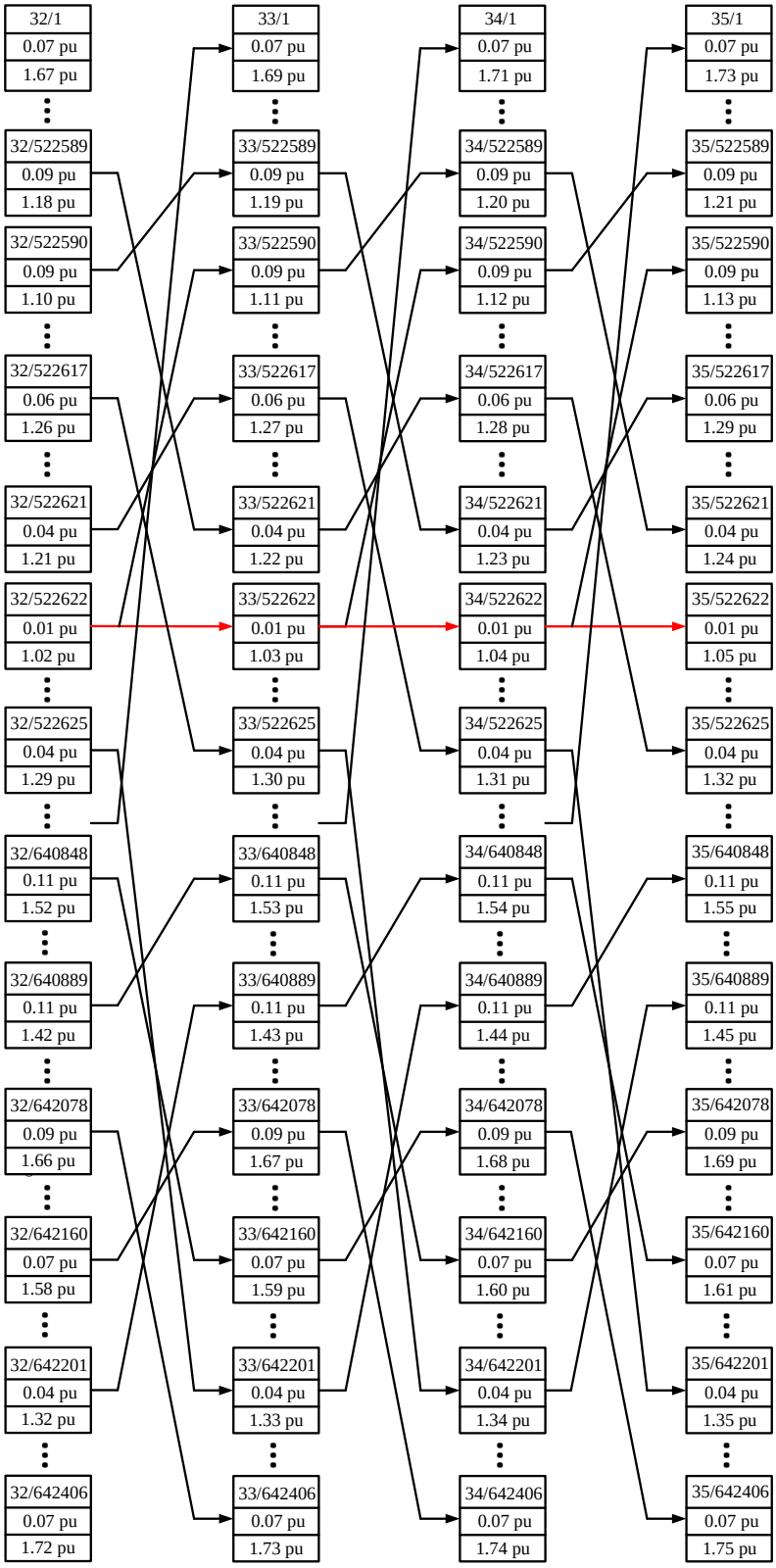

Figure 53 DP computation for the example system from stage 32 to 35 (optimal trajectory marked by red).

7.5 Summery

In this chapter, the DP-based DSR algorithm is tested on a relatively large system with 20 switches and is benchmarked with a two-level exhaustive search method. As shown in the simulation results, the proposed DP-based algorithm successfully obtains the optimal final topology found by the exhaustive search method and derives the 12-step optimal switching sequences leading to the final topology. As expected, the computation time of the exhaustive search method is shorter, since only potential feasible radial topologies are examined as opposed to examining both radial and meshed topologies for the DP-based approach. One proposed solution for reducing computation time of the DP-based algorithm is to limit the network size based on the final topology obtained by the exhaustive search. The most-time consuming part of the DP-based algorithm is the power flow calculation for all potential feasible topologies, which can be greatly expediated using simplified power flow routines or even closed-form power flow approximations.

CHAPTER 8. CONCLUSION AND FUTURE WORK DIRECTIONS

8.1 Conclusion

The contributions of this dissertation are: (1) development of an innovative DP-based DSR algorithm considering switch characteristics, which is capable of deriving the optimal switching sequence leading to the post-fault optimal system topology; (2) extension of the algorithm to consider system operational constraints including nodal voltage, line current, and radiality constraints through addition of a penalty term; (3) development of an efficient exhaustive search algorithm for single-stage DSR problem based on sequential exhaustive search, which can be used to aid the appropriate subsystem determination of the proposed DP-based algorithm, and (4) a distribution state estimation algorithm which leverages the switch measurements to obtain system states.

The proposed DP-based DSR algorithm does not require knowledge or estimates on the maximum number of switching operations, and can flexibly incorporate complex device models, contrary to the MIP-based counterparts. Instead of merely accounting for cumulative load interruption in the cost function, other factors such as switching costs of different switches and priority of different loads can also be incorporated.

8.2 Future Work Directions

The effectiveness of the proposed DP-based DSR framework on a 20-switch system has been validated in CHAPTER 7. Even though the proposed method can be reliably used as a proper offline operation tool, there remain multiple ways to improve its

scalability. First of all, not all states need to be initialized at the beginning. Similar to the branch-and-bound technique in integer programming, states with sufficiently high costs can be pruned and no further computation needs to be performed along those trajectories. Therefore, states that are only neighboring to high-cost states may be eliminated without power flow computation. Second, instead of using full power flow to check topology feasibility and constraint violation, there are many fast power flow routines and linear power flow approximations tailored for distribution systems [6, 63]. It can be expected that these approximations will significantly reduce the computation time of the initialization step, which is the most time-consuming part of the algorithm especially for system with large number of switches.

Another future direction is to incorporate more elaborate system devices, especially those with inter-temporal dependencies, such as dynamic load, DGs, and ESS, in the DP-based service restoration algorithm. The sequential service restoration approach provides an excellent framework to encompass the dynamic nature of the system and takes care of components that are time-dependent in the DSR process. This perspective has been considered in some of the existing publications [40–41] but has not been subjected to the examination of the proposed DP-based approach.

The proposed DP-based framework can be applied to other planning and operation problems that involve sequential or inter-temporal decision making, such as distribution system volt/var control, demand response, and microgrid black start.

Appendix A. Test System Data for State Estimation

The state estimation algorithm for distribution system discussed in CHAPTER 6 is demonstrated using a 33-bus system presented in [6]. The system is a hypothetical 12.66 kV distribution system with 1 feeder and 32 load buses. The base power is 1 MVA. Bus 0 is the feeder head bus which is modeled as a constant voltage source whose voltage is 1 p.u. The remaining 32 buses are modeled as PQ buses with base voltage 12.66 kV. The topology of the system is shown in Figure 54. There are five normally open tie switches, their corresponding branches are (7,20), (8,14), (11,21), (17,32), (24,28). The system line impedance and load data are shown in Table 23 and Table 24, respectively.

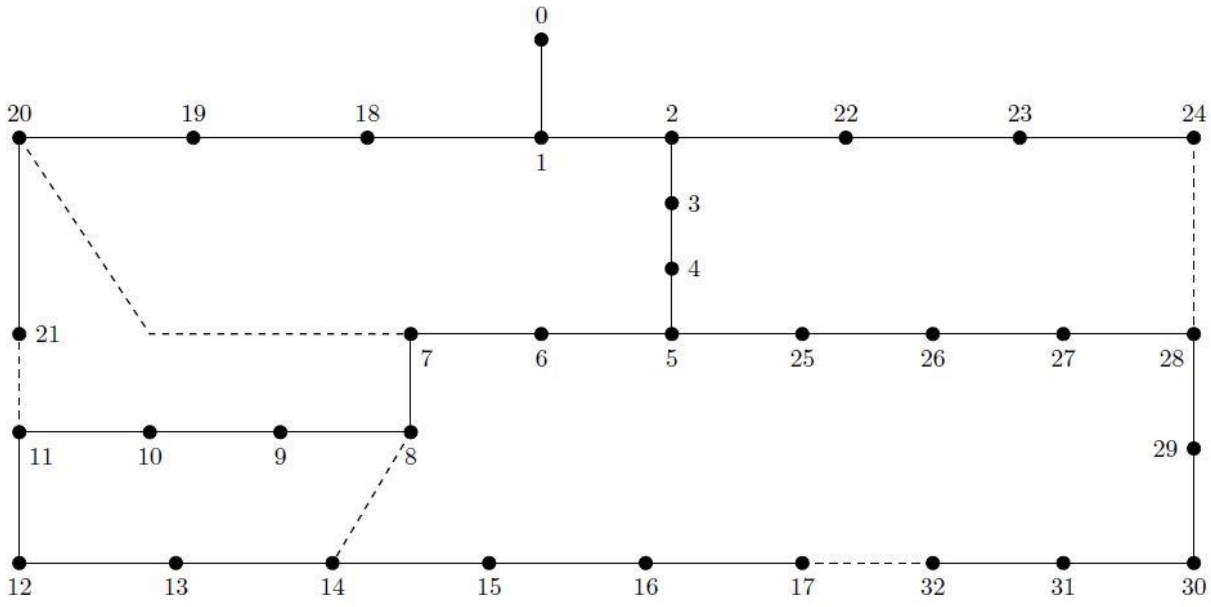

Figure 54 Topology of 33-bus system from [6].

Table 23 Line Impedance Data of the 33-Bus System From [6]

From bus	To bus	R (Ω)	X (Ω)	From bus	To bus	R (Ω)	X (Ω)
0	1	0.0922	0.0470	16	17	0.7320	0.5740
1	2	0.4930	0.2511	1	18	0.1640	0.1565
2	3	0.3660	0.1864	18	19	1.5042	1.3554
3	4	0.3811	0.1941	19	20	0.4095	0.4784
4	5	0.8190	0.7070	20	21	0.7089	0.9373
5	6	0.1872	0.6188	2	22	0.4512	0.3083
6	7	0.7114	0.2351	22	23	0.8980	0.7091
7	8	1.0300	0.7400	23	24	0.8960	0.7011
8	9	1.0440	0.7400	5	25	0.2030	0.1034
9	10	0.1966	0.0650	25	26	0.2842	0.1447
10	11	0.3744	0.1238	26	27	1.0590	0.9337
11	12	1.4680	0.1550	27	28	0.8042	0.7006
12	13	0.5416	0.7129	28	29	0.5075	0.2585
13	14	0.5910	0.5260	29	30	0.9744	0.9630
14	15	0.7463	0.5450	30	31	0.3105	0.3619
15	16	1.2890	1.7210	31	32	0.3410	0.5302

Table 24 System Load Data of the 33-Bus System From [6]

Bus No.	P_L (kW)	Q_L (kVAr)	Bus No.	P_L (kW)	Q_L (kVAr)
1	100.00	60.00	17	90.00	40.00
2	90.00	40.00	18	90.00	40.00
3	120.00	80.00	19	90.00	40.00
4	60.00	30.00	20	90.00	40.00
5	60.00	20.00	21	90.00	40.00
6	200.00	100.00	22	90.00	50.00
7	200.00	100.00	23	420.00	200.00
8	60.00	20.00	24	420.00	200.00
9	60.00	20.00	25	60.00	25.00
10	45.00	30.00	26	60.00	25.00
11	60.00	35.00	27	60.00	20.00
12	60.00	35.00	28	120.00	70.00
13	120.00	80.00	29	200.00	600.00
14	60.00	10.00	30	150.00	70.00
15	60.00	20.00	31	210.00	100.00
16	60.00	20.00	32	60.00	40.00

Appendix B. KEPCO Test System Data

The KEPCO test system data used in CHAPTER 7 is presented below. The system is a hypothetical distribution system with 12 feeders, 49 buses, and 27 switches. The base power is 100 MVA. Buses 1, 13, 20, 22, 24, 33, 35, 37, 46, and 48 are feeder head buses which are modeled as constant voltage sources whose voltage is 1 p.u. The remaining 37 buses are modeled as PQ buses with base voltage 13.8 kV.

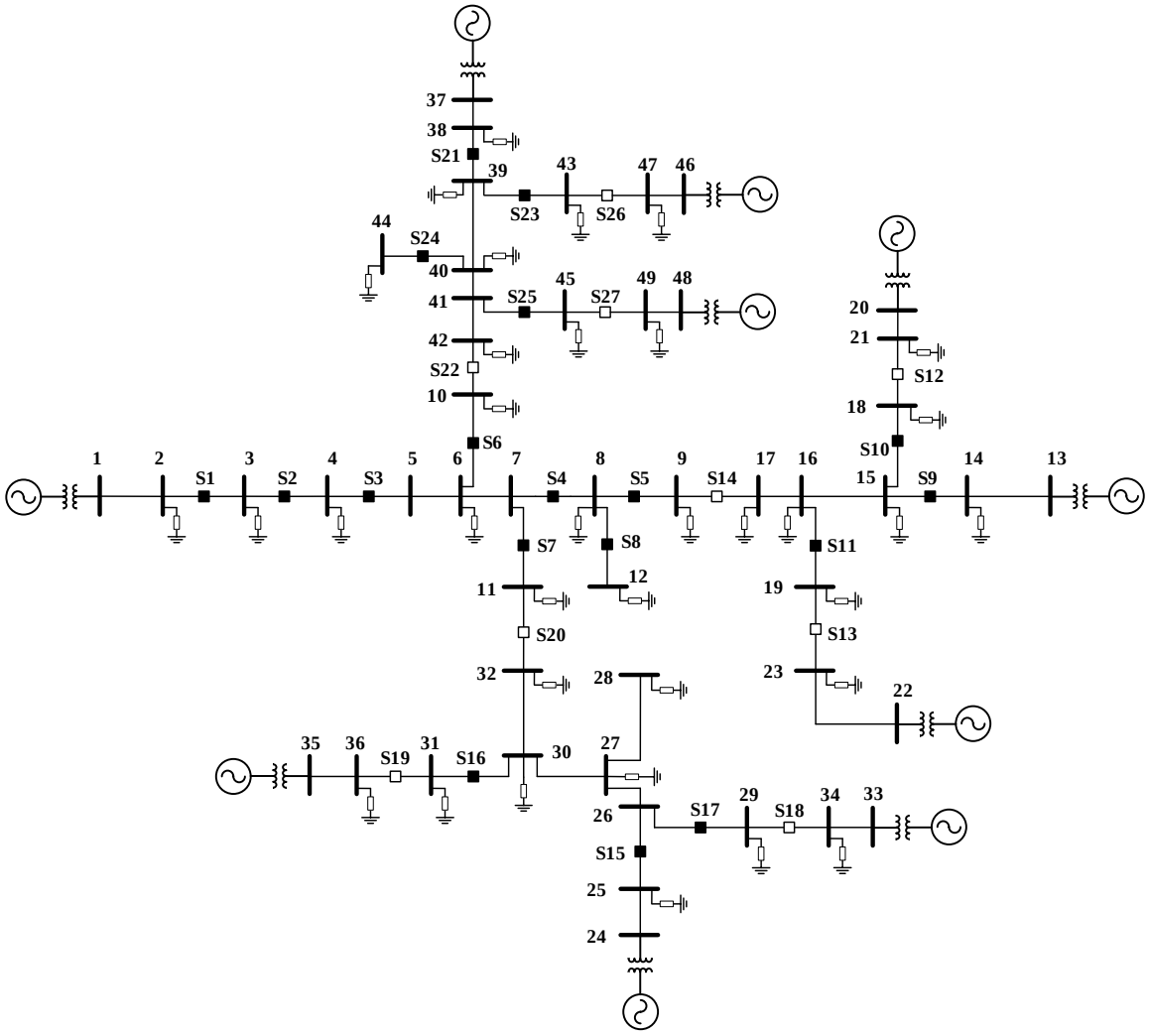

Figure 55 One line diagram of the 10-feeder system with 49 buses and 27 switches.

The topology of the system is shown in Figure 55. There are nine normally open tie switches: S14, S20, S22, S9, S13, S18, S19, S26, and S27. The system line data and load data are shown in Table 25 and Table 26, respectively. The switch reliability index in the last column of Table 25 is used in the exhaustive search method in CHAPTER 7 to rank candidate reconfigurations.

Table 25 Line Data of the 49-Bus System

From bus	To bus	R (Ω)	X (Ω)	Current capacity (kA)	Switch reliability
1	2	0.0661	0.1421	0.439	—
2	3	0.1322	0.2841	0.439	1
3	4	0.1322	0.2841	0.439	1
4	5	0.1322	0.2841	0.439	1
5	6	0.0661	0.1421	0.439	—
6	7	0.0661	0.1421	0.439	—
7	8	0.1982	0.4262	0.439	1
8	9	0.2870	0.4624	0.439	1
6	10	0.2209	0.3203	0.439	1
7	11	0.2209	0.3203	0.439	1
8	12	0.2209	0.3203	0.439	1
13	14	0.0661	0.1421	0.439	—
14	15	0.1322	0.2841	0.439	1
15	16	0.1322	0.2841	0.439	—
16	17	0.1765	0.3022	0.439	—
15	18	0.2209	0.3203	0.439	1
16	19	0.2209	0.3203	0.439	1
18	21	0.1765	0.3022	0.439	2
20	21	0.0661	0.1421	0.439	—
19	23	0.1765	0.3022	0.439	3
22	23	0.0661	0.1421	0.439	—
9	17	0.2209	0.3203	0.439	3
24	25	0.0661	0.1421	0.439	—
25	26	0.1322	0.2841	0.439	1
26	27	0.0661	0.1421	0.439	—
27	28	0.1765	0.3022	0.439	—
27	30	0.1322	0.2841	0.439	—
30	31	0.1765	0.3022	0.439	1
30	32	0.1765	0.3022	0.439	—
26	29	0.1765	0.3022	0.439	1
29	34	0.1765	0.3022	0.439	2

Table 25 (continued)

33	34	0.0661	0.1421	0.439	—
31	36	0.1765	0.3022	0.439	3
35	36	0.0661	0.1421	0.439	—
11	32	0.2209	0.3203	0.439	1
37	38	0.0661	0.1421	0.439	—
38	39	0.1322	0.2841	0.439	1
39	40	0.1322	0.2841	0.439	—
40	41	0.0661	0.1421	0.439	—
41	42	0.1765	0.3022	0.439	—
40	44	0.2209	0.3203	0.439	1
39	43	0.2209	0.3203	0.439	1
43	47	0.1765	0.3022	0.439	2
47	46	0.0661	0.1421	0.439	—
41	45	0.2209	0.3203	0.439	1
45	49	0.1765	0.3022	0.439	3
49	48	0.0661	0.1421	0.439	—
42	10	0.2209	0.3203	0.439	2

Table 26 System Load Data of the 49-Bus System

Bus No.	P_L (MW)	Q_L (MVAr)	V_{min} (p.u.)	V_{max} (p.u.)
1	0	0	0.95	1.05
2	1.00	0	0.95	1.05
3	1.00	0	0.95	1.05
4	1.00	0	0.95	1.05
5	0	0	0.95	1.05
6	1.00	0	0.95	1.05
7	0	0	0.95	1.05
8	1.00	0	0.95	1.05
9	1.00	0	0.95	1.05
10	1.00	0	0.95	1.05
11	1.00	0	0.95	1.05
12	1.00	0	0.95	1.05
13	0	0	0.95	1.05
14	3.00	0	0.95	1.05
15	1.00	0	0.95	1.05
16	1.00	0	0.95	1.05
17	1.00	0	0.95	1.05
18	1.00	0	0.95	1.05
19	3.00	0	0.95	1.05
20	0	0	0.95	1.05
21	6.00	0	0.95	1.05
22	0	0	0.95	1.05

Table 26 (continued)

23	6.00	0	0.95	1.05
24	0	0	0.95	1.05
25	1.00	0	0.95	1.05
26	0	0	0.95	1.05
27	1.00	0	0.95	1.05
28	1.00	0	0.95	1.05
29	2.00	0	0.95	1.05
30	1.00	0	0.95	1.05
31	1.00	0	0.95	1.05
32	1.00	0	0.95	1.05
33	0	0	0.95	1.05
34	6.00	0	0.95	1.05
35	0	0	0.95	1.05
36	7.00	0	0.95	1.05
37	0	0	0.95	1.05
38	1.00	0	0.95	1.05
39	1.00	0	0.95	1.05
40	1.00	0	0.95	1.05
41	0	0	0.95	1.05
42	1.00	0	0.95	1.05
43	1.00	0	0.95	1.05
44	1.00	0	0.95	1.05
45	2.00	0	0.95	1.05
46	0	0	0.95	1.05
47	8.00	0	0.95	1.05
48	0	0	0.95	1.05
49	8.00	0	0.95	1.05

REFERENCES

[1] J. Li, X.-Y. Ma, C.-C. Liu, and K. P. Schneider, "Distribution system restoration with microgrids using spanning tree search," *IEEE Trans. Power Syst.*, vol. 29, no. 6, pp. 3021–3029, Nov. 2014.

[2] A. Merlin and H. Back, "Search for a minimal-loss operating spanning tree configuration in an urban power distribution system," in *Proc. 5th Power System Computation Conf. (PSCC)*, Cambridge, UK, 1975, pp. 1–8.

[3] C.-C. Liu, S. J. Lee, and S. S. Venkata, "An expert system operational aid for restoration and loss reduction of distribution systems," *IEEE Trans. Power Syst.*, vol. 3, no. 2, pp. 619–625, May 1988.

[4] Y.-L. Ke, "Distribution feeder reconfiguration for load balancing and service restoration by using G-nets inference mechanism," *IEEE Trans. Power Syst.*, vol. 19, no. 3, pp. 1426–1433, Jul. 2004.

[5] Y.-C. Chuang, Y.-L. Ke, C.-S. Chen, and Y.-L. Chen, "Rule-expert knowledge-based Petri net approach for distribution system temperature adaptive feeder reconfiguration," *IEEE Trans. Power Syst.*, vol. 21, no. 3, pp. 1362–1370, Aug. 2006.

[6] M. E. Baran and F. F. Wu, "Network reconfiguration in distribution systems for loss reduction and load balancing," *IEEE Trans. Power Del.*, vol. 4, no. 2, pp. 1401–1407, Apr. 1989.

[7] S. Civanlar, J. J. Grainger, H. Yin, and S. S. H. Lee, "Distribution feeder reconfiguration for loss reduction," *IEEE Trans. Power Del.*, vol. 3, no. 3, pp. 1217–1223, Jul. 1988.

[8] S. K. Goswami and S. K. Basu, "A new algorithm for the reconfiguration of distribution feeders for loss minimization," *IEEE Trans. Power Del.*, vol. 7, no. 3, pp. 1484–1491, Jul. 1992.

[9] F. V. Gomes, S. Carneiro, Jr., J. L. R. Pereira, M. P. Vinagre, P. A. N. Garcia, and L. R. De. Araujo, "A new distribution system reconfiguration approach using

optimum power flow and sensitivity analysis for loss reduction," *IEEE Trans. Power Syst.*, vol. 21, no. 4, pp. 1616–1623, Nov. 2006.

[10] E. Dall'Anese and G. B. Giannakis, "Sparsity-leveraging reconfiguration of smart distribution systems," *IEEE Trans. Power Del.*, vol. 29, no. 3, pp. 1417–1426, Jun. 2014.

[11] Q. Peng, Y. Tang, and S. H. Low, "Feeder reconfiguration in distribution networks based on convex relaxation of OPF," *IEEE Trans. Power Syst.*, vol. 30, no. 4, pp. 1793–1804, Jul. 2015.

[12] R. A. Jabr, I. Dzafic, and Indira Huseinagic, "Real time optimal reconfiguration of multiphase active distribution networks," *IEEE Trans. Smart Grid*, to be published.

[13] R. J. Sarfi, M. M. A. Salama, and A. Y. Chikhani, "Distribution system reconfiguration for loss reduction: an algorithm based on network partitioning theory," *IEEE Trans. Power Syst.*, vol. 11, no. 1, pp. 504–510, Feb. 1996.

[14] D. Shirmohammadi and H. W. Hong, "Reconfiguration of electric distribution networks for resistive line losses reduction," *IEEE Trans. Power Del.*, vol. 4, no. 2, pp. 1492–1498, Apr. 1989.

[15] I. Roytelman, V. Melnik, S. S. H. Lee, and R. L. Lugtu, "Multi-objective feeder reconfiguration by distribution management system," *IEEE Trans. Power Syst.*, vol. 11, no. 2, pp. 661–667, May 1996.

[16] G. K. V. Raju and P. R. Bijwe, "An efficient algorithm for minimum loss reconfiguration of distribution system based on sensitivity and heuristics," *IEEE Trans. Power Syst.*, vol. 23, no. 3, pp. 1280–1287, Aug. 2008.

[17] A. A. M. Zin, A. K. Ferdavani, A. B. Khairuddin, and M. M. Naeini, "Two circular-updating hybrid heuristic methods for minimum-loss reconfiguration of electrical distribution network," *IEEE Trans. Power Syst.*, vol. 28, no. 2, pp. 1318–1323, May 2013.

[18] H.-D. Chiang and R. Jean-Jumeau, "Optimal network reconfigurations in distribution systems: part 1: a new formulation and a solution methodology," *IEEE Trans. Power Del.*, vol. 5, no. 4, pp. 1902–1908, Nov. 1990.

[19] H.-D. Chiang and R. Jean-Jumeau, "Optimal network reconfigurations in distribution systems: part 2: solution algorithms and numerical results," *IEEE Trans. Power Del.*, vol. 5, no. 3, pp. 1568–1574, Jul. 1990.

[20] R. Cherkaoui, A. Bart, and A. J. Germond, "Optimal configuration of electrical distribution networks using heuristic methods," in *Proc. 11th Power System Computation Conf.*, Avignon, France, 1993, pp. 147–154.

[21] C.-T Su, C.-F. Chang, and J.-P. Chiou, "Distribution network reconfiguration for loss reduction by ant colony search algorithm," *Electric Power Systems Research*, vol. 75, pp. 190–199, 2005.

[22] A. Ahuja and A. Pahwa, "Using ant colony optimization for loss minimization in distribution networks," in *Proc. 37th Annual North American Power Symp.*, 2005, pp. 470–474.

[23] K. Nara, A. Shiose, M. Kitagawa, and T. Ishihara, "Implementation of genetic algorithm for distribution systems loss minimum re-configuration," *IEEE Trans. Power Syst.*, vol. 7, no. 3, pp. 1044–1050, Aug. 1992.

[24] E. M. Carreno, R. Romero, and A. Padilha-Feltrin, "An efficient codification to solve distribution network reconfiguration for loss reduction problem," *IEEE Trans. Power Syst.*, vol. 23, no. 4, pp. 1542–1551, Nov. 2008.

[25] H. D. de Macedo Braz and B. A. de Souza, "Distribution network reconfiguration using genetic algorithms with sequential encoding: Subtractive and additive approaches," *IEEE Trans. Power Syst.*, vol. 26, no. 2, pp. 582–593, May 2011.

[26] A. Asrari, S. Lotfifard, and M. Ansari, "Reconfiguration of smart distribution systems with time varying loads using parallel computing," *IEEE Trans. Smart Grid*, vol. 7, no. 6, pp. 2713–2723, Nov. 2016.

[27] C.-T. Su and C.-S. Lee, "Network reconfiguration of distribution systems using improved mixed-integer hybrid differential evolution," *IEEE Trans. Power Del.*, vol. 18, no. 3, pp. 1022–1027, Jul. 2003.

[28] J.-P. Chiou, C.-F. Chang, and C.-T. Su, "Variable scaling hybrid differential evolution for solving network reconfiguration of distribution systems," *IEEE Trans. Power Syst.*, vol. 20, no. 2, pp. 668–674, May 2005.

[29] R. S. Rao, S. V. L. Narasimham, M. R. Raju, and A. S. Rao, "Optimal network reconfiguration of large-scale distribution system using harmony search algorithm," *IEEE Trans. Power Syst.*, vol. 26, no. 3, pp. 1080–1088, Aug. 2011.

[30] S. Toune, H. Fudo, T. Genji, Y. Fukuyama, and Y. Nakanishi, "Comparative study of modern heuristic algorithms to service restoration in distribution systems," *IEEE Trans. Power Del.*, vol. 17, no. 1, pp. 173–181, Jan. 2002.

[31] A. B. Morton and I. M. Y. Mareels, "An efficient brute-force solution to the network reconfiguration problem," *IEEE Trans. Power Del.*, vol. 15, no. 3, pp. 996–1000, Jul. 2000.

[32] W. Mayeda and S. Seshu, "Generation of trees without duplications," *IEEE Trans. Circuit Theory*, vol. 12, no. 2, pp. 181–185, 1965.

[33] A. Botea, J. Rintanen, and D. Banerjee, "Optimal reconfiguration for supply restoration with informed A* search," *IEEE Trans. Smart Grid*, vol. 3, no. 2, pp. 583–593, Jun. 2012.

[34] A. Borghetti, "A mixed-integer linear programming approach for the computation of the minimum-losses radial configuration of electrical distribution networks," *IEEE Trans. Power Syst.*, vol. 27, no. 3, pp. 1264–1273, Aug. 2012.

[35] J. A. Taylor and F. S. Hover, "Convex models of distribution system reconfiguration," *IEEE Trans. Power Syst.*, vol. 27, no. 3, pp. 1407–1413, Aug. 2012.

[36] R. Jabr, R. Singh, and B. Pal, "Minimum loss network reconfiguration using mixed-integer convex programming," *IEEE Trans. Power Syst.*, vol. 27, no. 2, pp. 1106–1115, May 2012.

[37] K. Chen, W. Wu, B. Zhang, and H. Sun, "Robust restoration decision-making model for distribution networks based on information gap decision theory," *IEEE Trans. Smart Grid*, vol. 6, no. 2, pp. 587–597, Mar. 2015.

[38] X. Chen, W. Wu, and B. Zhang, "Robust restoration method for active distribution networks," *IEEE Trans. Power Syst.*, vol. 31, no. 5, pp. 4005–4015, Sep. 2016.

[39] B. Chen, C. Chen, J. Wang, K. L. Butler-Purry, "Sequential service restoration for unbalanced distribution systems and microgrids," *IEEE Trans. Power Syst.*, to be published.

[40] O. Bassey, B. Chen, K. L. Butler-Purry, and A. Goulart, "Sequential service restoration in distribution system and microgrid integrating frequency response and varying switching interval," in *Proc. 2018 Texas Power and Energy Conference*.

[41] B. Chen, C. Chen, J. Wang, and K. L. Butler-Purry, "Multi-time step service restoration for advanced distribution systems and microgrids," *IEEE Trans. Smart Grid*, to be published.

[42] H. Ahmadi and J. R. Marti, "Linear current flow equations with application to distribution systems reconfiguration," *IEEE Trans. Power Syst.*, vol. 30, no. 4, pp. 2073–2080, Jul. 2015.

[43] H. M. Khodr, J. Martinez-Crespo, M. A. Matos, and J. Pereira, "Distribution systems reconfiguration based on OPF using Benders decomposition," *IEEE Trans. Power Del.*, vol. 24, no. 4, pp. 2166–2176, Oct. 2009.

[44] H. F. Zhai, M. Yang, B. Chen, and N. Kang, "Dynamic reconfiguration of three-phase unbalanced distribution networks," *Int. J. Electr. Power Energy Syst.*, to be published.

[45] N. C. Koutsoukis, D. O. Siagkas, P. S. Georgilakis, and N. D. Hatziargyriou, "Online reconfiguration of active distribution networks for maximum integration of distributed generation," *IEEE Trans. Autom. Sci. Eng.*, vol. 14, no. 2, pp. 437–448, Apr. 2017.

[46] Y. Xu, C.-C. Liu, K. P. Schneider, F. K. Tuffner, and D. T. Ton, "Microgrids for service restoration to critical load in a resilient distribution system," *IEEE Trans. Smart Grid*, to be published.

[47] S. Dimitrijevic and N. Rajakovic, "Service restoration of distribution networks considering switching operation costs and actual status of the switching equipment," *IEEE Trans. Smart Grid*, vol. 6, no. 3, pp. 1227–1232, May 2015.

[48] R. Perez-Guerrero, G. T. Heydt, N. J. Jack, B. K. Keel, and A. R. Castelhano, Jr., "Optimal restoration of distribution systems using dynamic programming," *IEEE Trans. Power Del.*, vol. 23, no. 3, pp. 1589–1596, Jul. 2008.

[49] R. O'Neill, R. Baldick, U. Helman, M. Rothkopf, and J. Stewart, "Dispatchable transmission in RTO markets," *IEEE Trans. Power Syst.*, vol. 20, no. 1, pp. 171–179, Feb. 2005.

[50] E. Fisher, R. O'Neill, and M. Ferris, "Optimal transmission switching," *IEEE Trans. Power Syst.*, vol. 23, no. 3, pp. 1346–1355, Aug. 2008.

[51] K. Hedman, R. O'Neill, E. Fisher, and S. Oren, "Optimal transmission switching with contingency analysis," *IEEE Trans. Power Syst.*, vol. 24, no. 3, pp. 1577–1586, Aug. 2009.

[52] A. Khodaei, M. Shahidehpour, and S. Kamalinia, "Transmission switching in expansion planning," *IEEE Trans. Power Syst.*, vol. 25, no. 3, pp. 1722–1733, Aug. 2010.

[53] K. Hedman, S. Oren, and R. O'Neill, "A review of transmission switching and network topology optimization," in *Proc. IEEE Power and Energy Society General Meeting*, Jul. 2011.

[54] M. Lavorato, J. F. Franco, M. J. Rider, and R. Romero, "Imposing radiality constraints in distribution system optimization problems," *IEEE Trans. Power Syst.*, vol. 27, no. 1, pp. 172–180, Feb. 2012.

[55] E. Romero-Ramos and J. Riquelme-Santos, "Discussion on 'imposing radiality constraints in distribution system optimization problems'," *IEEE Trans. Power Syst.*, vol. 28, no. 1, pp. 568, Feb. 2013.

[56] R. A. Jabr, "Radial distribution load flow using conic programming," *IEEE Trans. Power Syst.*, vol. 21, no. 3, pp. 1458–1459, Aug. 2006.

[57] R. A. Jabr, "Optimal power flow using an extended conic quadratic formulation," *IEEE Trans. Power Syst.*, vol. 23, no. 3, pp. 1000–1008, Aug. 2008.

[58] J. Lavaei and S. H. Low, "Zero duality gap in optimal power flow problem," *IEEE Trans. Power Syst.*, vol. 27, no. 1, pp. 92–107, Feb. 2012.

[59] B. Kocuk, S. S. Dey, and X. A. Sun, "Strong SOCP relaxations for the optimal power flow problem," *Operations Research*, vol. 64, no. 6, pp. 1177–1196, Nov. 2016.

[60] B. Kocuk, S. S. Dey, and X. A. Sun, “New formulation and strong MISOCP relaxations for AC optimal transmission switching problem,” *IEEE Trans. Power Syst.*, vol. 32, no. 6, pp. 4161–4170, Nov. 2017.

[61] J. C. Lopez, J. F. Franco, M. J. Rider, and R. Romero, “Optimal restoration/ maintenance switching sequence of unbalanced three-phase distribution systems,” *IEEE Trans. Smart Grid*, to be published.

[62] A. Abur and A. G. Exposito, *Power System State Estimation: Theory and Implementation*. New York: Marcel Dekker, Inc., 1994, ch. 9.

[63] S. Bolognani and S. Zampieri, “On the existence and linear approximation of the power flow solution in power distribution networks,” *IEEE Trans. Power Syst.*, vol. 31, no. 1, pp. 163–172, Jan. 2016.

VITA

Bai Cui was born in Beijing, China in 1989. He received the B.S. degree in Electrical Engineering from Shanghai Jiao Tong University in 2011, and the B.S. degree in Computer Engineering from the University of Michigan, Ann Arbor, MI, in 2011. He joined Georgia Institute of Technology in Fall 2011 to pursue his Ph.D. degree and is currently a Ph.D. candidate. He received the M.S. degree in Electrical and Computer Engineering from Georgia Tech in 2014. He has interned at Space-Time Insight and Eaton Corporation in 2014 and 2015, respectively.

He will join Argonne National Laboratory as a postdoctoral appointee in the Energy Systems Division in 2018. His research interests include distribution automation, power system stability and control, and power system optimization.

Bai is a student member of IEEE, a student member of IEEE Power & Energy Society, an active reviewer of several IEEE and IET journals, and an author of several journal and conference papers.